

Study of Plasma and Energetic Electron Environments and Effects

ESA contract 11974/96/NL/JG(SC)

WP 110 TECHNICAL NOTE (SPEE-WP110-TN)

Version 2.0

March 10, 1999

Analysis of Freja Charging Events: Charging Events Identification and Case Study

Prepared by

J.-E. Wahlund, L. J. Wedin, A. I. Eriksson, and B. Holback,
Swedish Institute of Space Physics, Uppsala Division

L. Andersson
Swedish Institute of Space Physics, Kiruna Division

ESA Technical Officer: A. Hilgers, Space Environments and Effects Analysis Section (TOS-EMA)
ESA Technological Research Programme, Space Environments and Effects Major Axis

TABLE OF CONTENTS

1. Introduction	3
1.1. Purpose of this document	3
1.2. Related documents	3
1.3. Why are spacecraft charging studies important ?	3
1.3.1. General on plasma-spacecraft interaction	3
1.3.2. Payload disturbances due to spacecraft charging	5
2. Previous Observations and Understanding of Spacecraft Charging	6
2.1. SCATHA and ATS studies (GEO)	6
2.2. DMSP studies (PEO/LEO)	7
3. The Freja Spacecraft and Payload Descriptions	9
3.1. Freja experiment descriptions	9
3.2. Instrumental restrictions and possible error sources	10
3.2.1. MATE data	10
3.2.2. TESP data	11
3.2.3. TICS data	11
3.2.4. Langmuir probe data	11
3.2.5. Plasma wave data	12
3.2.6. Magnetometer data	13
4. Methodology for Selection of Freja Charging Events	14
4.1. Selection criteria for Freja charging events	14
4.2. Determination of plasma density	15
5. Observational Characteristics of a Selected Subset of Freja Charging Events	16
5.1. Event 1: Orbit 487 (typical charging event)	16
5.2. Event 2: Orbit 542 (typical charging event)	25
5.3. Event 3: Orbit 790 (typical charging event)	33
5.4. Event 4: Orbit 1651 (typical charging event)	42
5.5. Event 5: Orbit 5802 (charging and ion heating)	47
5.6. Event 6: Orbit 1666 (largest charging potential)	54
5.7. Event 7: Orbit 1785 (charging during sunlight)	60
5.8. Event 8: Five low altitude survey orbits (suspected charging)	66
5.9. Event 9: Orbit 736 (variation with electron density)	69
5.10. Event 10: Orbit 7279 (low altitude charging)	79
6. Discussion of the Events	85
6.1. Identified Freja charging event types	85
6.2. Arcing ?	86
6.3. Comparisons with other spacecraft results	86
7. Conclusions from the charging events case study	88
8. References	90

1. INTRODUCTION

1.1 PURPOSE OF THIS DOCUMENT

This document presents the results provided by work package WP110, *Charging Events Identification and Case Study of a Subset of Them*. This work package includes a detailed analysis of 10 charging events detected by the Freja spacecraft in order to identify the precise mechanisms behind the charging processes that operate at Freja altitudes (1000 - 1800 km). The presented events aim to be a representative selection of the different types of charging processes detected in the Freja data set. The Freja spacecraft was in operation between October 1992 to April 1994 during declining solar activity conditions. The Freja mission objective was to study the polar (high latitude) auroral processes and was therefore equipped with a highly advanced plasma payload package, and the spacecraft itself was designed to be as electrically clean as possible. Such a payload package is, of course, also suitable for spacecraft charging studies. Numerous surface charging events did indeed occur with negative charging levels as large as -2000 Volts. Surface charging should therefore be of concern for future spacecraft designs. The analysis is complemented with precise electron and ion energy/pitch angle distributions, sunlight/eclipse characteristics, geomagnetic location and auroral activity conditions, as well as cold plasma information.

The work package also provides a detailed database of the Freja charging cases accessible by the SPEE WWW server (<http://www.geo.fmi.fi/spee>). The database includes all the 291 charging events found in the Freja data set. This database can be used for further studies of surface charging on the Freja spacecraft, but its primary aim is to provide an easy accessible database on environmental statistics for spacecraft charging. The SPEE WWW server is described in the *User and Software Requirements Document* to work package WP330 [SPEE-WP330-URD/SRD].

1.2 RELATED DOCUMENTS

The following documents are included in work package WP100, Analysis of Freja Charging Events:

- SPEE Final Summary Report
- Charging Events Identification and Case Study of a Subset of them (this document) [SPEE-WP110-TN]
- Modelling of Freja Observations by Spacecraft Charging Codes [SPEE-WP120-TN]
- Statistical Occurrence of Charging Events [SPEE-WP130-TN].

1.3 WHY ARE SPACECRAFT CHARGING STUDIES IMPORTANT ?

1.3.1 General on Plasma-Spacecraft Interaction

The discipline of spacecraft-environment interaction has developed in the past as a series of specific engineering responses to various space environment effects as they were discovered. The variation in current flows to/from a spacecraft in different space environments, can cause charge

accumulation on the spacecraft surface(s). This charge, in turn, can produce potential gradients between electrically isolated surfaces, as well as between the spacecraft ground and the surrounding space plasma. Spacecraft potentials of several tens of thousands of volts have been reported from several spacecrafts (e.g. ATS, DMSP, SCATHA) since its first detection [DeForest, 1972]. Such potential build-ups can give rise to destructive arc discharges or micro-arcs that generate electromagnetic noise and erode surfaces. For example, arcing on highly biased solar arrays are so severe that it destroys the array in a short time. The arcing associated with high amplitude surface charging by the magnetospheric plasma is believed to have caused the loss of at least one spacecrafts [Shaw *et al.*, 1976] and possibly several more, but also anomalies on several GEO satellites [Rosen, 1976; Leach and Alexander, 1995]. This started numerous efforts to understand and mitigate charge accumulation on surfaces in space. In fact, they led to the launch of a dedicated geosynchronous spacecraft (SCATHA, Spacecraft Charging AT High Altitudes) in 1979. With the development of more longer lived and more “environmental” active spacecrafts, with associated outgassing and thruster exhausts, it became obvious that the self-induced environment also influenced the charging state of the spacecraft. In effect, the plasma environment includes the ambient thermal and energetic magnetospheric plasma, secondary electrons emitted from the surfaces, as well as that released from plasma thrusters, that created by ionization of or charge exchange with the expelled or ambient neutral gas, that generated by arc discharges, and that created by micrometeorite impacts. The solar UV radiation will also contribute to the plasma environment through the induced emission of photo-electrons from the spacecraft surface. All these plasma sources affect the charge balance of the spacecraft. The accumulation of charged particles in the plasma on the surface cause charging, and produces electrostatic fields that extend from surfaces (or even deep into the spacecraft in the case of very energetic electron impacts) into space.

The natural space plasma environment depends, of course, on the spacecraft location. Over the years, several different regions have been identified where high amplitude spacecraft charging is more prone to arise. One such environment is the Polar Earth Orbit (PEO), which traverses the high-latitude auroral plasma regions. Other common charging environments are the Low Earth Orbit (LEO) of cold, dense ionospheric plasma, and the Geosynchronous Earth Orbit (GEO) immersed in the hot (high energy) plasmashet. Charging effects in all of these regions are heavily dependent on the magnetospheric substorm activity level, and therefore *Space Weather*. There are also many (inter-)planetary regions (explored and un-explored) which are known to cause environmental disturbances, especially in the magnetospheres of other planets. Another type of high amplitude surface charging was detected by the Voyager spacecrafts in the outer magnetosphere of Saturn. There the very hot (keV) and thin outer co-rotating Saturnian magnetosphere caused the Voyager spacecrafts to charge several hundreds of volts negative [e.g. Sittler *et al.*, 1983; Lazarus *et al.*, 1983; Eviatar and Richardson, 1986; D. A Gurnett, private communication]. The Freja measurements, reported here, add further to the knowledge on spacecraft surface charging in a Polar Earth Orbit (PEO). Only very few studies have been devoted to spacecraft charging in PEO (see below), with the exception of the DMSP (Defence Meteorological Satellite Program), which presented an extensive set of surface charging occasions from a lower altitude (840 km).

1.3.2 Payload Disturbances due to Spacecraft Charging

Modern spacecrafts often carry increasingly more complex, sensitive, and expensive payload, which is affected by the space environment (natural or self-induced). Many instruments have in the past experienced operation problems due to the plasma electrostatic environment, and the interpretation of data from measurements depend critically on the knowledge of spacecraft charging effects. For instance, any shift in potential relative to the spacecraft ground or the space plasma can affect instruments designed to collect or emit charged particles, but the spacecraft environment may also be a source of instrumental noise in general. Beside destructive arcing effects on surfaces, a charge buildup on a spacecraft can in itself attract charge contaminants to sensitive surfaces. This contamination, in turn, can alter the properties of the surface, e.g. changing its conductivity, thermal properties, or optical properties in the case of lenses or mirrors.

Plasma thrusters are under consideration by ESA to be used on small spacecrafts aimed for their planetary program. It is known that plasma thruster emission can lead to a back flow onto the spacecraft and cause contamination to be deposit on the surface. The back flow from plasma thrusters is sensitive to local electric fields and collective effects [*Carruth and Brady, 1981*], and can therefore be caused by differential charging between the resulting plasma plume and the spacecraft, which in turn set up an electrical attraction between the exhaust plasma and the spacecraft surfaces [*Newell, 1985*]. Another mechanism of importance is due to slow moving exhaust products near the thruster nozzle, which can re-circulate backward near the electrically charged spacecraft surface [*Detleff, 1991*]. Thus a large plasma cloud can develop around a spacecraft with a plasma thruster engine, which may lead to a current drain on high-voltage surfaces. The heavy metal ions from the thrusters (as well as from surface sputtering erosion) can easily adhere to the spacecraft surface, and the surface contamination may affect solar arrays, thermal control surfaces, optical sensors, communications, science instrumentation, properties (electrical, structural, chemical) of surface materials, and, of course, spacecraft charging. The level of charging is found to be reduced by the relatively cold thruster plasma, but the level of differential charging is thought to be increased by the occurrence of contaminants on the spacecraft surface. It is therefore important that plasma diagnostics accompany the first experimental spacecrafts with electrical propulsion, in order to identify the possible problems that may arise from the plasma back flow and give insight on how future such spacecrafts shall be designed to avoid these possible problems.

2. PREVIOUS OBSERVATIONS AND UNDERSTANDING OF SPACECRAFT CHARGING

2.1 SCATHA and ATS STUDIES (GEO)

The spacecraft charging processes and effects in both GEO and LEO/PEO orbits have been reviewed earlier [e.g. by, *Garrett*, 1981; and *Hastings*, 1995], and only a brief summary of the most relevant observations on spacecraft charging will be given here. *DeForest* [1972] was the first to report high-level charging on the geosynchronous orbiting Applied Technology Satellite (ATS 5). He found surface charging events with up to -10,000 V (negative) during eclipse, and up to -200 V in sunlight conditions. Later studies [e.g., *Gussenhoven and Mullen*, 1983; and *Mullen et al.*, 1986], using data from the ATS 5 and 6 as well as the P78-2 SCATHA missions, showed charging levels up to -19,000 V in eclipse and -2,000 V in sunlight when the spacecrafts entered the low density plasma sheet and intense fluxes of energetic electrons ($> 10 - 30$ keV) closely related to magnetospheric substorm activity. Also, significant amounts of differential charging between surfaces on the spacecraft, as well as discharges (both on the surface and internally) were detected [e.g. *Koons and Gorney*, 1991].

The SCATHA results can be summarised as follows:

- Surface charging occurred preferentially when the flux of tens of keV energy electrons was large [e.g. *Gussenhoven and Mullen*, 1983].
- Internal charging occurred preferentially when the flux of hundreds of keV energy electrons was large, while the flux of the tens of keV electrons was low [*Koons and Gorney*, 1991].
- The charging level was proportional to the electron flux with energy above 30 keV [*Mullen et al.*, 1986].
- The electron flux was insensitive to electron fluxes with energy below 10 keV where a critical electron peak energy threshold of 10 keV was necessary for high level charging to occur [*Olsen*, 1983]. The threshold effect is due to the shape of the secondary yield curve for the surface materials used, especially the high energy crossover where the secondary yield drops below 1, so that low energy electrons are balanced by their own produced secondary and back-scattered electron emission. This result was supported by the few percent eclipse events where a subtle change in the environment toward higher energy electron distribution produced a substantial change in spacecraft potential [*Katz et al.*, 1986; *Mullen et al.*, 1986].
- Discharges were weakly correlated with the relativistic electron flux [*Koons and Gorney*, 1991].
- Surface charging over -100 V occurred only for $K_p > 3+$ (i.e. when the auroral activity was large enough) [*Koons and Gorney*, 1991].

- Surface charging was strongly favoured during eclipse (i.e. when no photoelectron emission from the surface occurred), and therefore dominated in the midnight sector [*Koons and Gorney, 1991*].
- During sunlight surface charging levels occurred were modified by the spacecraft orientation with respect to the sun. In these cases it was thought that the low energy photo-electron emission returned back to the spacecraft by the action of the ambient magnetic field [*Mullen et al., 1986*].

2.2 DMSP STUDIES (PEO/LEO)

The very high charging levels as severe as -19,000 V detected in geosynchronous orbit by the ATS and SCATHA spacecrafts was not expected to occur at low altitudes, where a negative charging would be inhibited by a neutralising ion current from the dense ionospheric plasma. Even though theoretical predictions of negative charging of several kilovolts for large structures in polar LEO [*Katz and Parks, 1983*], and manned polar flights were believed to face hazards [*Hall et al., 1987*], it was a bit of a surprise when data from the Defence Meteorological Satellite Program (DMSP) revealed 184 events of negative surface charging in the range -47 to -1430 V within the auroral region at an altitude of only 840 km [e.g., *Gussenhoven et al., 1985*; *Yeh and Gussenhoven, 1987*; *Frooninckx and Sojka, 1992*; and *Stevens and Jones, 1995*].

The DMSP (F6, F7, F8, F9) results can be summarised as follows:

- high latitude charging events were detected in association with intense auroral energetic electron precipitation co-located with ionospheric plasma depletions [e.g. *Gussenhoven et al., 1985*],
- precipitating electrons with energies as low as 2-3 keV may contribute to surface charging, although higher-energy electrons make a greater contribution [*Frooninckx and Sojka, 1992*],
- incident energetic electron fluxes of at least 10^{12} electrons/m²-s-str existed during the charging events [*Gussenhoven et al., 1985*],
- the charging level was better correlated with the ratio of the integral electron flux over the cold thermal plasma density, than just the integral electron flux alone [*Yeh and Gussenhoven, 1987*],
- secondary electron production at the surface by the incident electrons with energies below 1 keV inhibited charging, most probably due to the large secondary yields at these low incident electron energies [*Frooninckx and Sojka, 1992*],
- the charging events always occurred during eclipse, i.e. in the absence of photoelectron emission from the spacecraft surface [*Gussenhoven, private communication*; *Gussenhoven et al., 1985*],
- the highest thermal plasma density observed during charging events was 10^{10} m⁻³ [*Frooninckx and Sojka, 1992*],
- the distribution of the charging events was modulated by the solar activity, i.e. the charging were most frequent and severe during solar minimum. Since the incident

electron flux did not vary significantly over a solar cycle, while the cold thermal plasma density varied with several orders of magnitude, it was suggested that the increased ionisation, and resulting increased thermal plasma density, during solar maximum inhibited charging [*Frooninckx and Sojka, 1992*],

- theoretical comparisons with the POLAR code [see SPEE-WP120-TN on spacecraft charging models and simulations] suggested, except for the material secondary electron yield properties, that the spacecraft orientation, fraction of conductive areas in the velocity direction, the cold thermal plasma density, and the ion composition modified the charging level to the greatest extent [*Stevens and Jones, 1995*].

In order to predict the charging level of a LEO/PEO spacecraft, one therefore needs to know precisely the incident electron spectral distribution as well as the surface material properties (especially the secondary yield versus incident energy), since the current balance is largely determined by the ratio between the flux of the incident electrons and the flux of re-emitted secondary electrons [e.g., *Katz et al., 1986*; and *Yeh and Gussenhoven, 1987*; see also *Olsen, 1983*, regarding similar ATS and SCATHA results].

We would like to note that the thermal plasma densities were estimated from the SSIE instrument on board the DMSP satellites, which consisted of a spherical Langmuir probe and a retarding potential analyser. Both these instruments will, according to our analyses, be severely affected by the high negative charging levels in that no thermal electrons will have enough energy to even reach the instruments (see below). The ion densities inferred from the RPA might be in order, but we are rather cautious in overly interpreting the DMSP plasma densities as true ones. These measurements may be strongly affected by the spacecraft charging.

3. THE FREJA SPACECRAFT AND PAYLOAD DESCRIPTIONS

3.1 FREJA EXPERIMENT DESCRIPTIONS

The Freja* spacecraft (Figure 3.1.1) was launched in October 6, 1992, and ended its operations in October, 1996, two years after its planned operation time. This study is limited to the time period October, 1992, to May, 1994, when most on-board plasma instruments provided good measurements. This time period covered a declining phase of the solar cycle from medium solar activity to minimum solar activity. The Freja spacecraft orbits Earth with a 63° inclination, an apogee in the northern hemisphere of 1756 km, and a perigee in the southern hemisphere of 601 km. Freja therefore passes along the auroral region almost tangentially each orbit, and can therefore be considered to be a Polar Earth Orbit (PEO) spacecraft. The perigee is 601 km above the southern hemisphere, and the apogee is 1756 km above the northern hemisphere. Only low-resolution survey data exist below an altitude of 1000 km. Freja is a spin-stabilised sun-pointing spacecraft with a spin period of 6 seconds, and its structure and surface materials are presented in SPEE-WP120-TN.

The Freja project was designed to give high temporal/spatial resolution measurements of the auroral plasma characteristics, and therefore contained 73 kg of the state of the art plasma diagnostic experiments. The Freja data set therefore allows detailed studies of spacecraft charging events. The following payload existed

<i>Experiment</i>	<i>Measurement</i>	<i>Principal Investigator</i>
F1 Electric Fields	3 pair of wire booms (< 3 kHz)	Göran Marklund
F2 Magnetic Fields	3-axis fluxgate magnetometers (< 64 Hz)	Lawrence Zanetti
F3H Hot Plasma	2D electron spectrometer (MATE, 0.1-115 keV)	Lars Eliasson
	2D ion composition spectrometer (TICS, 1 eV-10 keV)	
F3C Cold Plasma	3D ion/electron distr. (<300 eV)	Brian Whalen
F4 Plasma Waves	3 pair of wire booms, 3-axis search coil magnetometers, HF booms (E, B, dn/n, 1 Hz-4 MHz)	Bengt Holback
F5 Auroral Imager	2 UV CCD Cameras	John S. Murphee
F6 Electron Beam	3 electron guns (3D of E-field)	Götz Paschmann
F7 Electron Spectrometer	2D electron spectrometer (TESP, 0.01-20 keV)	Manfred Boehm

A detailed description of all experiments onboard Freja can be found in a special Freja instrumentation issue of *Space Science Reviews* [Lundin et al., 1994].

*) **Freja**, the goddess of fertility in Nordic mythology, was not a gentle "Afrodite of the north". She was the empress of Folkvang, the estate of the Nordic Gods, and she stood close to Odin, the almighty. She is a female warrior like Pallas Athena in Greek mythology. Her power encompassed life and death, love and battle, fertility and black magic. Half of the heroes killed in battle were her toll, sent to her for her amusement.

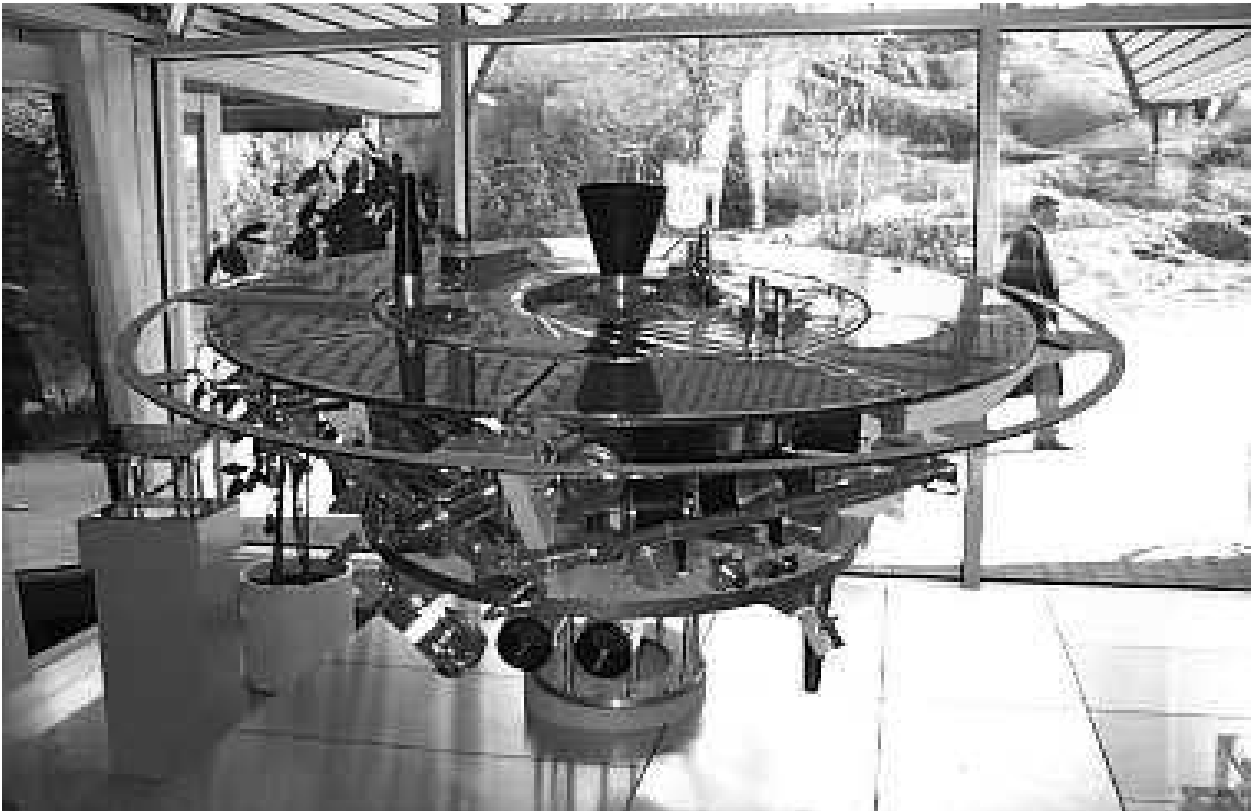


Figure 3.1.1: The Freja satellite mockup in the entrance hall at the Swedish Space Corporation, 1997.

3.2 INSTRUMENT RESTRICTIONS AND POSSIBLE ERROR SOURCES

3.2.1 MATE Data

The MAgnetic imaging Two-dimensional Electron spectrometer (MATE), measures electron energy and angular distributions in the energy range 0.1-100 keV. MATE consist of a 360° field-of-view sector magnet energy analyser with 90° deflection angle for simultaneous energy and pitch-angle determination. The sampling rate for the full energy range is 10 ms, and a collimator system enables measurements of the energy spectrum at 16 energies (with resolution $\Delta E/E = 30\%$), and 30 angular sectors.

Unfortunately, the MATE instrument was not deployed completely and was to 1/3 blocked by the Freja spacecraft itself and only every 4th angular sector have data. Also, the MATE instrument did only work properly up to orbits around 1600, where after only the integrated flux of the high-energy electrons (with some pitch-angle information) could be obtained after that. In addition, the lowest energy channels was found to give uncertain data. This instrument is otherwise the only instrument onboard Freja that could give accurate information on the high energy electrons.

3.2.2 TESP Data

The Two-dimensional Electron SPectrometer (TESP) on Freja consists of a "top-hat" style sweeping electrostatic analyser. The energy range of 20 eV-25 keV is covered in 32 sectors to complete a spectrum. Depending on instrument mode, 16 or 32 spectra are returned each second (31.25 ms resolution). The angular field-of-view is the full 360° and electrons are counted in 32 equally spaced bins, yielding an angular resolution of 11°. The entrance aperture of the TESP also contains a set of electrostatic deflectors which allows the plane of acceptance to be "warped" into a cone.

The TESP experiment started working around orbit 720, when the instrument software were sent to the spacecraft after the launch. The TESP data covers only energies up to 25 keV, but give nevertheless important information regarding the high-energy electrons. Since low energy electrons may cause an excess emission of secondary electrons (and thereby mitigate charging), the information from this experiment is very useful. Note though that the energy channels below about 30 eV was found to give uncertain data.

3.2.3 TICS Data

The Three-dimensional Ion Composition Spectrometer (TICS) measures the positive ion distributions in the energy range 0.5 eV/q-5 keV/q. TICS carry out measurements perpendicular to the spacecraft spin plane and thus gives 3D ion measurements every 3 s. TICS consists of a spherical "top-hat" electrostatic analyser with 16 or 32 energy steps sampled each 10 ms. This means that one 16 step energy sweep takes 160 ms + 40 ms for adjusting the high voltage. TICS also gives limited ion composition information in the range 1-40 amu/q. This instrument gives the best measurement of the degree of negative charging, since the whole ion population is accelerated toward the spacecraft (and TICS) and will be detected at energies corresponding to the potential of the spacecraft. Even as small negative potentials as -5 V can be seen in the TICS data.

3.2.4 Langmuir Probe Data

There exist 4 possible spherical Langmuir probes (P3-P6) situated on wire booms, and a cylindrical Langmuir probe (CYLP) onboard Freja. The CYLP is almost always available, but the operation of the spherical Langmuir probes (LP) depends on the measurement mode for a certain orbit in question. The spherical LP's are 6 cm in diameter and coated with graphite (DAG 213). They are situated 5.5 m (P5 and P6) and 10.5 m (P3 and P4) from the spacecraft respectively. The CYLP is 57 cm long and 1 cm in diameter, and is made of carbon fibre. It is mounted on the DC

magnetometer stiff boom (2 m from the spacecraft) parallel to the spin axis. As the spin axis is "sun-pointing" within 30°, this will minimise the projected surface area and thus the photoelectron emission. The CYLP data is not used in the statistical study because of difficulties in interpreting (correctly modelling) the results from this probe.

A Langmuir probe samples all current contributions in a plasma at a certain biasing potential, with respect to the spacecraft floating ground, according to its current-voltage characteristics. Therefore, a LP is a direct measurement of the charge state of the probe (and spacecraft). Most often this fact gives information on the density and electron temperature of the ambient thermal plasma, since the sampled probe current usually is directly proportional to $n_e / \sqrt{T_e}$ and because the ambient thermal electron current usually dominates the current collection for positive probe potentials. However, when the spacecraft (and probe) attains a large negative potential (i.e. a large negative charge) with respect to the surrounding plasma, the thermal electrons will start to be repelled from the LP. If the negative potential becomes much larger than the average energy of the thermal electrons (typically below 2 eV), a majority of these electrons cannot easily reach the negatively charged LP, and the probe current drops sharply to the very low values more characteristic for the collected ion thermal current. A LP current below $5 \cdot 10^{-8}$ A therefore either indicates a negative charging event of at least a few Volts negative (it is biased -8 V with respect to the spacecraft), or a very low electron density below 10^7 m^{-3} . If the threshold current represents an O^+ ram current, I_i , with ram velocity, v_i , and density, n_i , then

$$I_i \approx e n_i v_i A_p \Rightarrow n_i \approx 10^{10} / \sqrt{U} \quad [\text{m}^{-3}]$$

where A_p is the sample area of the probe, and U the absolute value of the spacecraft potential in Volts. A current of $5 \cdot 10^{-8}$ A therefore corresponds well with typical thermal plasma densities encountered by Freja when the charging levels were several tens of Volts negative. The sampled LP current is therefore a very sensitive measurement for spacecraft charging, even though it does only give a threshold value for the negative potential during high level charging events.

3.2.5 Plasma Wave Data

The plasma wave experiments (F4) did measurements in basically three frequency regimes, LF (5-2000 Hz), MF (5 Hz-16 kHz) and HF (10 kHz-4 MHz). The LF measurements most often consisted of 4 simultaneously sampled waveform components of several possible types, and the MF consisted most often of 2 simultaneous waveform components. All the wave measurements were normally made in snapshots of various lengths and duty cycle, depending on sampling rate, telemetry allocations, etc. There are 3 pairs of spherical probes, P1-P2 (21 m), P3-P4 (21 m), and P5-P6 (11 m) mounted on three wire boom pairs in the satellite spin plane. Four of the probes (P3, P4, P5, and P6) could be used for either electric field measurements (potential mode) or plasma density measurements (current mode). Probes P1 and P2 was only used for electric field measurements. The HF measurements were either made with the P12 probe pair or a special short (1.2 m) antenna probe pair (PAB) mounted on one of the magnetometer booms. There is also a Search Coil Magnetometer (SCM) assembly consisting of three identical coils which are mounted orthogonally with one

parallel to the spin axis and the other two in the spin plane. All signals are transmitted to the ground as waveforms and there is no onboard treatment except filtering, A/D conversion and intermediate storage.

During charging events the LF and MF electric field measurements were strongly disturbed up to rather large frequencies due to the fact that the probes had large negative potentials. This is due to the fact that the potential between the spacecraft and each of the probes was measured separately and the electric field was derived by the difference between these measurements. Unfortunately the work point of these measurements only allowed for a ± 50 V change, which obviously can be exceeded during charging events. The HF measurements on the other hand made use of the short PAB booms and measured the relative difference in potential between these probes directly. Therefore no large disturbances occurred on the HF measurements during charging events.

3.2.6 Magnetometer Data

The FluxGate Magnetometer (FGM) is mounted on a 2 m long boom, and gave the full 3D vector measurements of the dc geomagnetic field as well as magnetic variations with 128 samples/s. The magnetic fluctuation level is often a good measure of the "auroral activity", and the magnetic measurements seems not to be affected by charging events in any profound way.

We conclude the instrument section by noting that knowledge about charging processes is the key issue regarding good data analysis. This knowledge is specifically used in this study to differ between events of true ion heating and events of charging, which otherwise looks very much the same in the TICS data. Also, this knowledge helps us to interpret the Langmuir probe measurements correctly and it give a reason for the failures of the MF and LF plasma wave measurements. Several more effects can be detected in the operation of the scientific instruments.

4. METHODOLOGY FOR SELECTION OF FREJA CHARGING EVENTS

4.1 SELECTION CRITERIA FOR FREJA CHARGING EVENTS

Several selection criteria are necessary for identification of charging events on the Freja spacecraft in order to distinguish these events from naturally occurring plasma processes (e.g. transverse ion heating events in connection with plasma density cavities, [e.g. *André et al.*, 1998; *Wahlund et al.*, 1998]). One very sensitive indicator for a negative charging events is that the langmuir probe (LP) current drops to values below about

$5 \cdot 10^{-8}$ A, due to that very few thermal electrons will reach the very negatively charged probe. A strong negative potential of the spacecraft will also cause the surrounding ion populations to accelerate toward the spacecraft. The ion spectrometers onboard Freja (e.g. TICS) will detect a general increase in energy of all ion components when this happens. This general increase have a different appearance in the data compared to naturally occurring ion heating events, in that a "string" of enhanced flux is detected at all pitch-angles rather than showing conic characteristics. Unfortunately, ion heating events and spacecraft charging events occur simultaneously at times. A third indicator is that the low frequency electric field measurements becomes strongly disturbed.

In this study the following methodology to identifying surface charging events on the Freja spacecraft was employed:

- 1) The sampled Langmuir probe currents of the spherical probes (P3, P4, P5, P6) as well as the cylindrical (CYLP) probe is below $2 \cdot 10^{-8}$ A. This either means the plasma density is extremely low or the probes are negatively charged to a few Volts.
- 2) The narrow-band Langmuir emission (in the HF) indicates a larger density than the Langmuir probe currents would indicate. During charging events the narrowband HF emission is often unaffected, while the LP currents drop to very low values, thus suggesting that the density is much larger than the LP current would suggest.
- 3) The TICS data show a clear lift in energy of the whole ion population at least 5 eV, and the ion distribution characteristics show a well defined energy "strip" at most pitch angles. If the ion distributions have characteristics similar to transverse ion heating events (ion conics), they are only kept as suspect charging events if there is a clear miss-match between the density inferred from the Langmuir probes and the HF narrow-band emissions.
- 4) The events should show disturbances in the LF and MF electric field data. This is not a requirement for identifying a charging event though.

4.2 DETERMINATION OF PLASMA DENSITY

The HF measurements of narrow-band Langmuir waves, and/or the upper cutoff of electrostatic whistler type waves, give us the best estimate for the electron density from

$$f_{pe} = \frac{1}{2\pi} \sqrt{\frac{n_e e^2}{\epsilon_0 m_e}} \Leftrightarrow n_e = \frac{\epsilon_0 m_e}{e^2} (2\pi f_{pe})^2$$

The electron density inferred in this way varies most of the time almost exactly as the probe current measured by the LPs. This correlation strongly supports the interpretation of both the narrow-band HF signals and the probe current as measures of the plasma density. However, during surface charging events the sampled LP current drops to very low values (see above) and cannot longer be a good estimate for the plasma density. In such cases the narrow-band Langmuir emission (if existing) is a very accurate tool for determining the electron density (with about 10 % accuracy).

The conversion factors between plasma density and sampled LP currents are based on calibrations against the HF plasma frequency emissions for a statistically significant data-set. The following conversion factors have been obtained [Carlson, 1994]:

Probe	[m ⁻³ /A] in Eclipse	[m ⁻³ /A] in Sunlight
Spherical Probes	1.2·10 ¹⁵	7.5·10 ¹⁴
CYLP	8.8·10 ¹⁵	2.1·10 ¹⁵

These conversion factors are accurate to within 95 % confidence.

Another check of the plasma density can be gained from the lower frequency cutoff of whistler waves belonging to the dispersion surface connected to the lower hybrid waves. This cutoff usually occurs around a few kHz. During a charging event the MF electric field measurements are strongly disturbed, but the weak magnetic component of the whistler emission (as measured by the SCM) is often sufficient to determine this cutoff. The cutoff occurs near the lower hybrid frequency, given by

$$f_{LH} = \frac{f_{pi}}{\sqrt{1 + f_{pe}^2 / f_{ce}^2}}$$

and is therefore dependent on the ion composition. This cutoff therefore gives a rough estimate of the plasma density.

5. OBSERVATIONAL CHARACTERISTICS OF A SELECTED SUBSET OF FREJA CHARGING EVENTS

5.1 EVENT 1: ORBIT 487 (TYPICAL CHARGING)

Overview Data, 92.11.12, Prince Albert:

Figure 5.1.1 displays the TICS and MATE data for the whole Prince Albert passage of orbit 487. The high energy particles related to the radiation belts are detected around 0404:00-0407:00 UT in all the ion data (panels 1-3, O⁺, He⁺, and H⁺ respectively) as well as in the MATE data (panel 5). No TESP data were available during this particular orbit. Spacecraft charging events are detected as an increase in energy of the ion populations during the time interval 0409:00-0421:00 UT. Simultaneous with these "lifted" ion populations, enhanced fluxes of electrons with peak energy around a few keV and high energy tails reaching up to 50-100 keV are detected by the MATE experiment (panel 5). The charging events occur during eclipse (panel 4, thick line), between 21-03 MLT, 63°-75° CGLAT, and in the altitude interval 1720-1770 km. A generally good correspondence between the intensity of the energetic electron precipitation and the up-lifted ion population exists except near 0415:00 UT where a simultaneous transverse ion heating event occurred (see below).

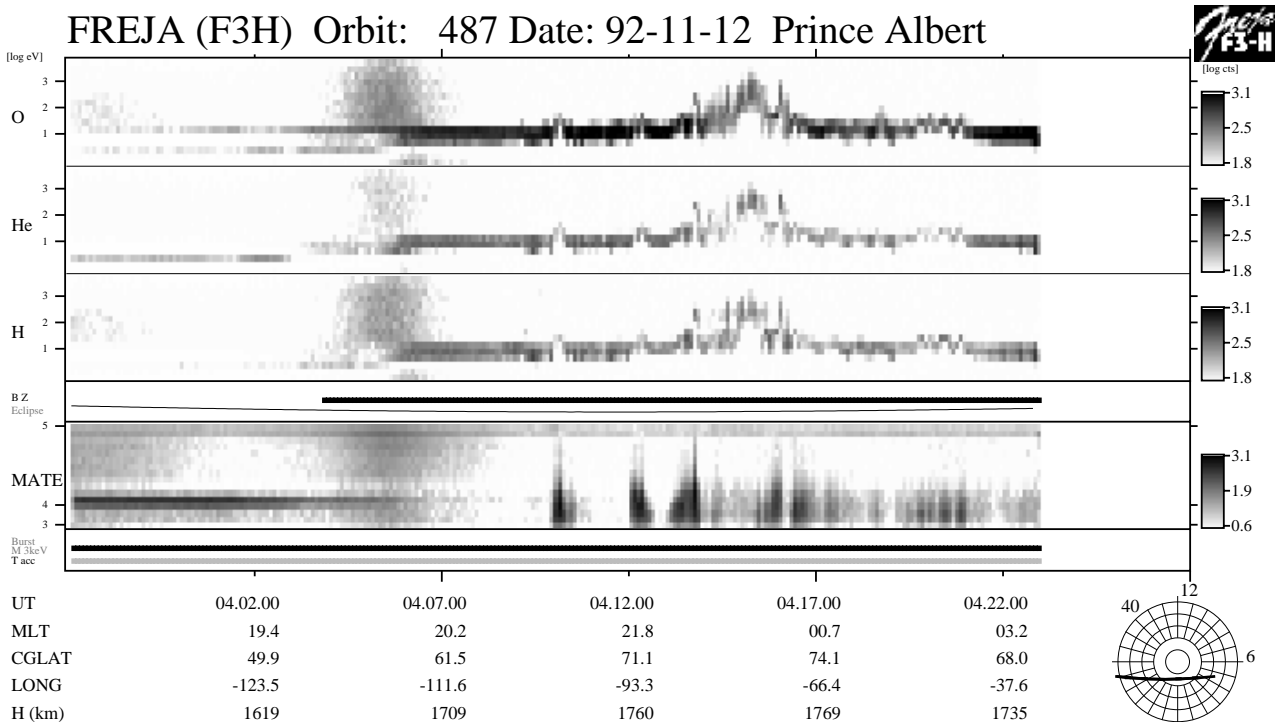


Figure 5.1.1: Overview particle data from orbit 487. A number of high-energy (up to 80 keV) electron events (panel 5) occurs in eclipse (panel 4) between 0409:00 UT and 0422:00 UT. They are all associated with "uplifted" in energy ion populations (panels 1 - 3, O⁺, He⁺, and H⁺ respectively) characteristic for spacecraft charging. An auroral transverse ion heating event is detected near 0415:00 UT, which is not due to spacecraft charging despite similar ion distribution behaviour.

Particle Data (TICS, MATE):

We divide the time period of the charging events into two shorter consecutive periods (Figure 5.1.2a and 5.1.2b) in order to see more details. Figure 5.1.2a (0408:00-0415:00 UT) show three clear charging events with uplifted ion energies in panels 1-3 near 0410:10 UT, 0412:10 UT, and 0413:20 UT. Each such uplifted ion event has an associated increased energetic electron flux (panel 5). The higher the electron energy and electron flux reach in these events, the higher the uplifted ion energy becomes. The uplifted ion energies reach a couple of 100 eV near 0413:40 UT. The continuous enhanced ion flux with energy around 10 eV is due to the ram flow caused by the moving satellite (7 km/s). A transverse ion heating event starts at 0413:50 UT and continues to around 0416:20 UT in Figure 5.1.2b (0415:00-0422:00 UT). The energy increase during this heating event is probably not due to charging (see below), except for times after 0415:40 UT where the high energy electron fluxes correlates again well with the uplifted ion energies. Figure 5.1.2a and 5.1.2b illustrate the fact that charging events in the Freja data-set most often are contained below a few tens of Volts negative [compare Figure 3.1.1 in SPEE-WP130-TN], even though the primary cause of the charging still seems to be the energetic electron precipitation (1-100 keV). The times where the sampled LP current drops sharply (Figure 5.1.3a and 5.1.3b, panel 5) is clearly the same time periods as when the supposed charging events and accompanied energetic electrons appear.

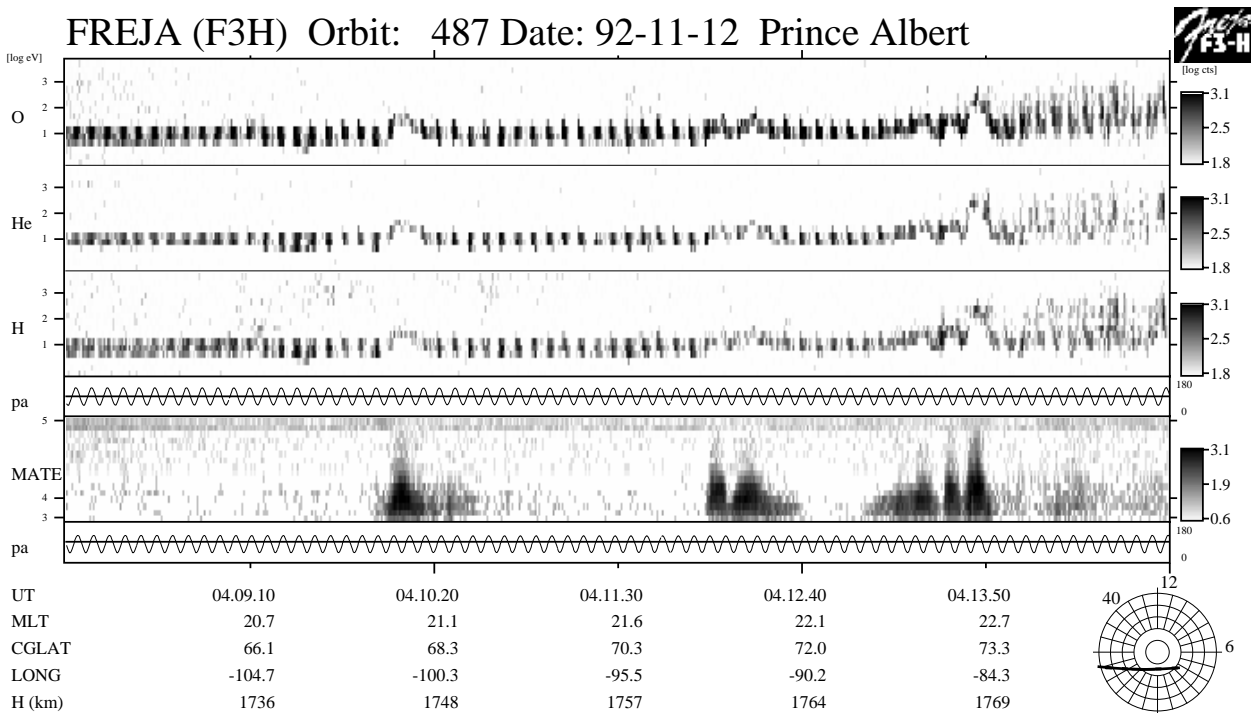


Figure 5.1.2a: Detailed spectrograms from the first half period of Figure 5.1.1. When energetic electron precipitation hits Freja (panel 5), the ion populations are lifted in energy in rough proportion to the intensity and energy tail extension of the energetic electrons.

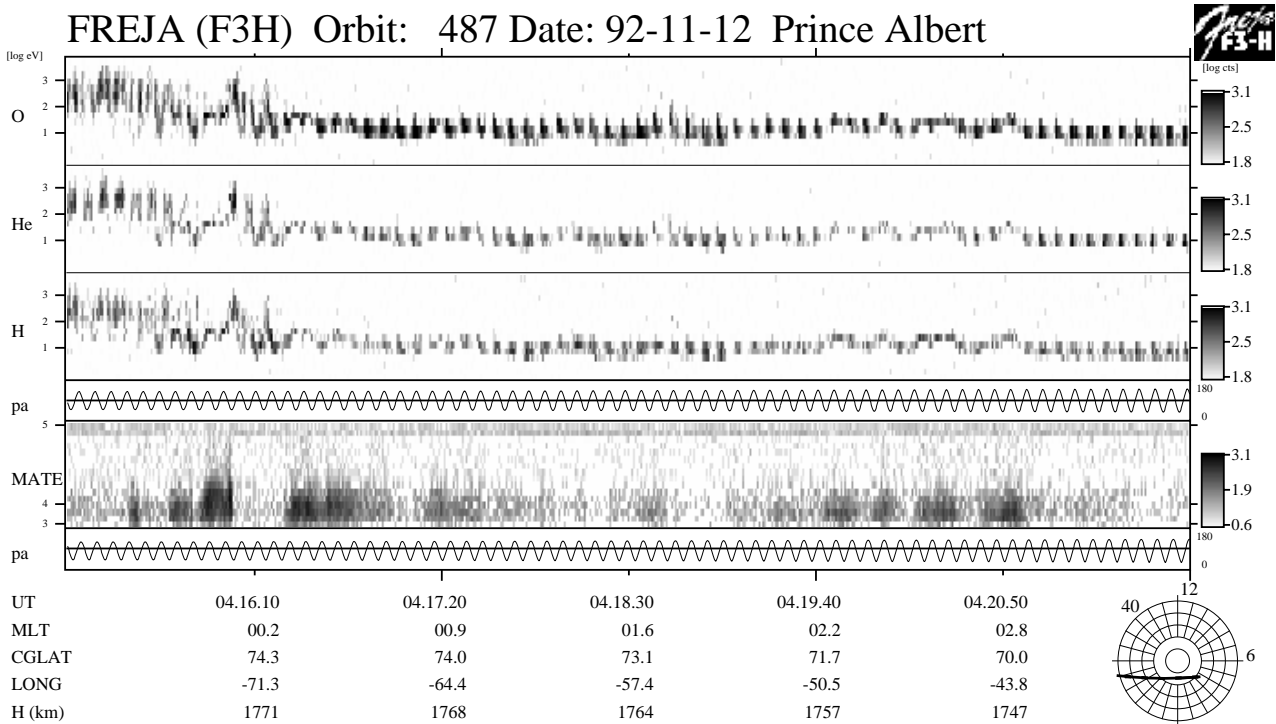


Figure 5.1.2b: Same as Figure 5.1.2a, but for the second half period of Figure 5.1.1. Again, the intensity and high energy tail extension of the energetic electron precipitation is matched by a corresponding rise in energy of all ion populations.

Wave Data (F4, F2):

The plasma wave data corresponding to the particle data in Figure 5.1.2a and 5.1.2b are presented in Figures 5.1.3a and 5.1.3b respectively. The Langmuir probe current (panel 5) and HF narrow-band emission (panel 1) corresponds both to a plasma densities of about $5\text{-}6 \cdot 10^8 \text{ m}^{-3}$ near, for example, 0408:00 UT + 170 s (Figure 5.1.3a). The density becomes lower ($1 \cdot 10^8 \text{ m}^{-3}$) during the ion heating event near +400 s (Figure 5.1.2a), which is also confirmed by the estimated density from both the LP current and the narrow-band HF emissions. The uplift in ion energy during the signatures of transverse ion heating can thus be natural, and do not require an additional charging potential. On the other hand, disruptions in the MF electric field data occasionally appears at the same times as when the LP current drops sharply in a way not matched by the frequencies of the HF narrow-band emissions (e.g. near +130 s or +340 s). These features are therefore due to charging of the Freja spacecraft. Thus, even charging of Freja of only a few tens of volts negative cause serious operational effects in certain instruments.

We have investigated one Langmuir probe sweep in order to confirm the validity of the statement that only ions are sampled by this instrument during charging. The LP sweep near 0415:00 UT + 330 s is shown in Figure 5.1.3c. A sweep consist of one "down" sweep from +15 V to -11 V during three seconds, followed by an "up" sweep. The two uppermost rows show the linear response, while the lowest panels show the logarithmic current response. We have assumed 50% Oxygen and 50%

Hydrogen in the theoretical fits. It is quite obvious that the electron current is gone, while the remaining measured current can be explained in terms of an ion current.

Printed: 22-Feb-99 17:06:21 WahlundClient v2.0

Freja F4 Wave Data, Orbit: 487
Seconds fr. 1992 11 12 040800.000000 UT

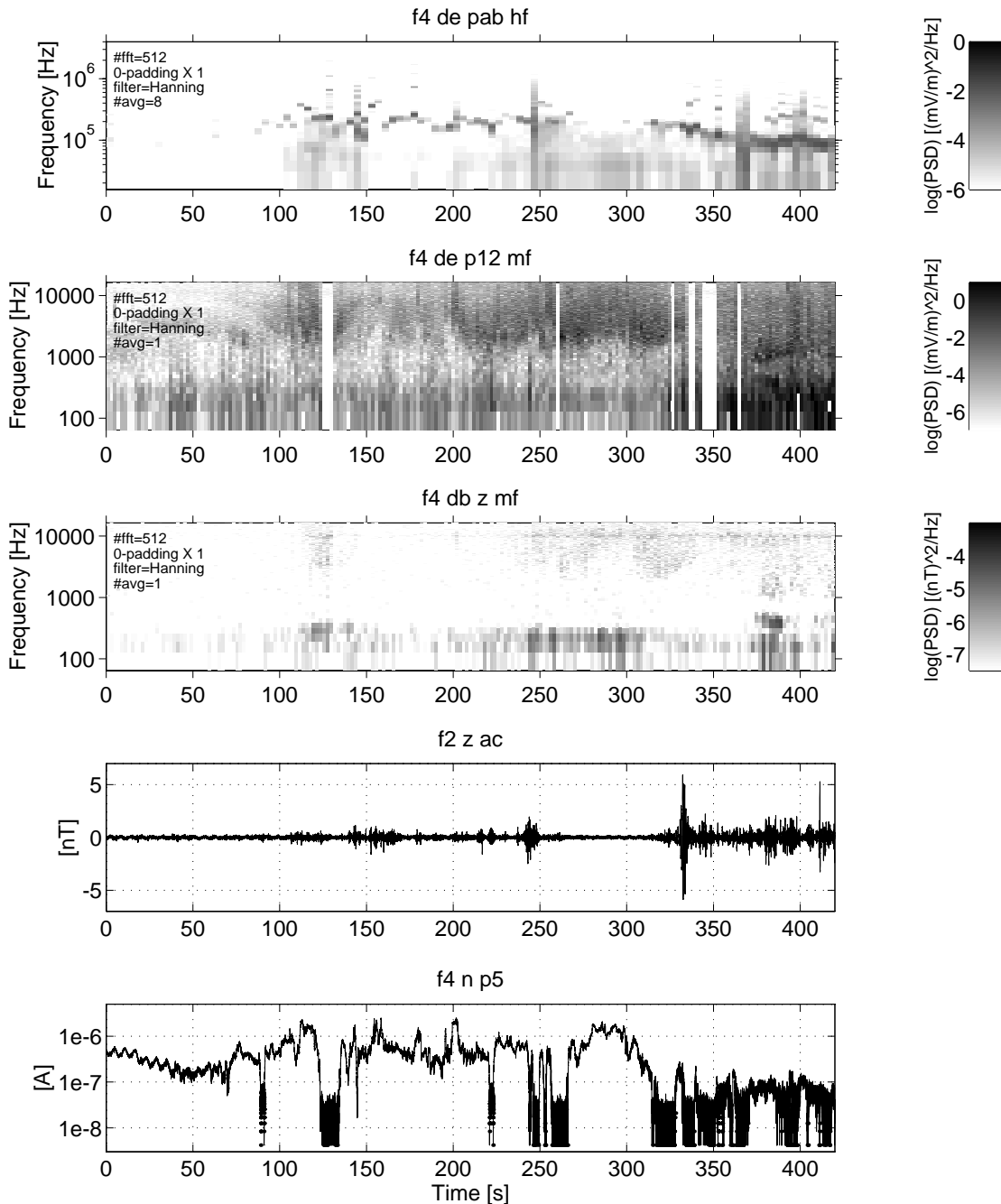


Figure 5.1.3a: The narrow-band HF emissions (panel 1) can be used for plasma density estimation. The Langmuir probe current drops to 10^{-8} A when negative charging occurs (i.e. when no thermal electrons reach the probe, +130 s, +250 s, and +320 s). A similar drop in LP current occurs after +350 s, which is matched by a corresponding decrease in frequency of the HF narrow-band emission and thus is interpreted instead as a real decrease in plasma density. Disturbances in the MF electric field measurements can be detected during charging.

Freja F4 Wave Data, Orbit: 487
Seconds fr. 1992 11 12 041500.000000 UT

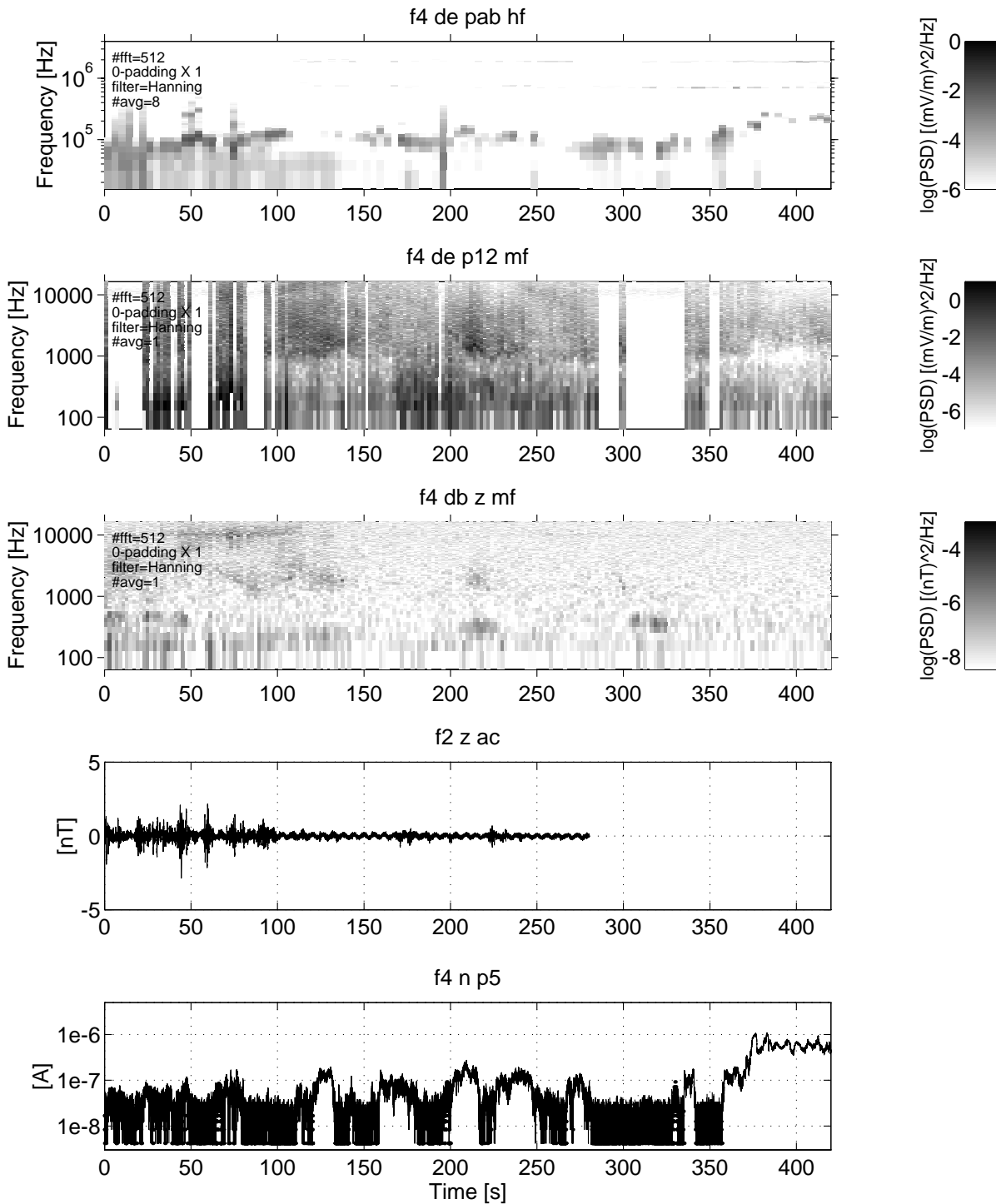


Figure 5.1.3b: Same as in Figure 5.1.3a, but for the second half period of 5.1.1. LP current drops during charging events, while the narrow-band HF emissions indicate a rather constant plasma density. Disturbances in the MF electric field measurements can be detected during charging.

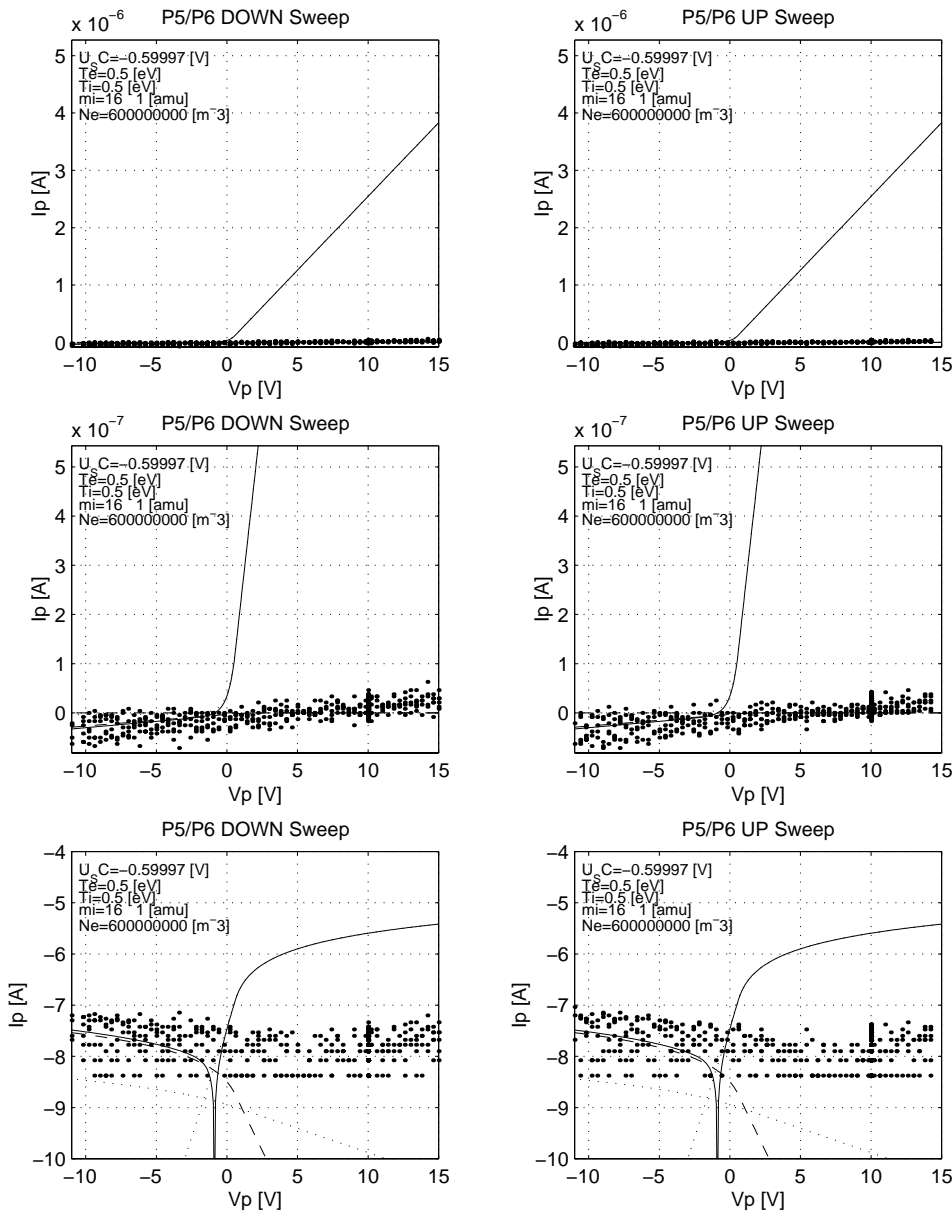


Figure 5.1.3c: A Langmuir sweep occurred at +330 s in Figure 5.1.3b during a charging event. The first two rows shows a linear scale, the last a logarithmic scale. As expected the electron current is absent in the measured sweep, and the sweep can be explained by the ion current alone (50% O^+ and H^+ each) assuming a density estimated from the HF narrowband emissions.

Detailed Case Near 0413:40 UT (TICS, MATE):

Detailed MATE spectra with 6 s resolution around the highest attained charging level are shown in Figure 5.1.4. The first panel corresponds to the maximum in the charging event. It is clear that rather large fluxes of high energy electrons occurs during charging (panel 1). Energy fluxes above $1 \cdot 10^6$ eV/cm²-eV-s-str are detected below an energy of 100 keV, and the energy fluxes were enhanced by at least an order of magnitude in the energy range 5-30 keV. The first data point (outside plot) and the last three data points (one outside plot) are uncertain, and may be influenced by instrumental effects. The one count level is indicated well below the measured electron spectra.

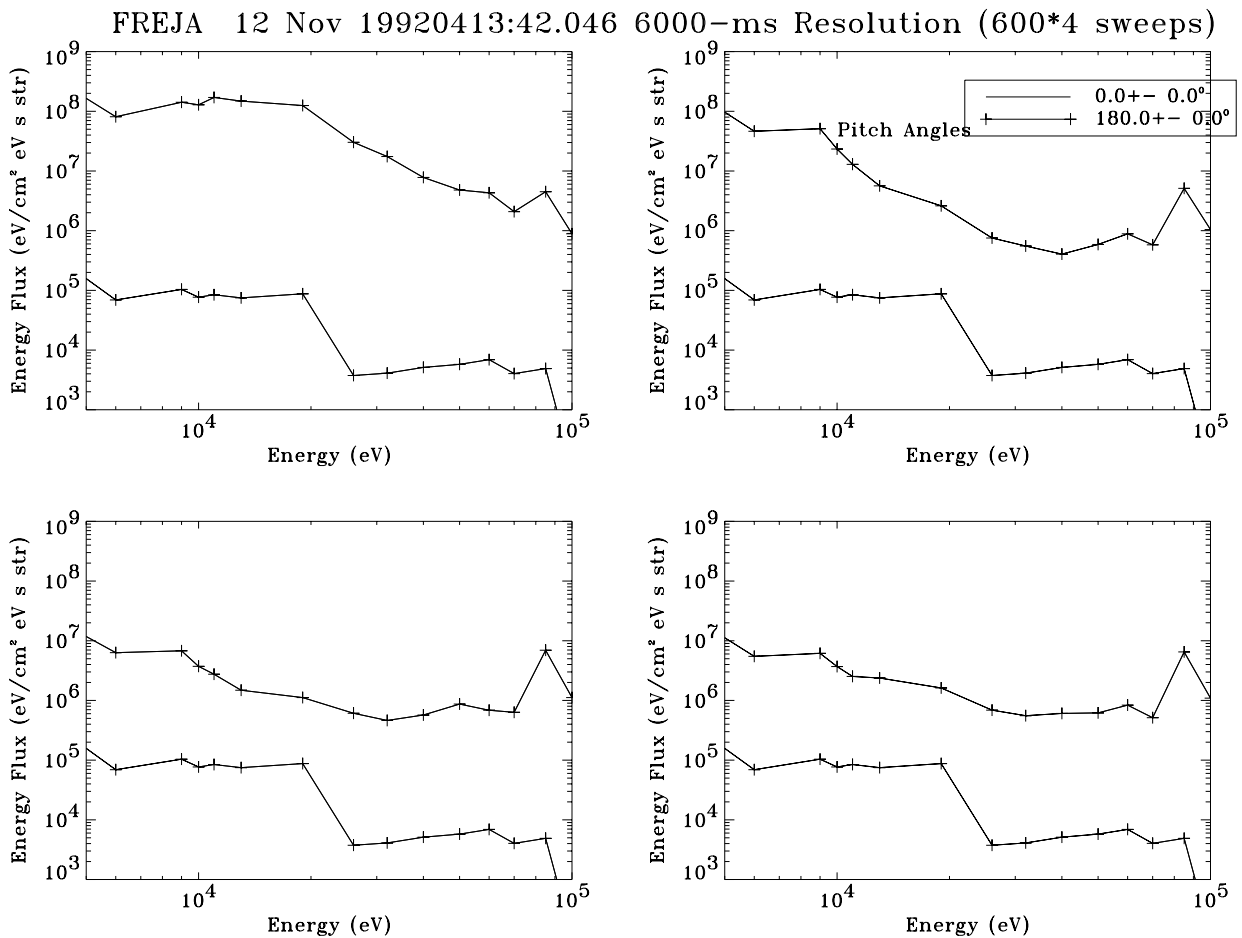


Figure 5.1.4: Electron spectra from the MATE instrument. The lower curve is the one count level. The first panel occurs during maximum charging, and large electron fluxes can be detected near the inverted-V peak (around 15 keV) as well as at larger energies.

Detailed ion distributions are displayed in Figures 5.1.5a to 5.1.5c. Figure 5.1.5a occurs within the charging event preceding the time of the highest reached charging level shown in Figure 5.1.5b (panels 2 and 3), while a typical ion conic due to transverse ion heating follows in Figure 5.1.5c. Charging events, in contrast to ion conic distributions, are characterised by an uplifted ion distribution at all pitch-angles. The charging level as read from panel 2 in Figure 5.1.5b is about -250 V. There are also enhanced fluxes below the main uplifted ion distribution, which may be due to either

- high energy electrons in the MeV range penetrating into the ion detector, or to
- uplifted ion distributions at different charging levels within the 2.8 s integration period.

FREJA 12 Nov 19920413:13.750 2800-ms Resolution Energy Flu

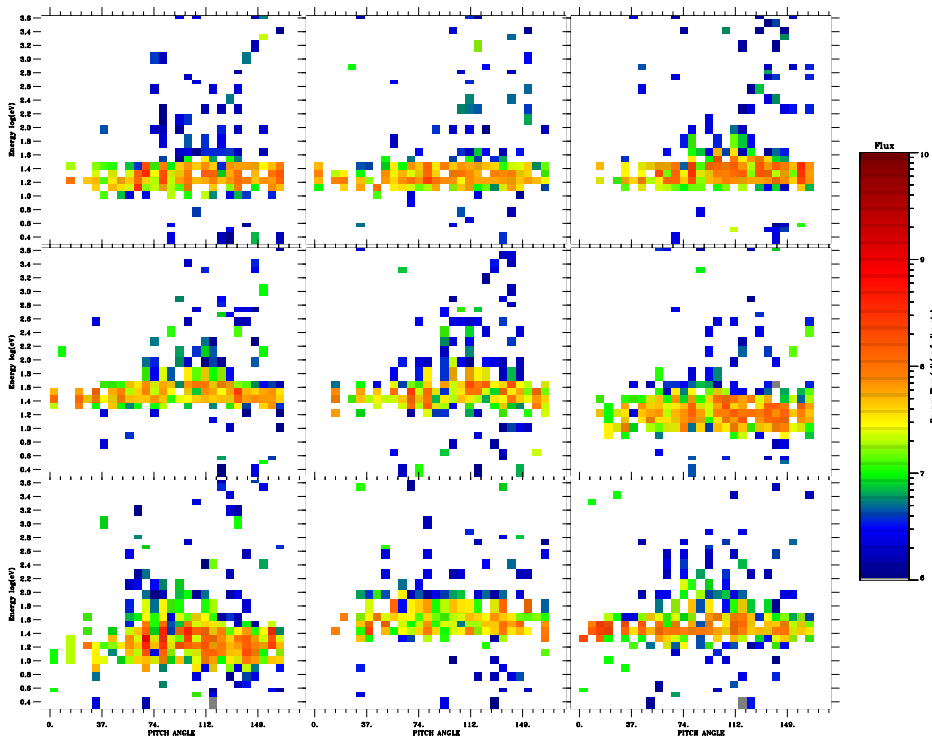


Figure 5.1.5a: The O^+ energy - pitch-angle distribution during a typical charging event. The ion population is lifted in energy at all pitch-angles simultaneously (i.e. the ions are accelerated toward the spacecraft from all angles). The charging is about -30 V.

FREJA 12 Nov 19920413:38.951 2800-ms Resolution Energy Flu

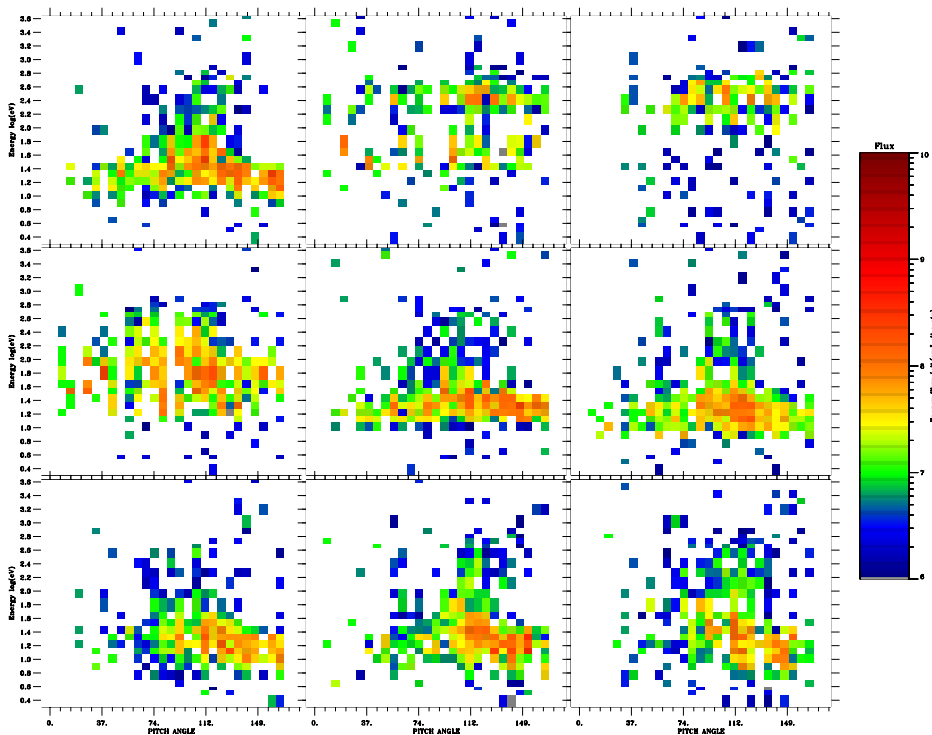


Figure 5.1.5b: The O^+ distribution during maximum charging on orbit 487. Charging levels around -250 V can be detected in the second panel.

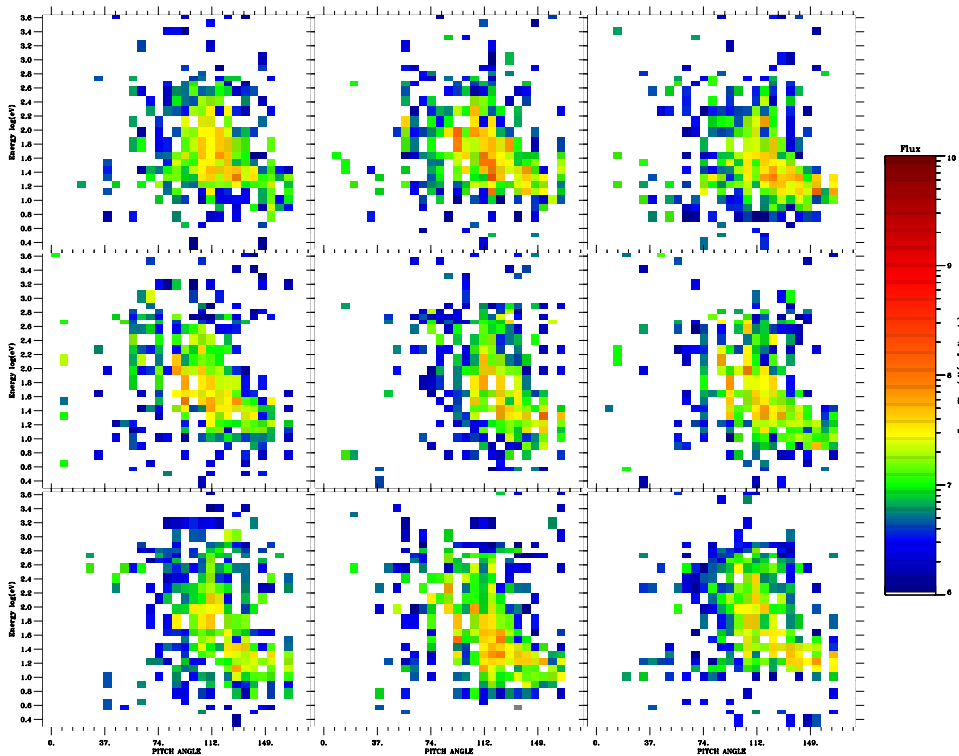


Figure 5.1.5c: A different O^+ distribution appears when auroral transverse ion heating occurs, as compared to when spacecraft charging occurs (compare Figure 5.1.5a).

Conclusions regarding orbit 487:

- The thermal plasma density did not change significantly during the charging events as compared to the surrounding plasma environment (which differs from the DMSP results).
- There was an almost one-to-one correlation between charging events and energetic electron flux (as well as energy) increases. Even the low level charging events of a few volts negative were associated with the presence of energetic electrons.
- There was at least one order of magnitude increase in the electron flux in the energy range 5-30 keV during the most extreme charging event up to -250 V.
- Clear measurement disturbances were observed in the Langmuir probe and the LF and MF plasma wave measurements, as well as in the TICS data.

5.2 EVENT 2: ORBIT 542 (TYPICAL CHARGING)

Overview Data, 92.11.16, Prince Albert:

The overview particle data are presented in Figure 5.2.1. Two periods of uplifted ion events exist during this orbit at 0809:00 - 0814:00 UT, and 0819:00 - 0824:00 UT (panels 1-3). Both periods are associated with high energy electron precipitation with peaks around a few keV and reaching up to 100 keV (panel 5). Both the events occur during eclipse (panel 4, thick line). The ion and electron spectrograms for these charging event periods are presented in Figure 5.2.2a and 5.2.2b, and the plasma wave data are presented in Figure 5.2.3a and 5.2.3b.

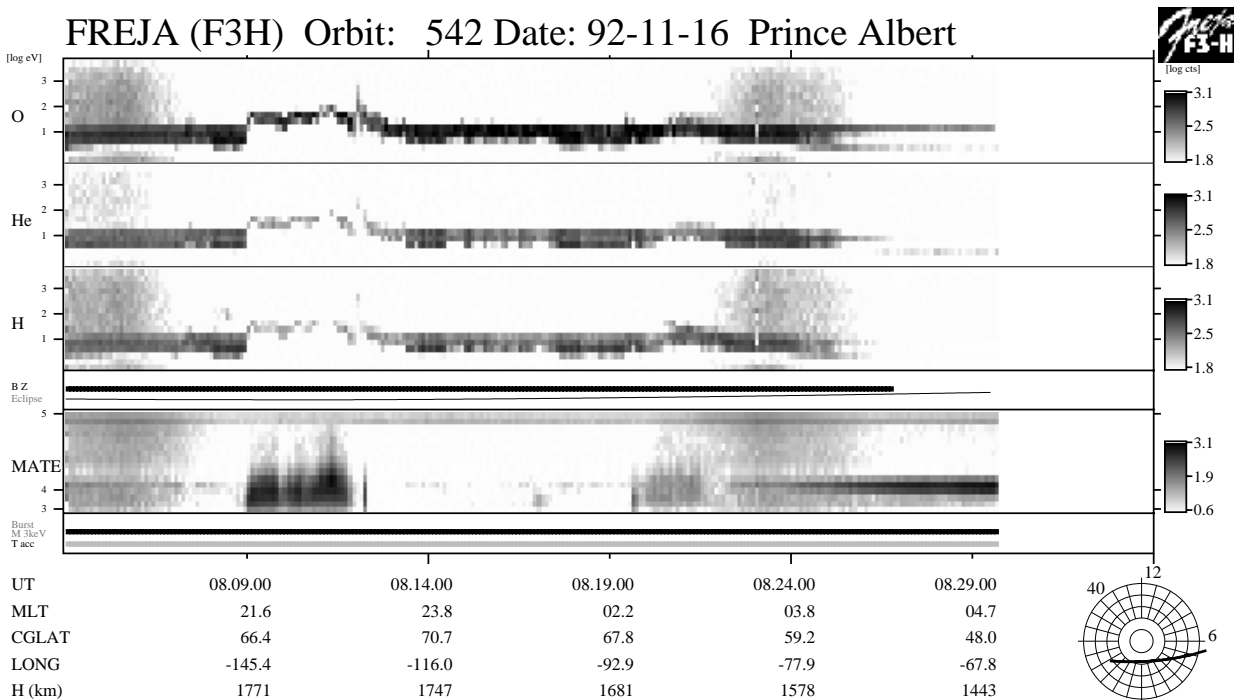


Figure 5.2.1: Overview particle data from orbit 542. High-energy (up to 80 keV) electron events (panel 5) occurs in eclipse (panel 4) near 0811:00 UT and near 0821:00 UT. They are associated with “uplifted” in energy ion populations (panels 1 - 3, O^+ , He^+ , and H^+ respectively), which is characteristic for spacecraft charging.

First Event:

The charging potential as estimated from the uplifted ion populations for the first period (panels 1-3, Figure 5.2.2a) varies between -30 V to -100 V. The maximum peak ion energy around 100 eV is obtained near 0811:20 UT, and the short lived event near 0812:10 UT reaches similar energy levels. There is a short lived ion heating event in between. The intensity of the high energy electrons (MATE, panel 5, Figure 5.2.2a) correlates rather well with the amount of ion acceleration toward the spacecraft (TICS detector) for these events. However, the small uplift in ion energy of up to 10 eV after 0812:10 UT does not show any associated high energy electrons.

The period when the CYLP collects almost zero current (Figure 5.2.3a, panel 5) corresponds best with the time period of uplifted ions. The HF emissions (panel 1, Figure 5.2.3a) indicate cold

plasma densities between $2\text{-}6\cdot 10^8\text{ m}^{-3}$, and the CYLP current, outside the times when it has anomalously dropped, corresponds to cold plasma densities between $4\text{-}8\cdot 10^8\text{ m}^{-3}$ in agreement with the HF estimates. These low densities are rather unusual for cold plasma conditions encountered by Freja. We make the conclusion that the times when the CYLP current drop are due to spacecraft charging, but that the period after 0812:10 UT lacks the simultaneous occurrence of high energy electrons. Thus, spacecraft charging to low levels may occur without simultaneous intense energetic electron fluxes. One possible explanation for this behaviour is that Freja enters a region with large electron temperature and rather low density, causing the CYLP current to become small (which is then proportional to $n_e/\sqrt{T_e}$), while the density still corresponds to plasma densities in agreement with the HF emissions. A large negative equilibrium potential of about -10 V can be maintained by the large electron temperature. Unfortunately no information exist for the electron temperature during this time, but an electron temperature of only $2\text{-}3\text{ eV}$ would be able to cause the desired effect, perhaps produced from various plasma instability processes near auroral arcs. However, since no supporting data exist that could verify this hypothesis for the charging mechanism any further speculation is meaningless. Also, it is very seldom that low level charging above a few Volts is detected in the Freja data set without simultaneous energetic electron precipitation, and electrons above a few keV is for certain the most dominant source of Freja charging events.

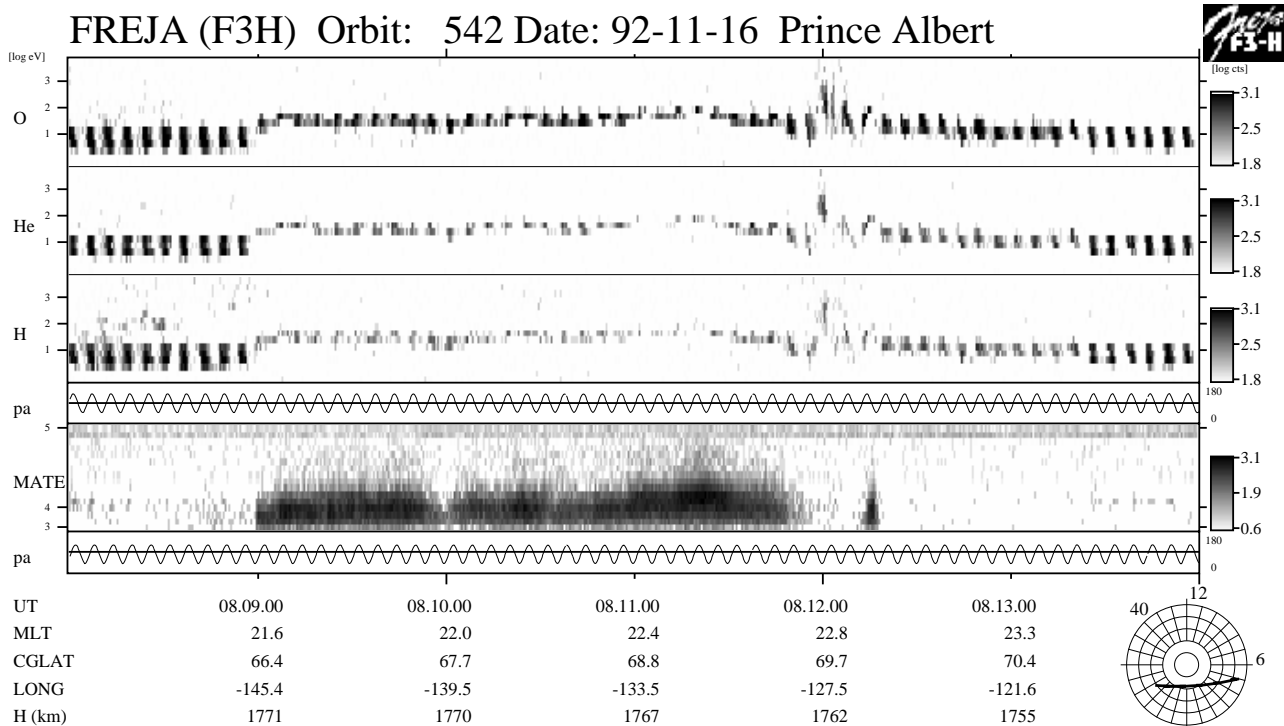


Figure 5.2.2a: Charging levels of -30 V to -100 V is reached during this typical eclipse charging event. The ion population stays lifted with about 10 eV energy after the event until 0813:30 UT, perhaps due to an electron temperature increase up to $2\text{-}3\text{ eV}$ of the thermal plasma.

Freja F4 Wave Data, Orbit: 542 Seconds fr. 1992 11 16 080800.000000 UT

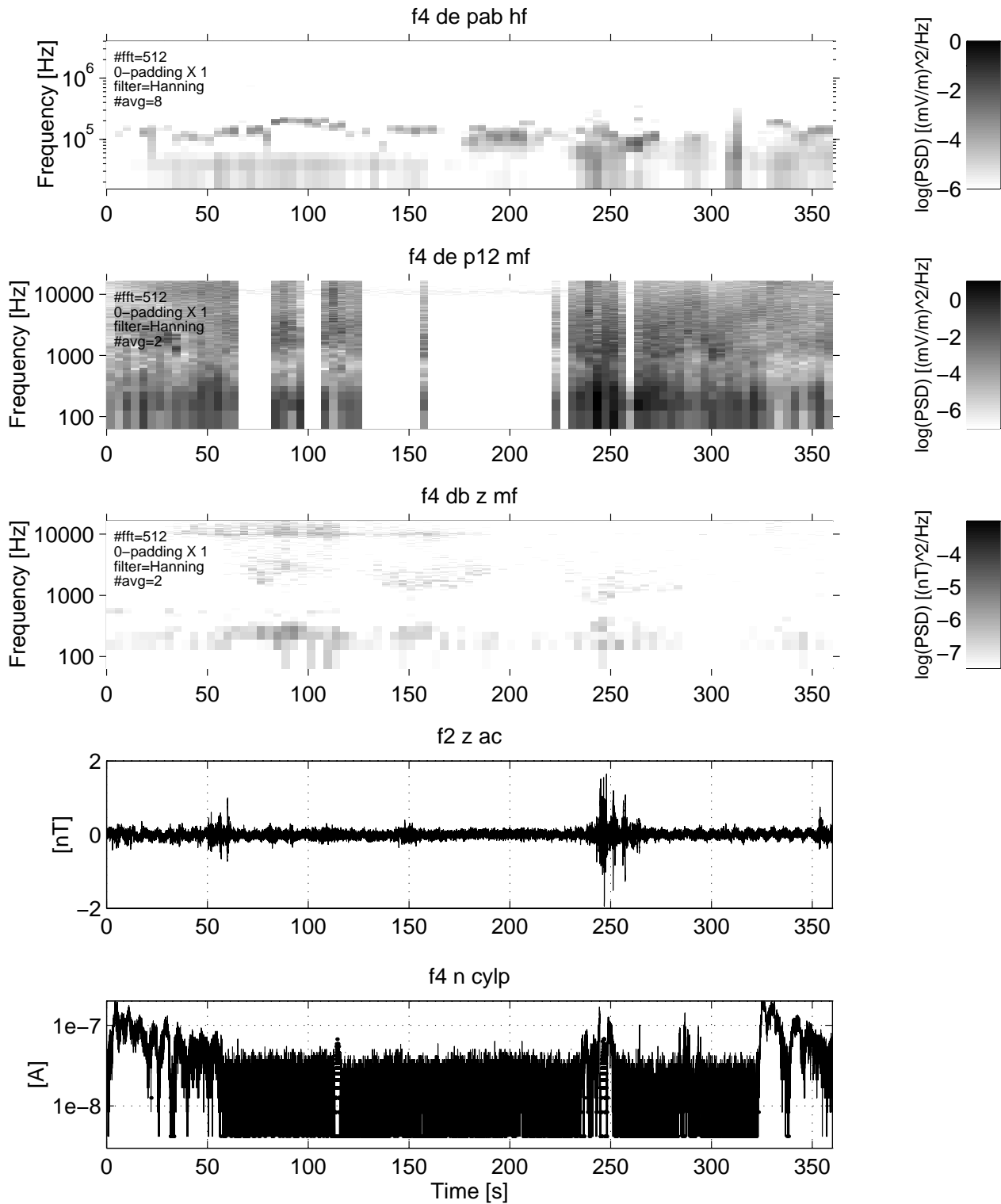


Figure 5.2.3a: The plasma density stays rather constant during this charging event (panel 5), while the LP current drops anomalously due to lack of thermal electrons and the MF electric field measurements more or less fails.

Details of First Charging Event:

Detailed 6 s average MATE spectra from the highest level charging around 0811:20 UT are displayed in Figure 5.2.4. Large electron fluxes are detected at high energy levels, and indications of an energetic tail exists in the energy range 20 - 80 keV above the main peak near 12 keV.

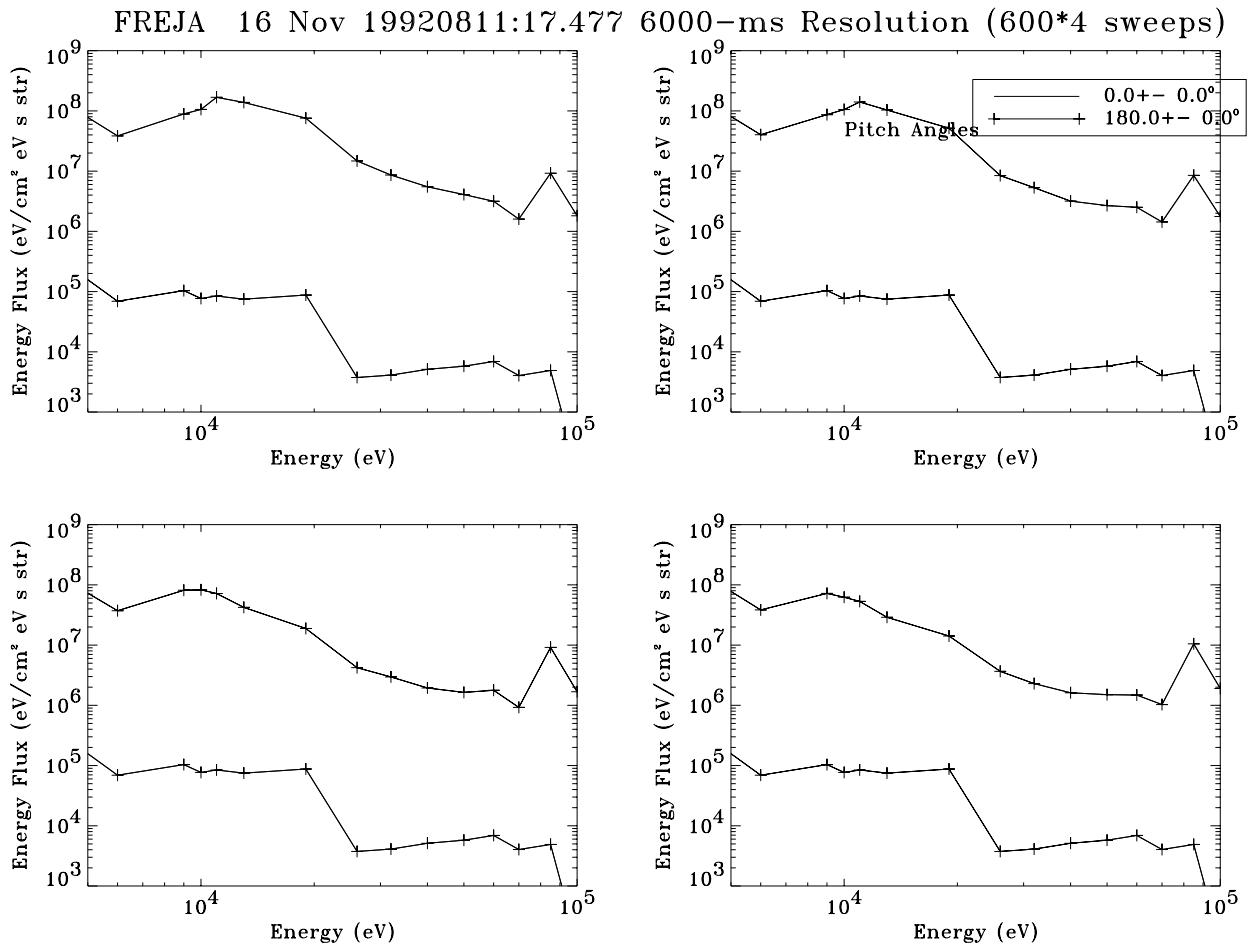


Figure 5.2.4: MATE electron spectra from the time period of highest negative charging during orbit 542. Large fluxes well above 10^6 eV/cm²-s-str-eV are detected at energies above the electron peak near 10 keV energy. The first point (outside plot and the two last points are not trustable).

The corresponding detailed ion distributions are shown in Figure 5.2.5, where clear uplifted ion distributions covering all pitch-angles due to spacecraft charging up to -100 V can be detected. At the beginning of the charging event near 0809:00 UT the ion distribution changes from the normal ram distribution to a typical charging distribution as shown in Figure 5.2.6. A charging distribution looks very much like a ring-distribution, and could of course be taken as such if it was the only information available.

FREJA 16 Nov 19920811:16.507 2800-ms Resolution Energy Flu

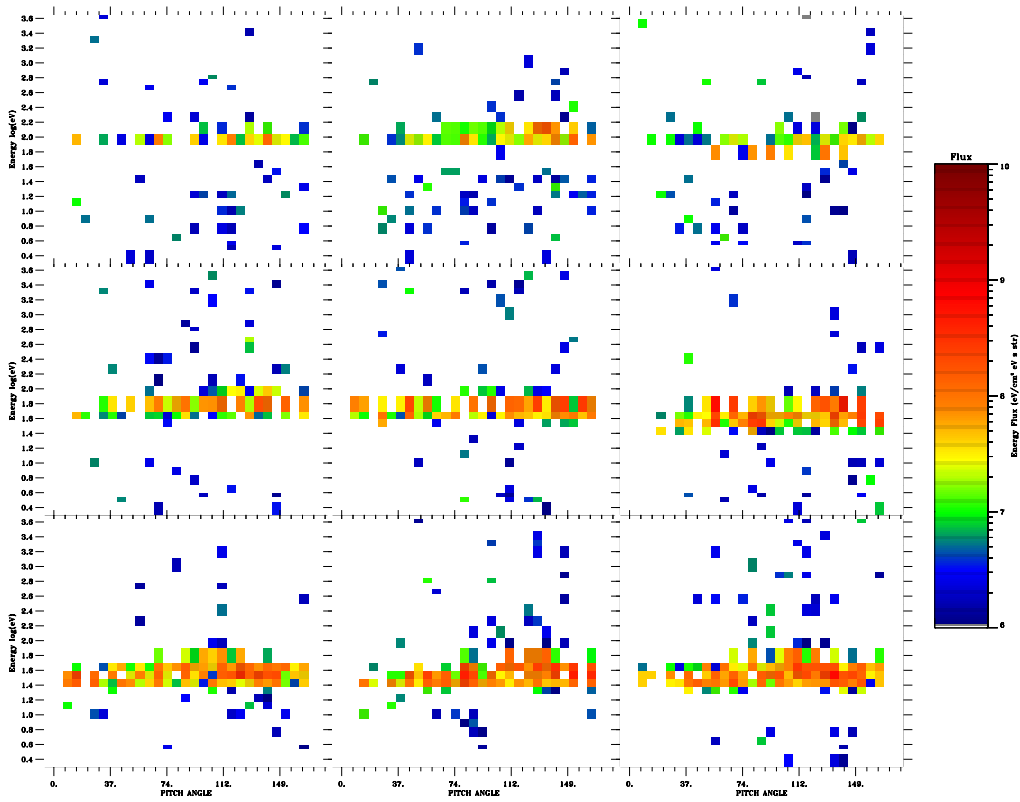


Figure 5.2.5: The O^+ distribution functions reveal the typical charging distribution with ion acceleration toward the spacecraft from all pitch-angles. Charging levels of about -100 V can be inferred.

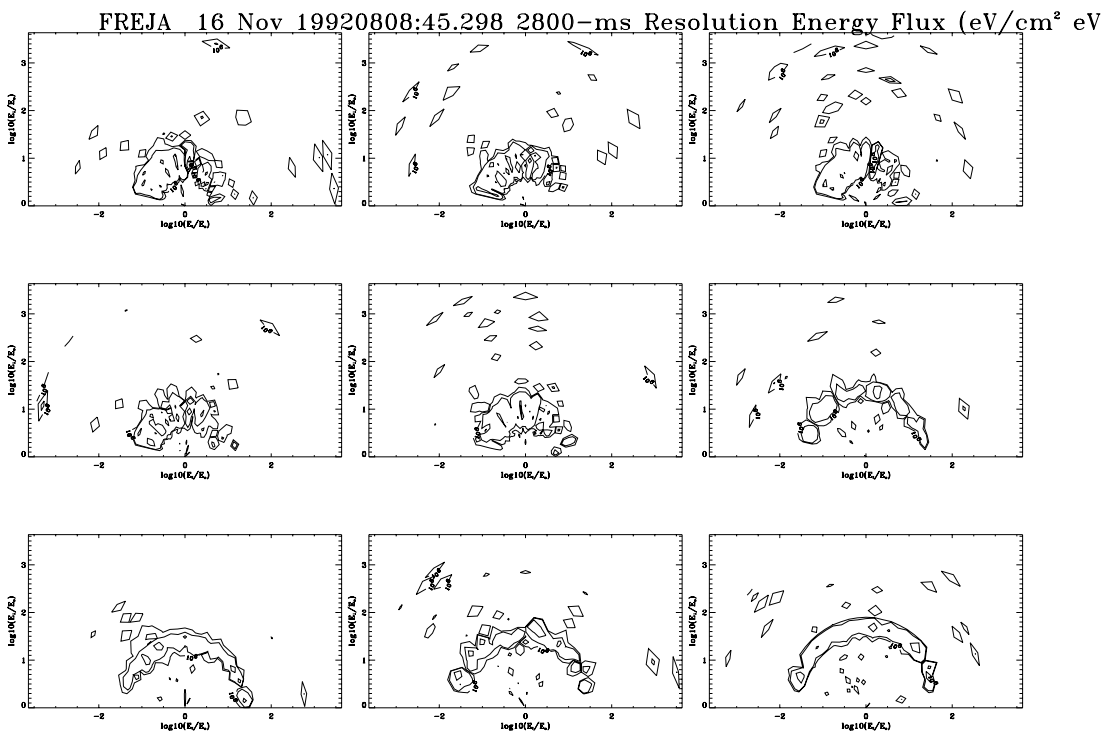


Figure 5.2.6: The usual ram distribution due to the spacecraft velocity (panels 1 - 5) is evolving toward a ring-like distribution typical for spacecraft charging.

Second Event:

The second period (Figure 5.2.2b and 5.2.3b) is characterised by three periods of possible spacecraft charging, near 0817:00 UT, near 0819:40 UT, and the period after 0820:20 UT. The two first periods are associated with CYLP current drops (Figure 5.2.3b, panel 5) below the density level indicated by the HF emissions (panel 1). The density near +50 s is about $3 \cdot 10^8 \text{ m}^{-3}$ as estimated from the narrow-band Langmuir emission, while the CYLP current at that time corresponds to a density of close to $5 \cdot 10^8 \text{ m}^{-3}$. This can be considered to be within the error limits, since the CYLP behaviour during the Freja mission is not well understood (modelled). The CYLP and HF measurements near +120 s give comparable plasma density estimates of about $1\text{-}2 \cdot 10^8 \text{ m}^{-3}$. Unfortunately, no estimates for the plasma density can be obtained from the HF measurements after +250 s (0820:20 UT), and it is therefore uncertain whether a true charging event occurs or not. The two first events are correlated with only weak high energy electron fluxes (Figure 5.2.2b, panel 5), while the last event indeed is associated with high energy electrons although the coincidence with the dropouts of the CYLP current and the energy uplift of the ions is not striking. It is interesting to note that electron flux enhancements below 10 keV (the two first cases) indeed seem to cause low level charging events. As in the first event on this orbit, a charging event appear to continue even if the high energy electron precipitation have ended. However, in this case the charging event continues into the radiation belt region with other types of high energy electrons present which make the cause of the charging more obscure.

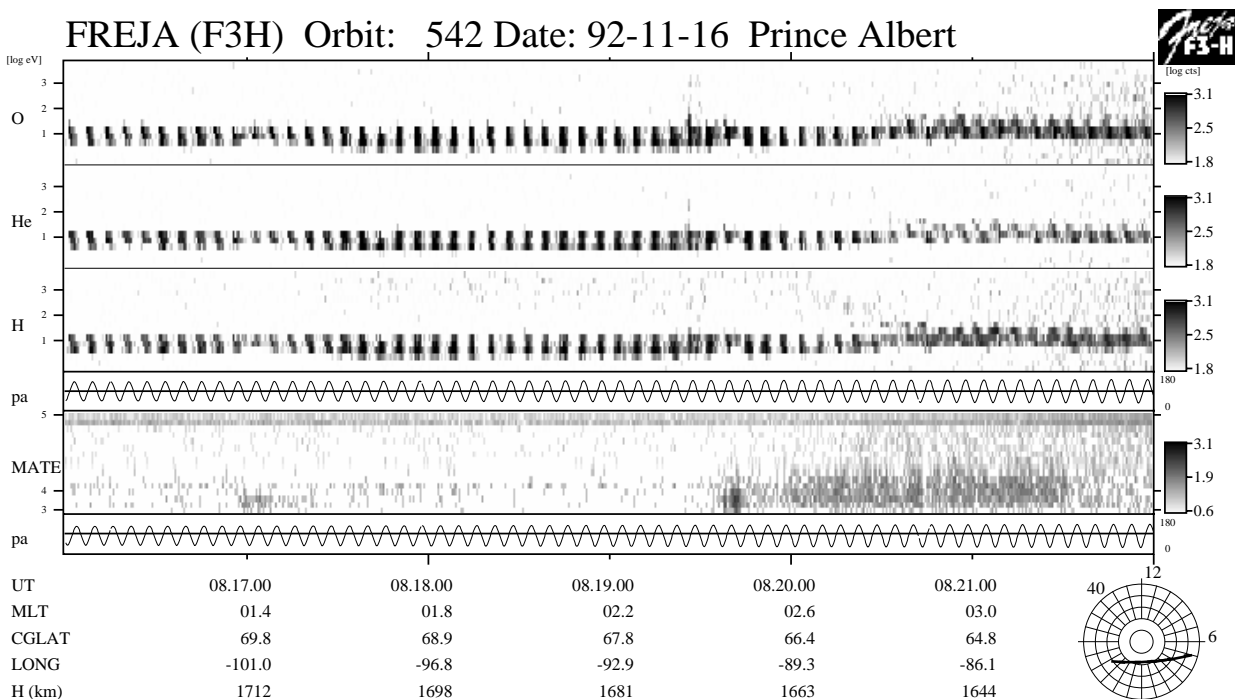


Figure 5.2.2b: Weak energetic electron fluxes (panel 5) are associated with this low level charging event near 0821:00 UT.

Freja F4 Wave Data, Orbit: 542 Seconds fr. 1992 11 16 081600.000000 UT

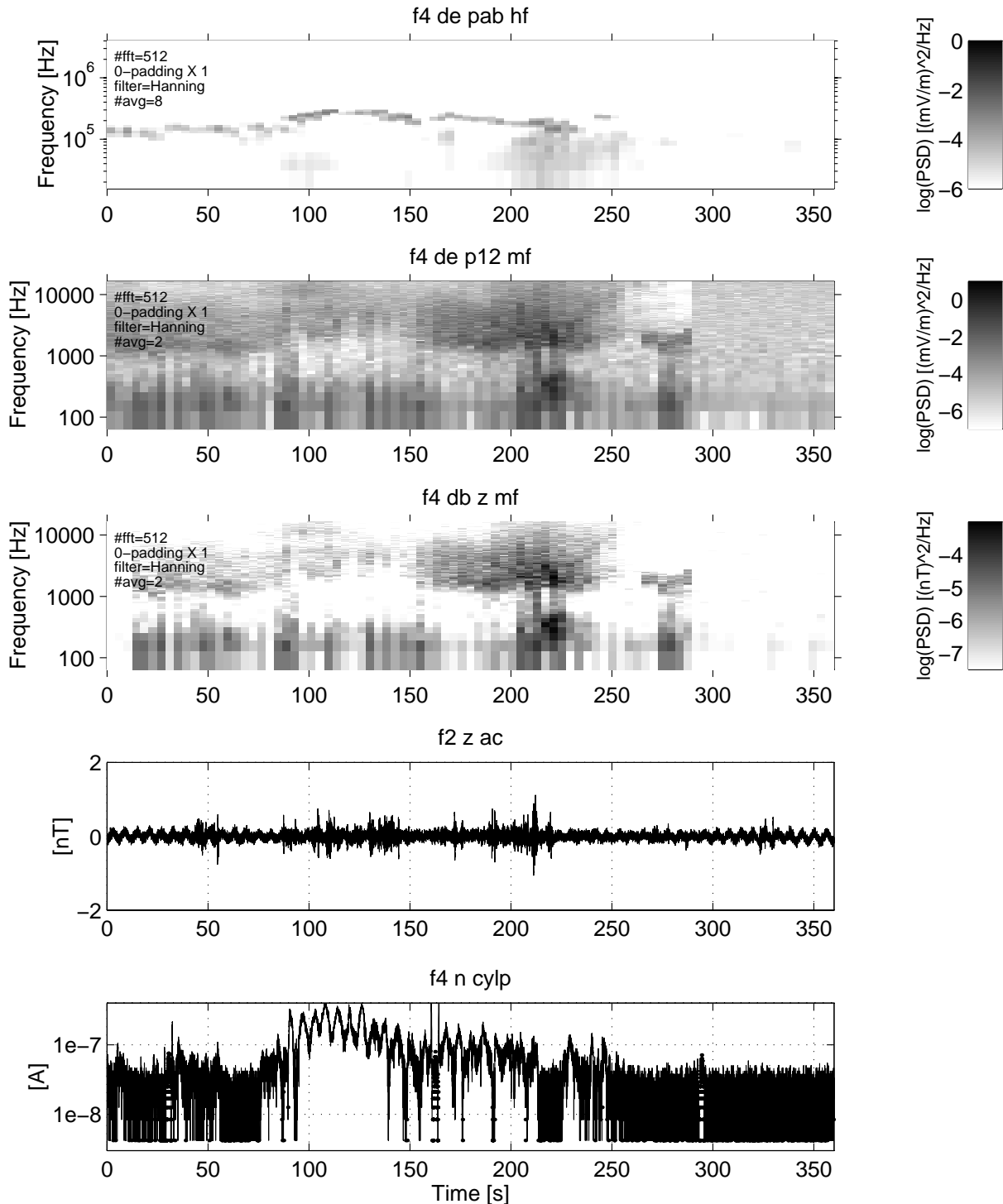


Figure 5.2.3b: Even the very low level charging events near +60 s and +220 s give as significant LP current drops (compare with Figure 5.2.2b) as the larger scale charging event after +250 s. Unfortunately the narrow-band HF emissions (panel 1) disappear after +250 s, and the plasma density is therefore unknown after that time.

Conclusions from orbit 542:

- The dominant source for charging of the Freja spacecraft appears to be intense electron fluxes in the energy range 5 - 80 keV. A high energy tail in the energy range 20-80 keV existed during the highest charging levels (around -100 V).
- Low level charging were detected when enhanced electron fluxes below an energy of 10 keV occurred. This is an important result, since Freja is to the largest extent covered with ITOC that has a crossover energy (secondary yield = 1) of 2.5 - 3 keV, and the second most common surface material is a thermal blanket with a crossover energy of just under 4 keV. Thus, the high-energy tail (10 – 80 keV) is not necessary for charging in these observed cases.
- Low level charging events that were not caused by energetic electron precipitation were detected. These charging events may be explained by a large electron temperature (2-3 eV) of the thermal plasma.
- Even if the plasma densities are unusually low for typical Freja conditions, there is no detection of sudden drops in density when the charging events started to occur as was suggested from the DMSP measurements.
- There are instrument disturbances due to the charging events in the Langmuir probe, MF and LF electric, and the TICS measurements.

5.3 EVENT 3: ORBIT 790 (TYPICAL CHARGING, SUNSET CASE)

Overview data, 92.12.05, Prince Albert

Orbit 790 is famous in the Freja scientific community, since a well developed auroral substorm passed during this orbit, and several papers have been written about this substorm. However, no-one have addressed the charging event that seems to exist in the middle of the auroral activity and transverse ion heating. Figure 5.3.1 display the overview particle data. Between 0233:00 UT and 0243:00 UT a large auroral disturbance occurs with large fluxes of high energy electrons as measured by both the TESP instrument (panel 7) and the MATE instrument (panel 5). The ion population is uplifted in energy in the time interval 0234:00 - 0239:00 UT. Most of this particular time interval occurs during sunlight conditions (panel 4), and only the later part of the event is in eclipse. The eclipse is, of course, more gradual than the sharp time indicated in panel 4, and the whole uplifted ion event can be considered to occur during terminator conditions with a more smooth transition from sunlight to darkness as more and more of the Earth's atmosphere inhibit the solar radiation. The two Freja photometers were unfortunately not available during this event. The first part of the auroral event between 0233:00 - 0236:00 UT is most probably due to transverse ion heating, since no dropout exist in the LP current during these times. The later part is presented in more detail in Figure 5.3.2 and 5.3.3.

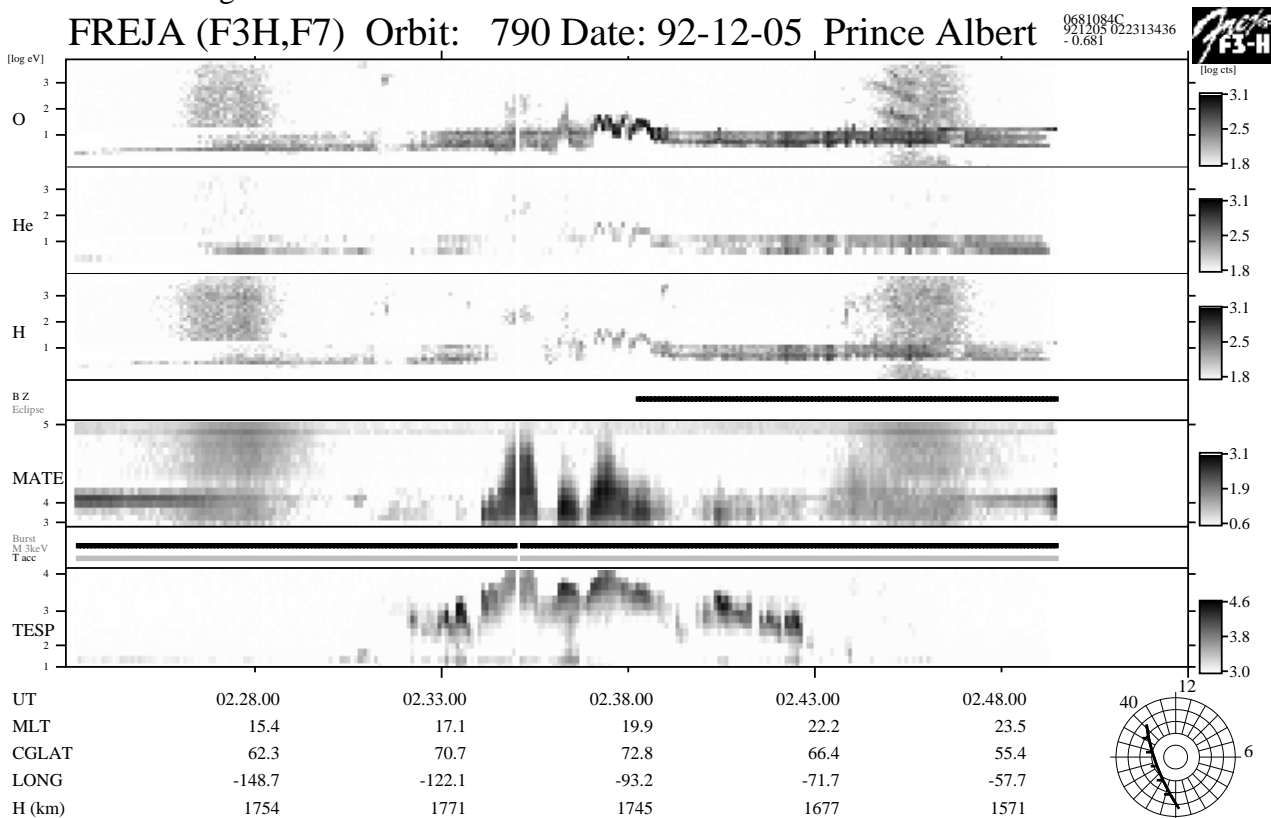


Figure 5.3.1: Overview particle data from orbit 790. Both MATE (panel 5) and TESP (panel 7) electron data existed when a full scale auroral substorm passed. A charging event occurred during this substorm around 0238:00 UT near the terminator (as seen in panel 4).

The estimated density from the HF narrow-band emissions (Figure 5.3.3, panel 1) is rather constant for the whole displayed interval and attains values close to $1.2\text{-}2.8 \cdot 10^8 \text{ m}^{-3}$, while the CYLP current (panel 5) occasionally drops to very low values. Spacecraft charging is therefore suggested during those current drops. The ions are uplifted in energy to almost 100 eV (Figure 5.3.2, panels 1-3) during the CYLP current dropouts, and enhanced fluxes of high energy electrons (panels 5 and 7) correlates well in both flux intensity and maximum energy attained for these periods. We interpret these results that the electron flux and peak energy are major factors determining the charging level for a given plasma density.

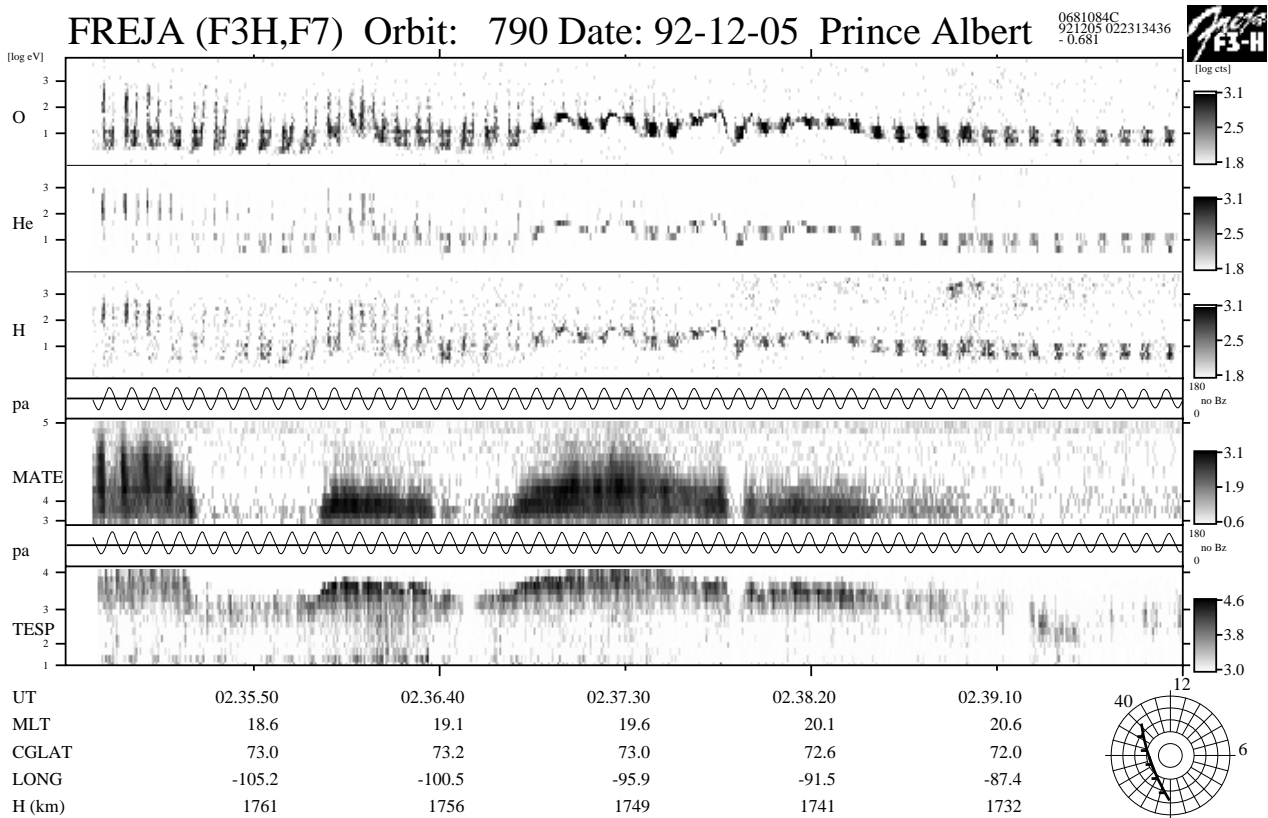


Figure 5.3.2: An enlargement of the data in Figure 5.3.1 around the charging period. Transverse ion heating related to the auroral substorm can be detected before 0237:00 UT.

Freja F4 Wave Data, Orbit: 790 Seconds fr. 1992 12 05 023500.000000 UT

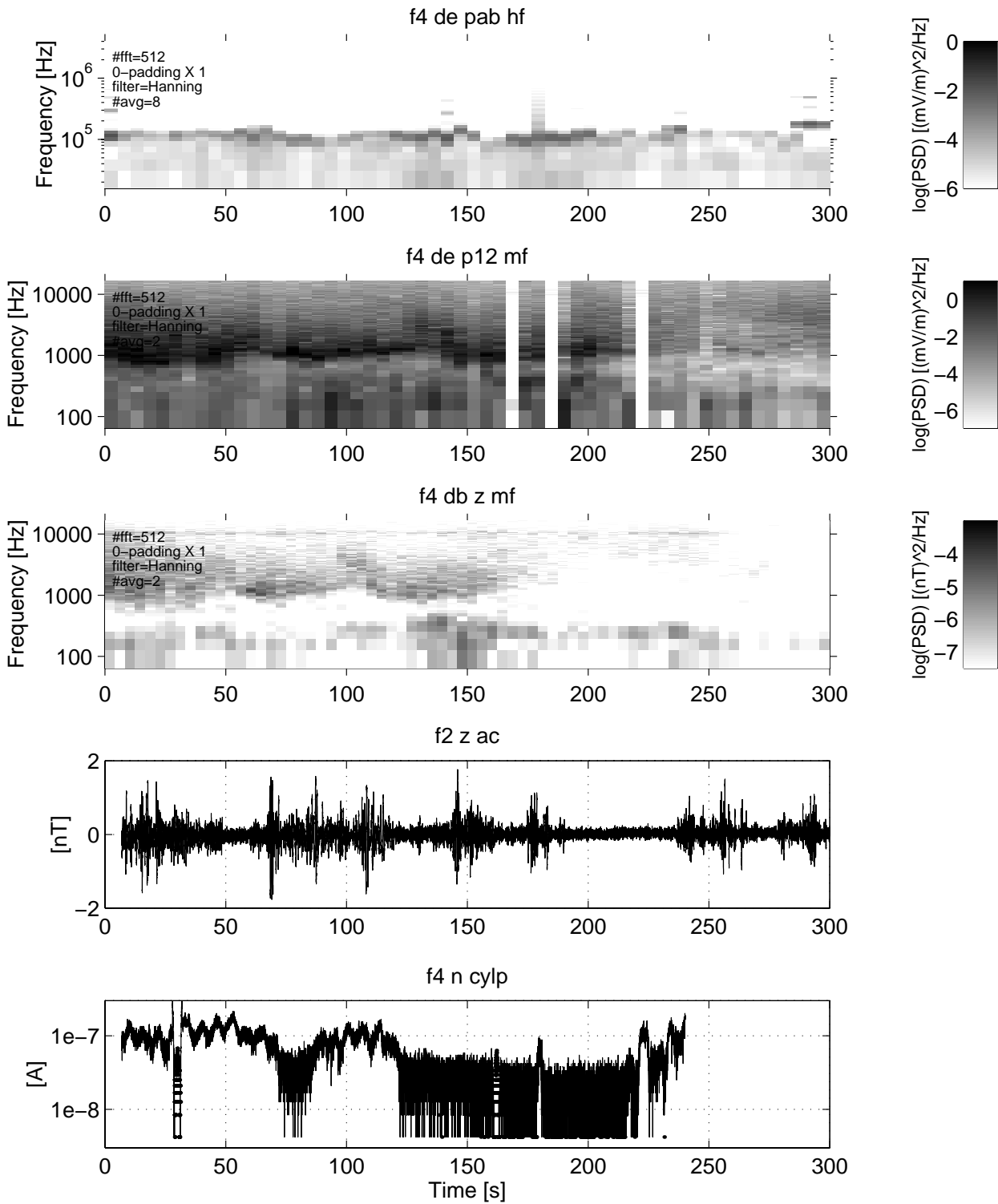


Figure 5.3.3: Narrow-band Langmuir emissions (panel 1) indicate an almost constant plasma density during the charging event. The periods of charging is inferred from the sudden drops in the sampled LP current near +80 s and around 170 s.

Detailed Distributions Around 0237:30 UT:

A series of TESP and MATE particle flux spectra are presented in Figures 5.3.4a - 5.3.4c and 5.3.5a - 5.3.5d respectively, which together covers the time period 0236:40 - 0238:10 UT. Note how these spectra evolve with time when the charging event starts, reaches its maximum, and then relax. The maximum of the inverted-V peak reaches large energies up to 10 keV during maximum charging (Figure 5.3.4b, all panels; Figure 5.3.5b, all panels; Figure 5.3.5c, panels 3 and 4), where also the largest electron fluxes at these highest energies of a few keV occurs. The precipitating electron fluxes are close to isotropic and belongs to an auroral inverted-V event. Thus, during the charging event the maximum flux of energetic electrons at the peak moves above the crossover energies of ITOC (2.5-3 keV) and the thermal blanket (just below 4 keV). This suggests that the flux of the emitted secondary electrons cannot longer balance the incident energetic electron flux, and in this way cause the observed negative charging. Also, the flux levels in the high energy tail up to 60 keV increases with about an order of magnitude, which further contribute to the excess negative charge accumulation.

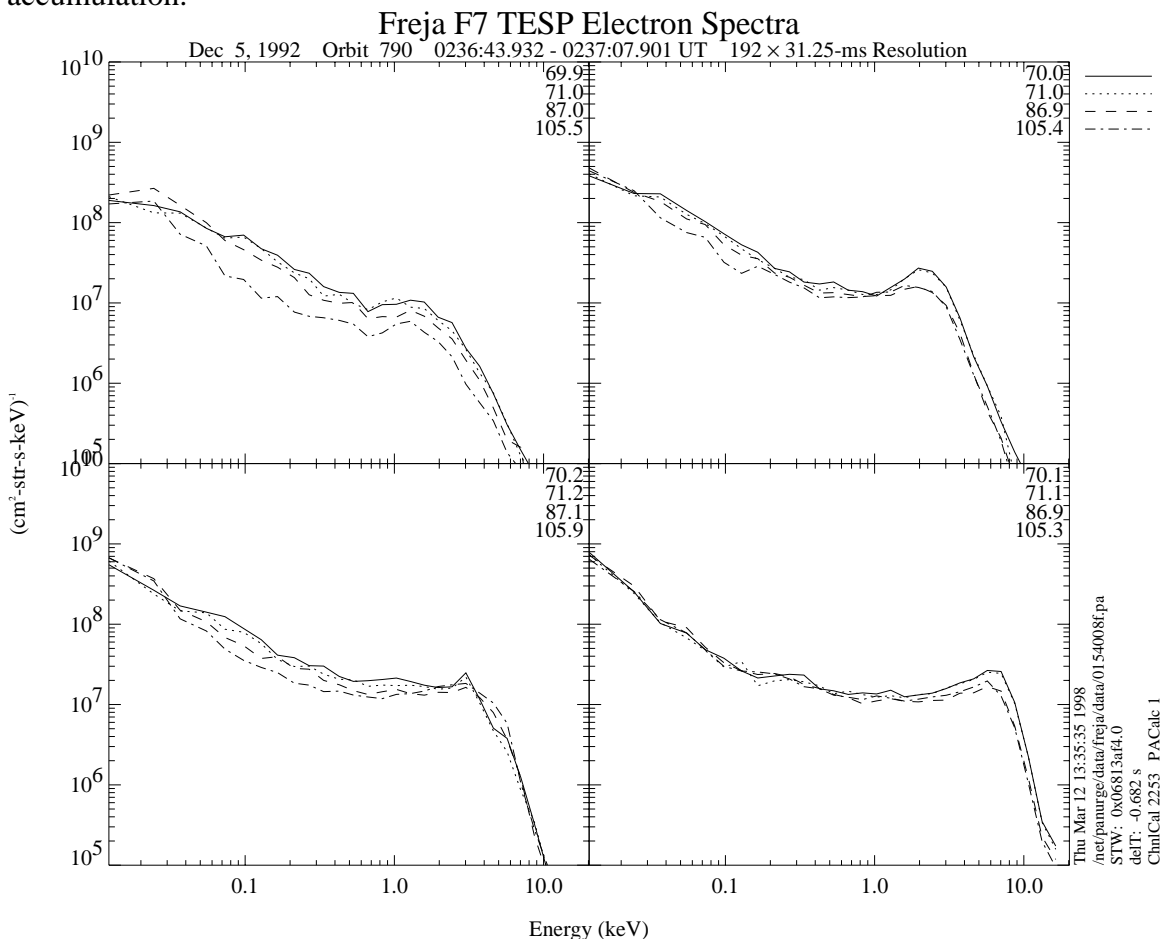


Figure 5.3.4a: The following three Figures with TESP data and four Figures with MATE data show the evolution of the electron spectra during the charging event. For the TESP measurements the charging start evolve in panels 2-3, to continue through Figure 5.3.4b, and start decline in panel 3-4 in Figure 5.3.4c. As soon as almost isotropic inverted-V peak reach above about 5 keV charging appears. Similarly, for the MATE data (Figure 5.3.5a-d) the charging event start in Figure 5.3.5b (panel 1) where the inverted-V peak reach 10 keV and continue to rise in energy (and flux) to panel 2-3 in Figure 5.3.5c, where after it declines in Figure 5.3.5d.

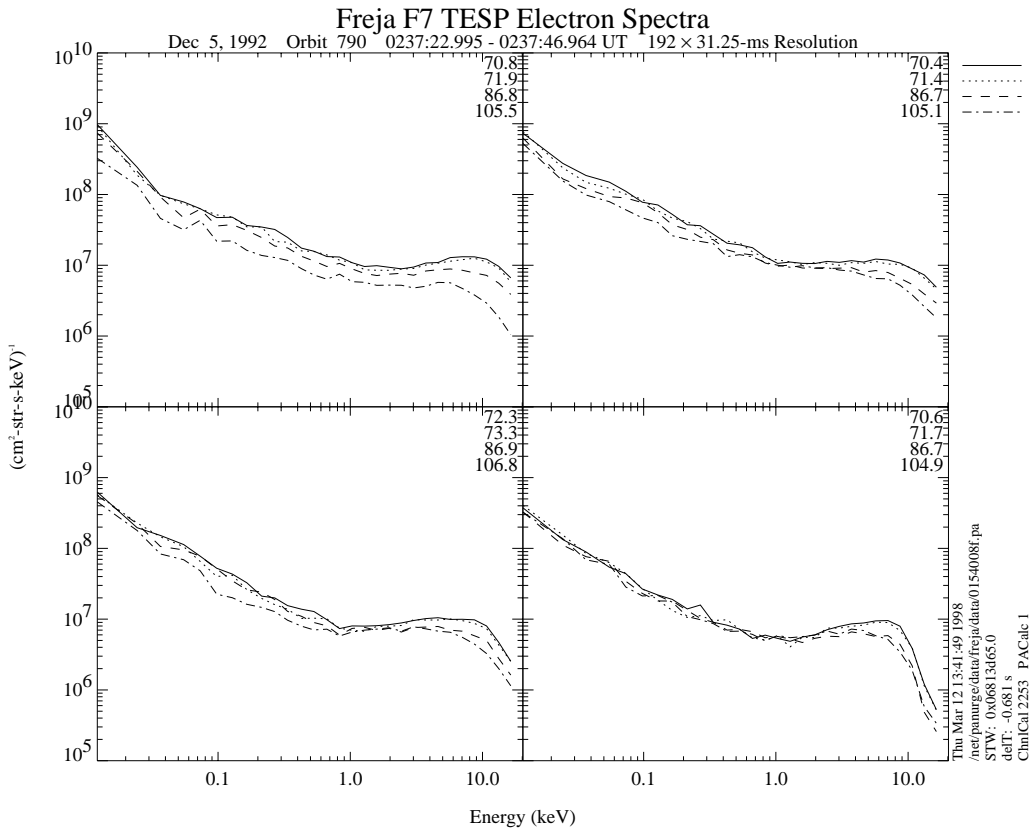


Figure 5.3.4b: See Figure 5.3.4a.

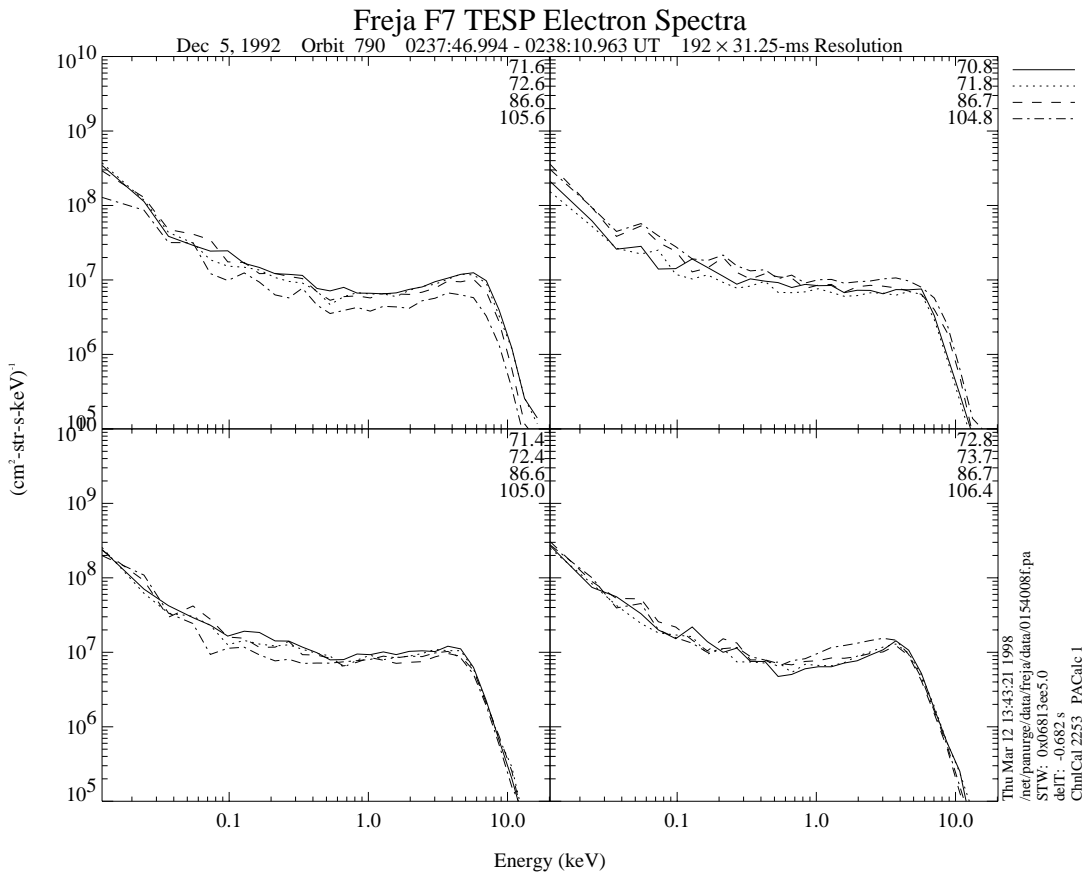


Figure 5.3.4c: See Figure 5.3.4a.

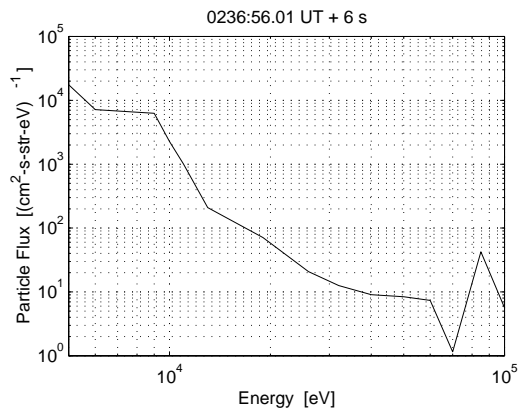
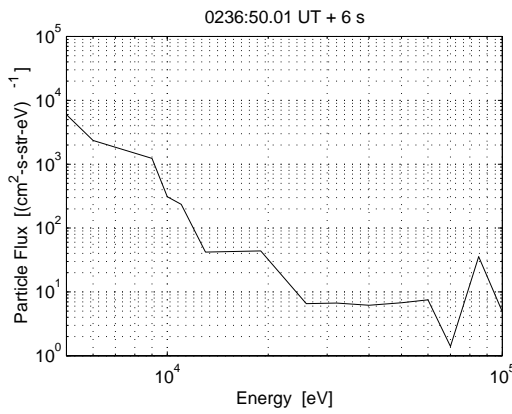
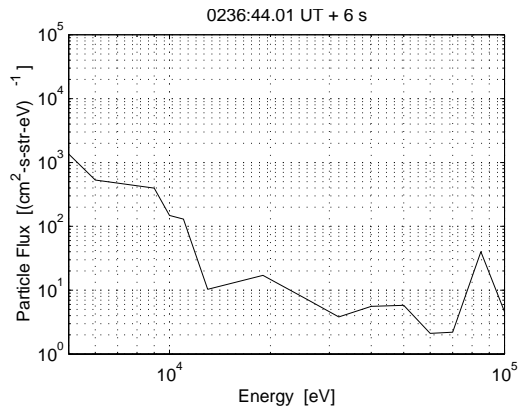
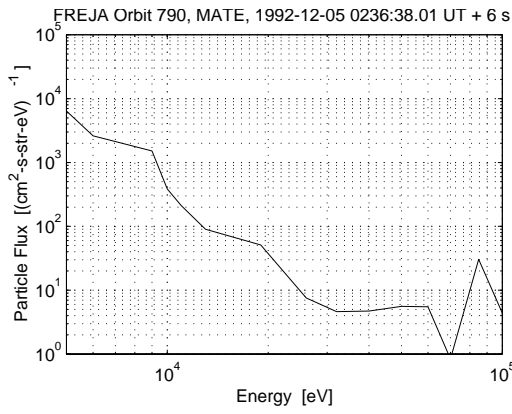


Figure 5.3.5a: MATE data. See Figure 5.3.4a.

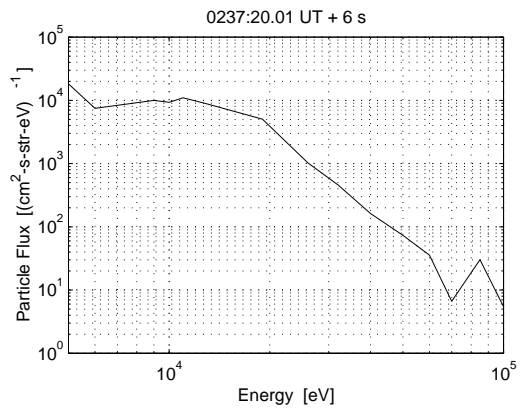
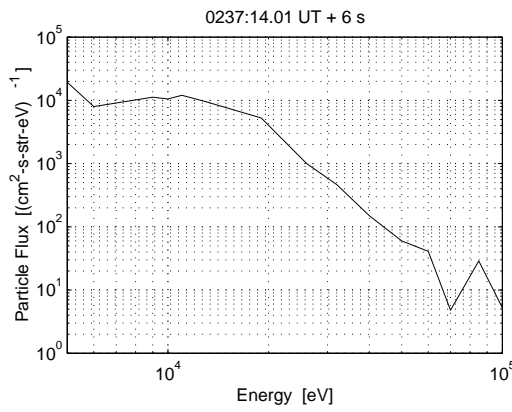
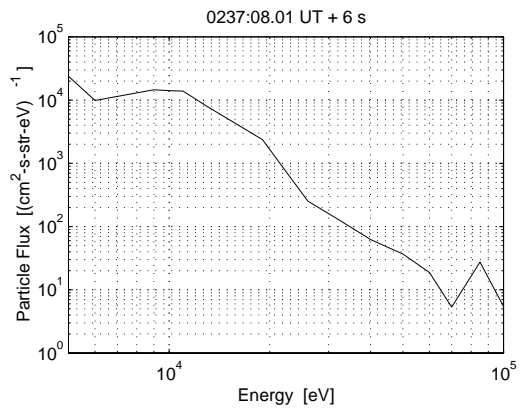
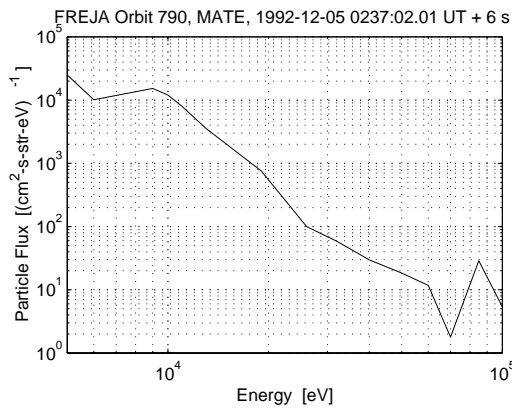


Figure 5.3.5b: MATE data. See Figure 5.3.4a.

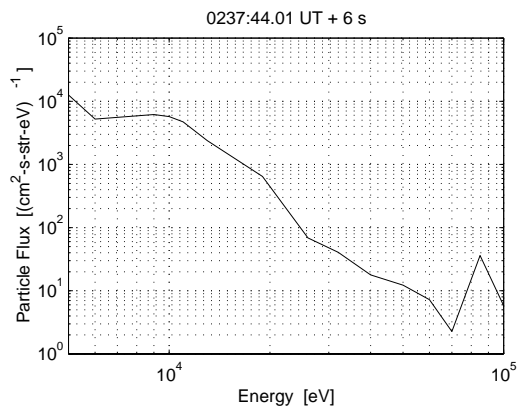
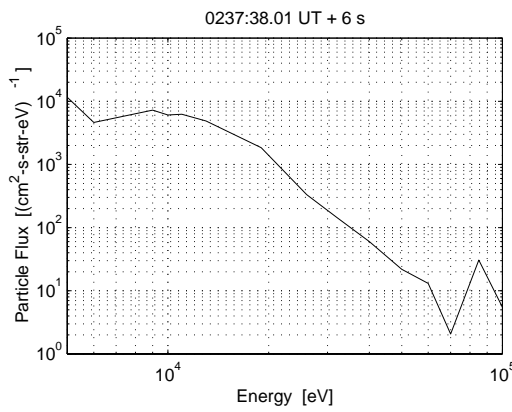
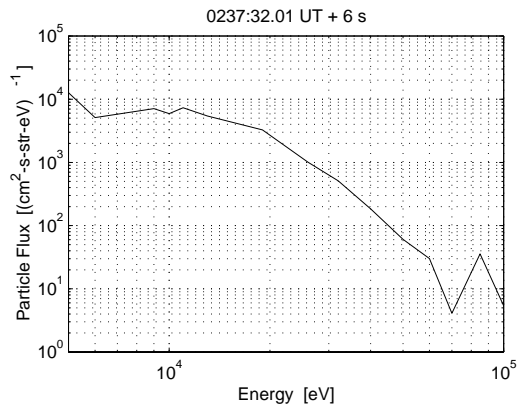
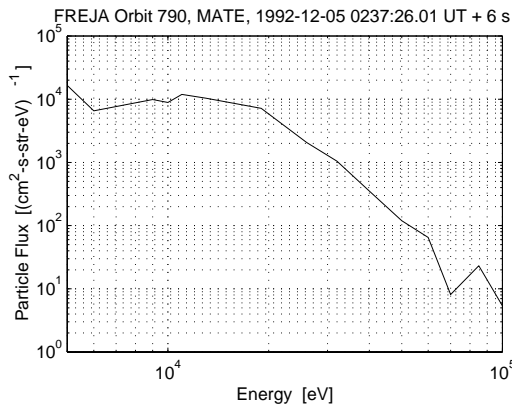


Figure 5.3.5c: MATE data. See Figure 5.3.4a.

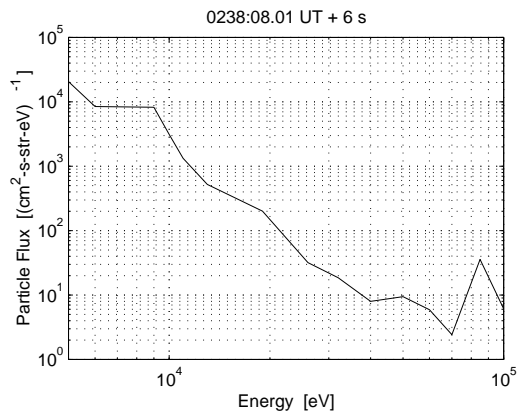
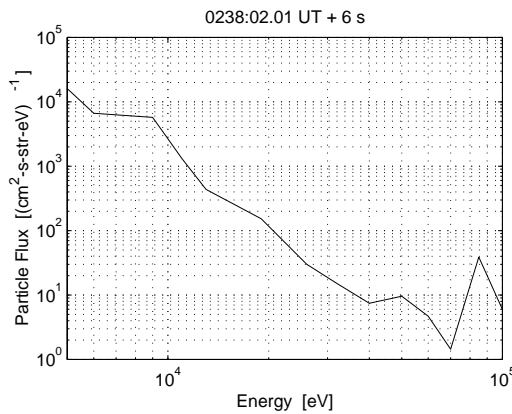
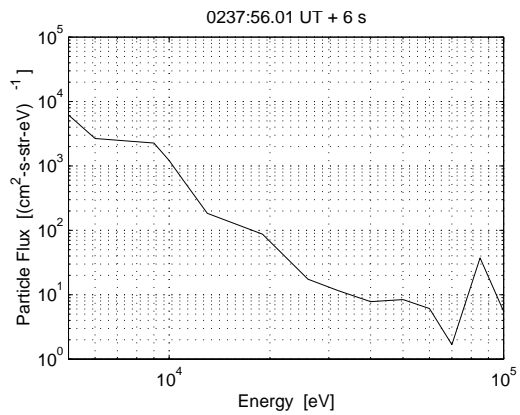
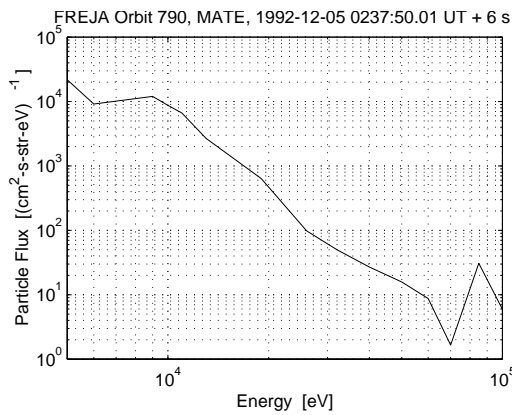


Figure 5.3.5d: MATE data. See Figure 5.3.4a.

Ion distributions around maximum charging are displayed in Figure 5.3.6a. They show the typical lifted-in-energy all-pitch-angle distribution of a charging event of about -65 V. Some indications of simultaneously occurring ion conics can be seen around 90° pitch-angle. For comparison, ion distributions from the ion conic event preceding the charging event, are presented in Figure 5.3.6b, where clear ion conics with energies up to 1.5 keV can be detected.

FREJA 05 Dec 19920237:24.163 2800–ms Resolution Energy Flu

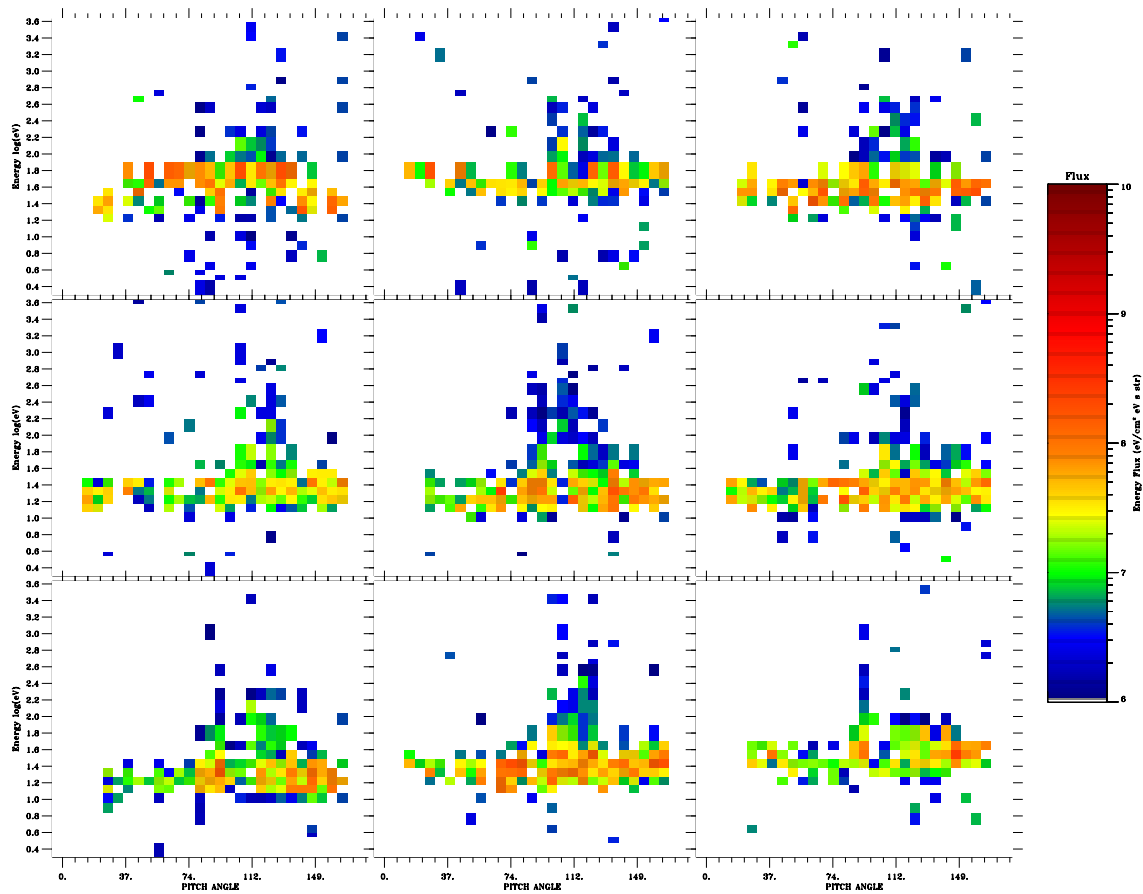


Figure 5.3.6a: The O^+ distributions during maximum charging (panel 2, -65 V).

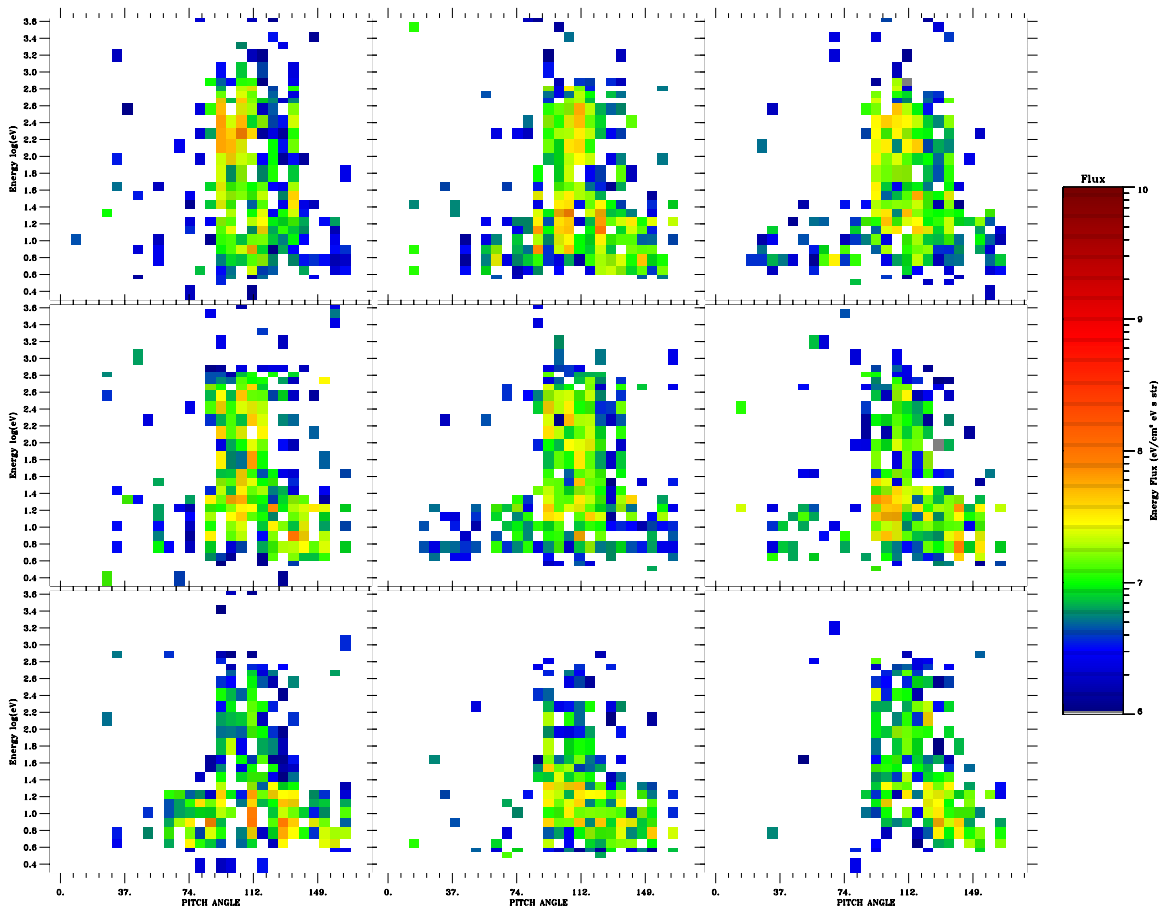


Figure 5.3.6b: Ion distributions from the ion conic event preceding the charging event. Ion conics with energies up to 1.5 keV can be detected.

Conclusions from orbit 790:

- The charging events started when the inverted-V electron energy peak reached above a few keV and the electron flux increased by an order of magnitude above these energies.
- Both electron peak energy and flux increased simultaneously, i.e. they were correlated.
- Spacecraft charging may occur during terminator conditions, i.e. when photoelectron emission from the spacecraft surface is expected to be significant. On the other hand, no charging was detected in the preceding full sunlight conditions despite heavy energetic electron precipitation associated with an auroral substorm.
- There are instrument disturbances due to the charging events in the Langmuir probe, MF and LF electric, and the TICS measurements

5.4 EVENT 4: ORBIT 1651 (TYPICAL CHARGING)

Overview Data, 93.02.08, Prince Albert

The overview data for the particle measurements are presented in Figure 5.4.1. The ions are lifted in energy between about 0558:00 - 0600:00 UT (panels 1-3) at the same time as enhanced fluxes of high energy electrons are detected (TESP, panel 7). The event occurs during eclipse (panel 4). The MATE measures only the integrated flux during this orbit.

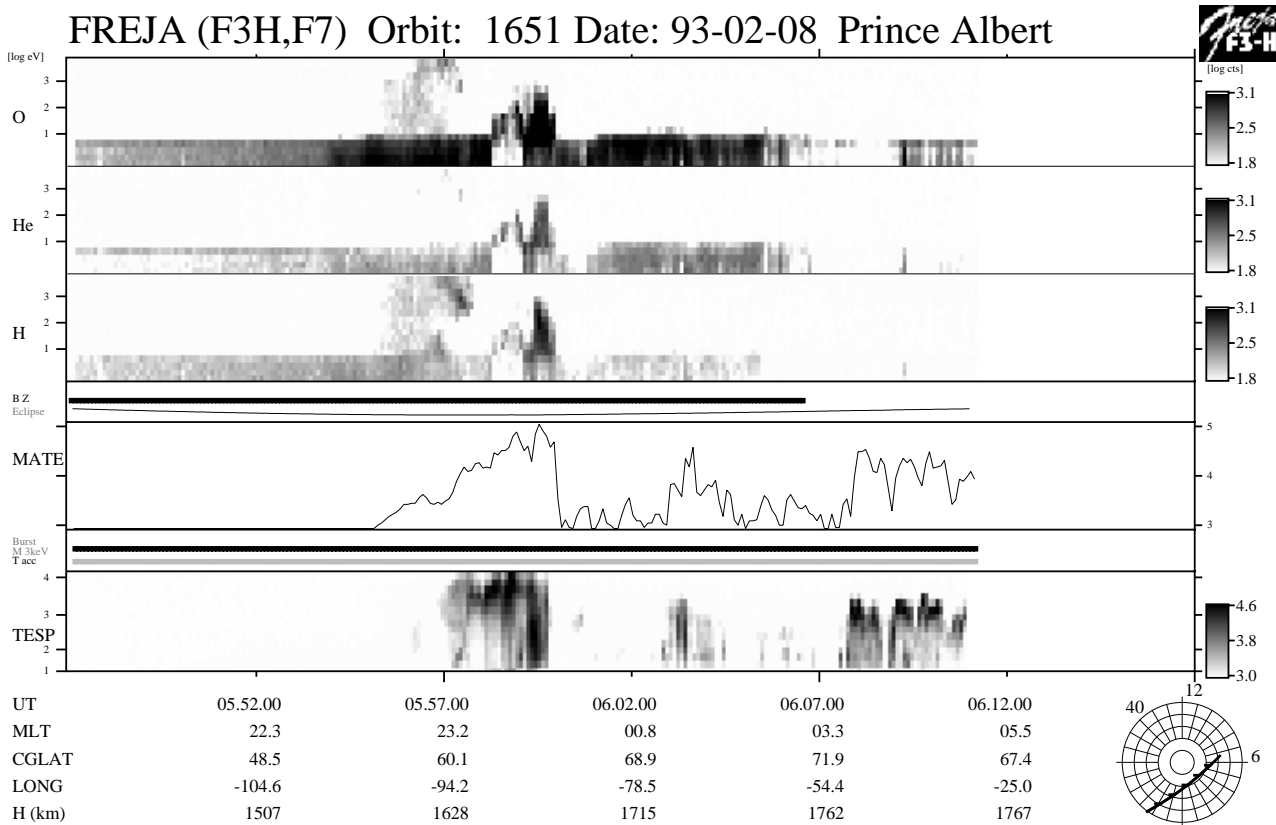


Figure 5.4.1: Overview particle data from orbit 1651. A typical charging event occurs during eclipse (panel 4) near 0558:30 UT just to be followed by a transverse ion heating event. A clear inverted-V structure (panel 7) can be seen in the TESP electron data when charging appears.

Figures 5.4.2 and 5.4.3 show a blow up of the particle and plasma wave data around the uplifted ion event in the interval 0558:10 - 0600:00 UT. After 0959:10 UT the ion energy increase is not accompanied with a clear dropout in the LP current, and is therefore likely to be due to ion heating rather than spacecraft charging. The HF narrow-band emission based estimates for the electron density correspond to densities inferred from the LP current, except for times of LP current dropout. The cold plasma density varies between $5 \cdot 10^8 - 3 \cdot 10^9 \text{ m}^{-3}$. Charging levels of a few tens of volts negative are inferred from the ion data, and the charging events are correlated with auroral inverted-V events with high energy electrons. Both the peak energy and the electron flux increase during charging times.

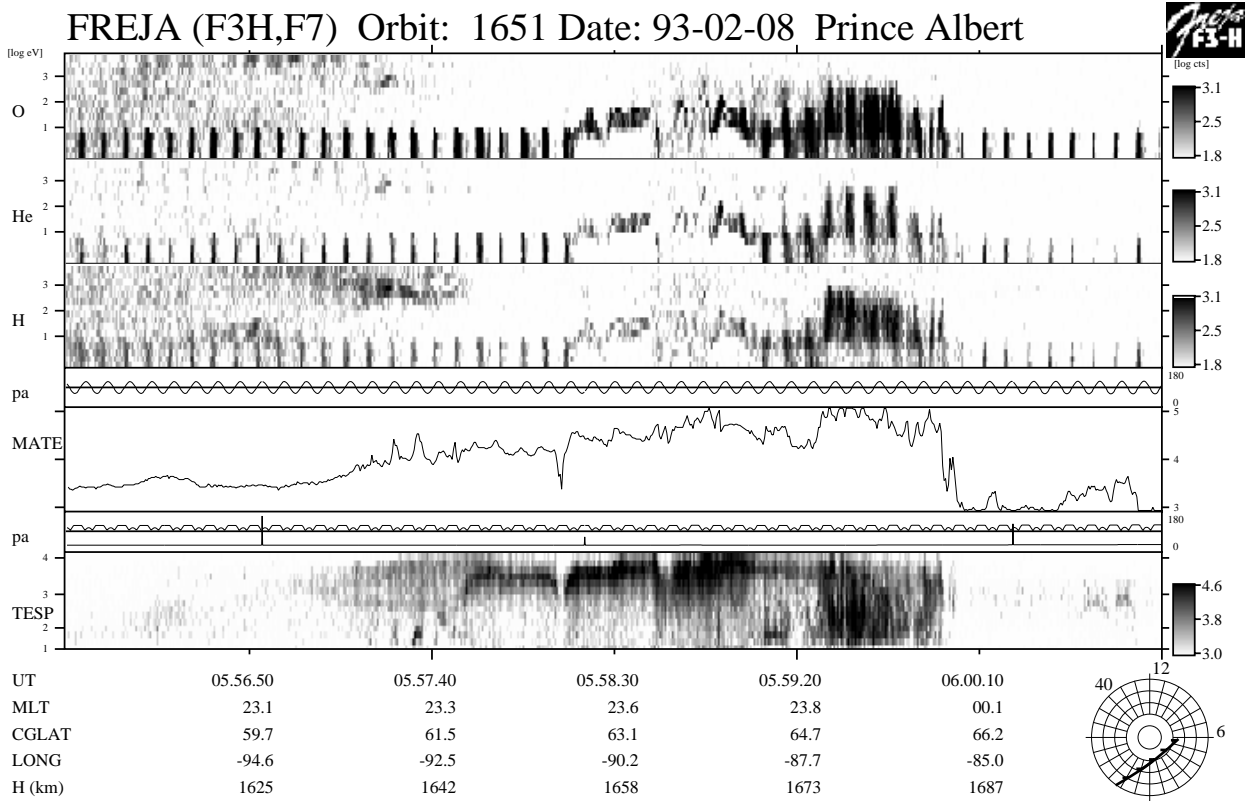


Figure 5.4.2: A blowup of Figure 5.4.1 around the charging event. Both the peak energy and electron flux increases during negative charging of Freja.

Freja F4 Wave Data, Orbit: 1651 Seconds fr. 1993 02 08 055600.000000 UT

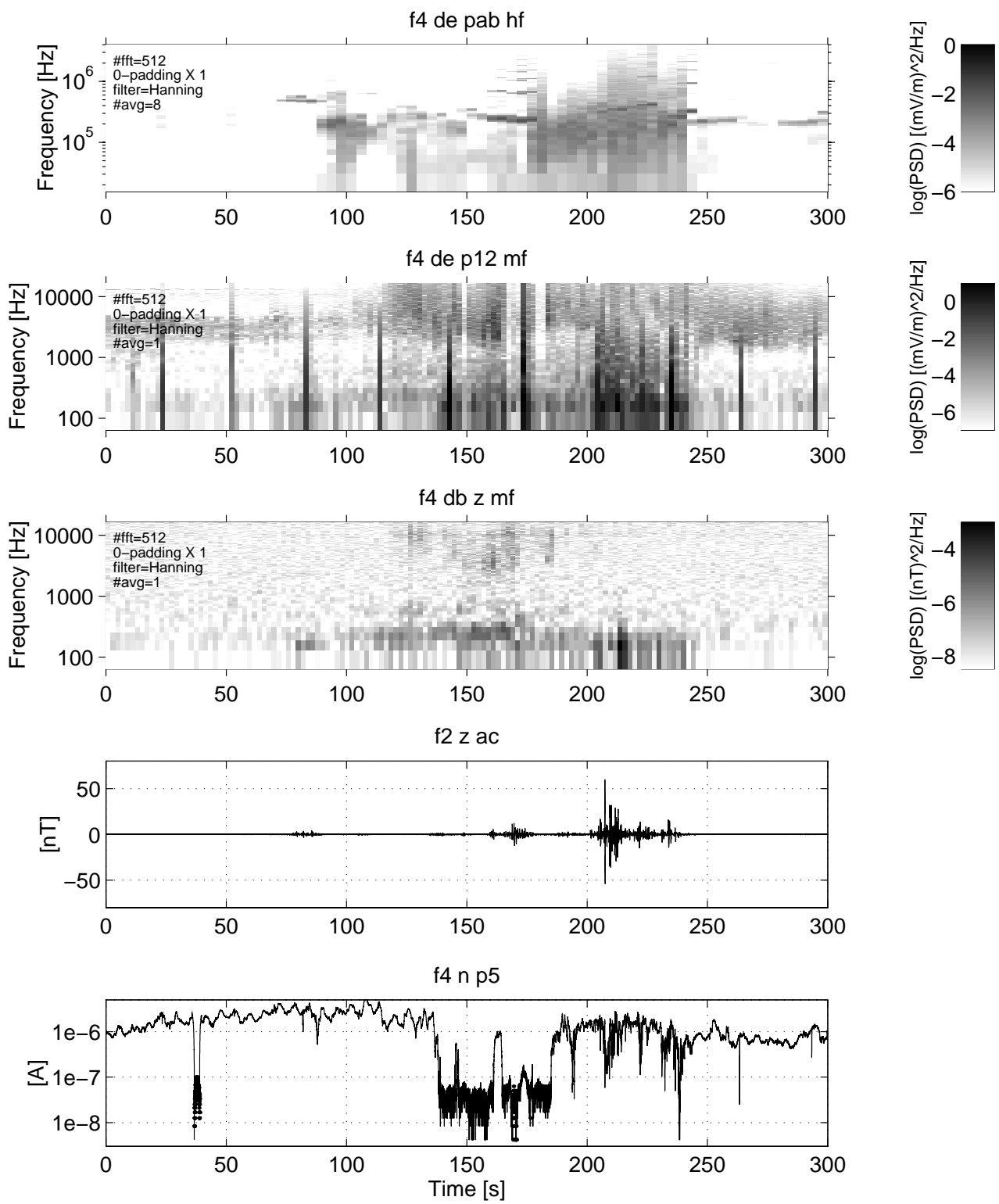


Figure 5.4.3: Plasma wave data corresponding to the particle data in Figure 5.4.2.

Detailed Particle Distributions

The TESP electron spectra during the charging event are shown in Figure 5.4.4. A typical inverted-V like electron spectrum with a clear energy peak near 7 keV can be seen in panel 2, which is replaced by a somewhat more energetic distribution in panel 3, to be relaxed in panel 4 (compare with panel 5 in Figure 5.4.2). The peak flux does not change significantly in panels 3 and 4. Instead an increased flux of lower energy electrons appears in panels 3 and 4, which may inhibit charging by producing an excess of secondary electrons. The detailed ion distributions are shown in Figure 5.4.5, where charging levels up to -40 V is inferred in panels 2 - 4.

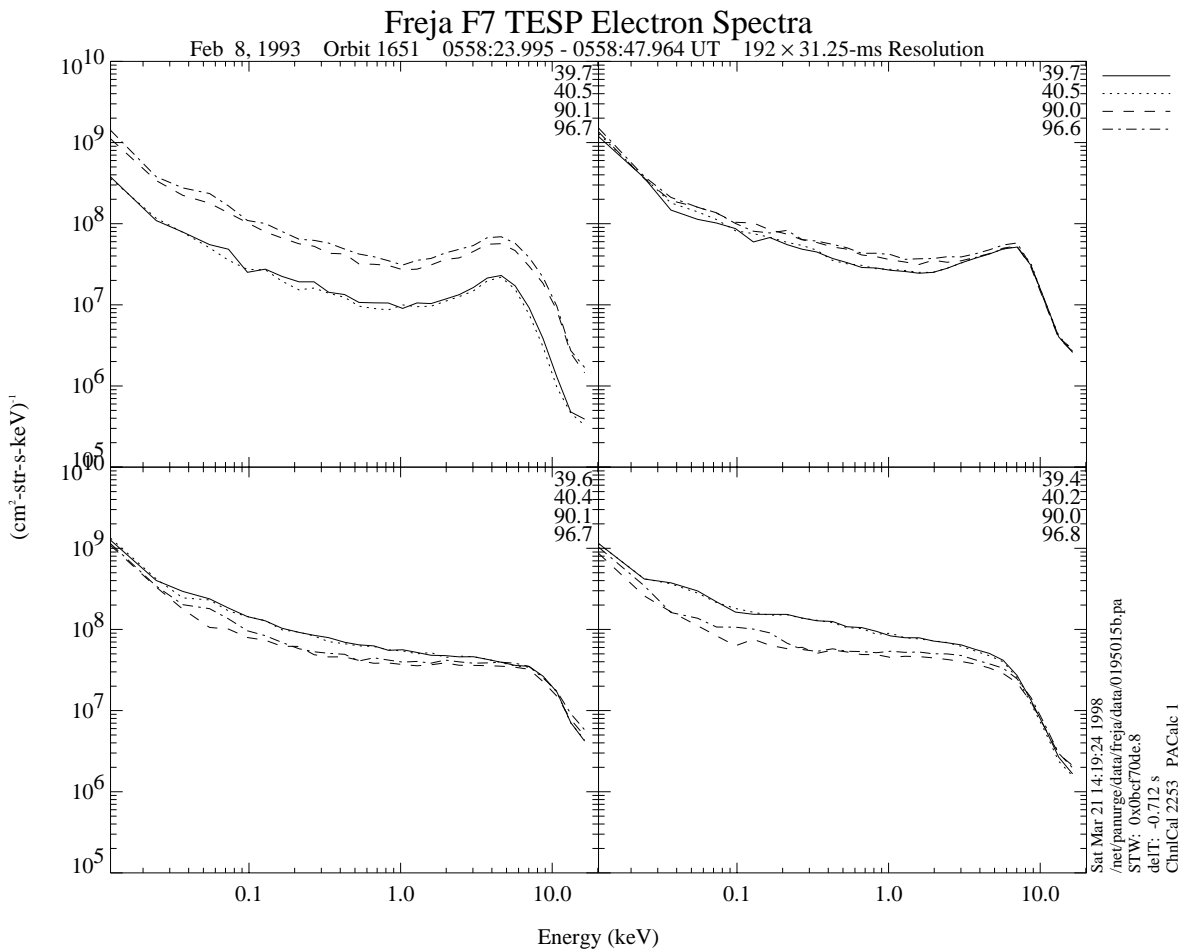


Figure 5.4.4: TESP electron spectra corresponding to the charging event displayed in Figure 5.4.2.

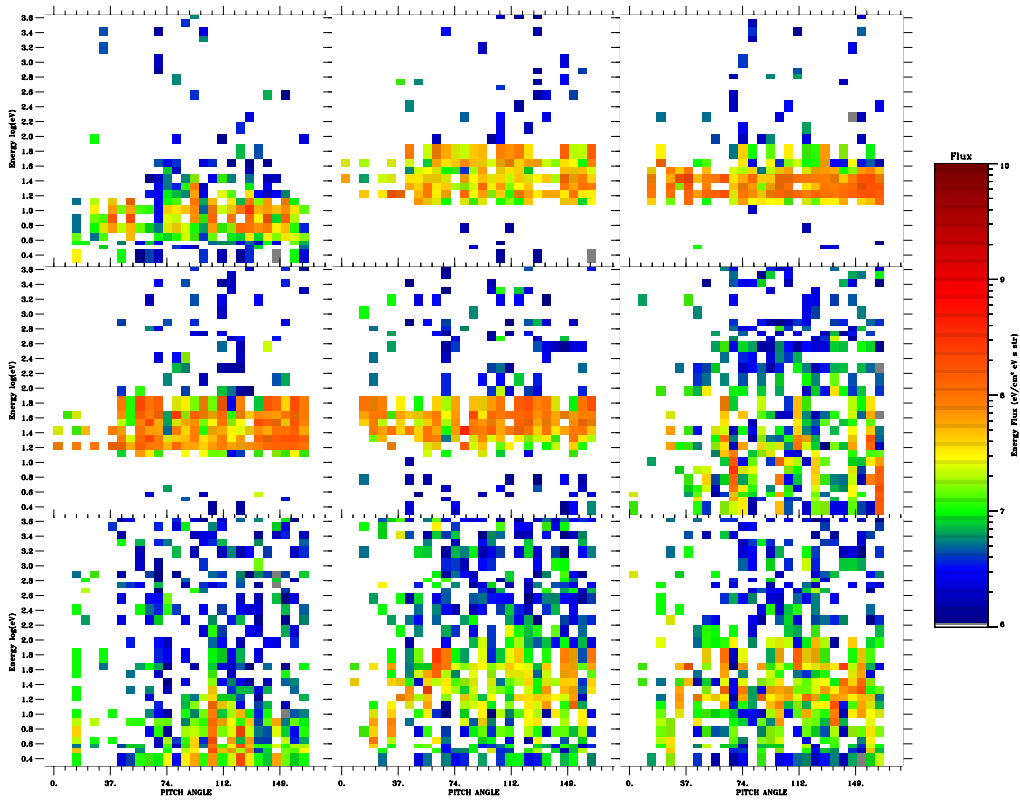


Figure 5.4.5: The O^+ distributions reveal negative charging of about -40 V in panels 2 to 4.

Conclusions from orbit 1651:

- both the inverted-V electron peak energy and flux increased during the charging event,
- an enhanced level of low energy (< 1 keV) electrons seemed to inhibit the charging,
- no sudden drop in plasma density seems to have occurred during the charging event,
- there are instrument disturbances due to the charging event in the Langmuir probe and the TICS measurements.

5.5 EVENT 5: ORBIT 5802 (CHARGING AND ION HEATING)

Overview Data, 93.12.19, Prince Albert

The overview data for the particle measurements from orbit 5802 are presented in Figure 5.5.1. The ions are lifted in energy between 0747:00 - 0752:00 UT (panels 1-3). However, only the first part of this period seems to be associated with enhanced fluxes of high energy electrons (panel 7), even though the information above 25 keV is unknown. The whole event occurs during eclipse (panel 4). The MATE measures only the integrated flux during this orbit.

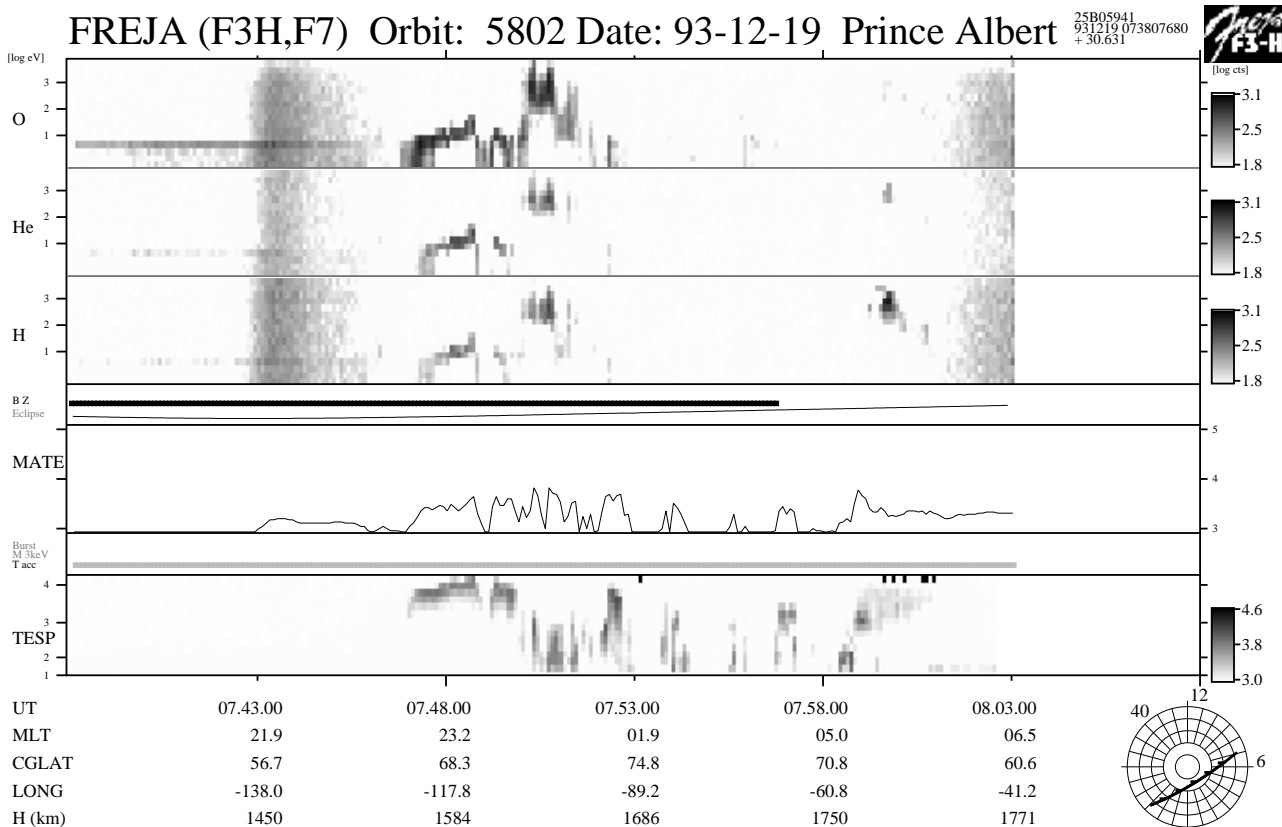


Figure 5.5.1: Overview particle data from orbit 5802. This orbit present two events with “uplifted” ion populations around 0748:00 UT and 0750:30 UT. Both events occur in eclipse. The first event is associated with energetic inverted-V type electrons, the other with lower energy so called field-aligned suprathermal electron bursts. The first event is a charging event, the following is an auroral transverse energization event.

Figures 5.5.2 and 5.5.3 show a blow up of the particle and plasma wave data around the uplifted ion event, which can be divided into three regions (0747:00 - 0750:00 UT, 0750:00 - 0751:30 UT, and the event after 0752:00 UT, Figure 5.5.2, panels 1-3). The events in the first part are associated with dropouts in the CYLP current, when the HF emissions still indicate large plasma densities of $2 \cdot 10^8 \text{ m}^{-3}$. The middle event period shows very low densities below $7 \cdot 10^7 \text{ m}^{-3}$ according to the HF emissions and the CYLP current dropouts are not completely in the bottom. Also, there are no enhanced high energy electron fluxes associated with this event. Rather the TESP data show evidence for suprathermal electron bursts with energies below a few hundred eV. The third event

after 0752:00 UT is associated with both high energy electrons and CYLP current dropouts, but there is no detectable uplift in ion energies. We interpret these data as follows; the event in the first period are due to spacecraft charging, the event in the middle period is due to ion heating, and the last event is also a charging event, but with fast intermittent fluctuations of low level charging not readily detectable by the TICS instrument. In the first event the charging starts when the inverted-V peak energy approaches 10 keV, while no charging occurs if the inverted-V peak energy is below about 5 keV. Thus, a threshold energy for charging seems to be present also for this charging event, which can be due to in the crossover secondary emission yield energy of the Freja surface materials.

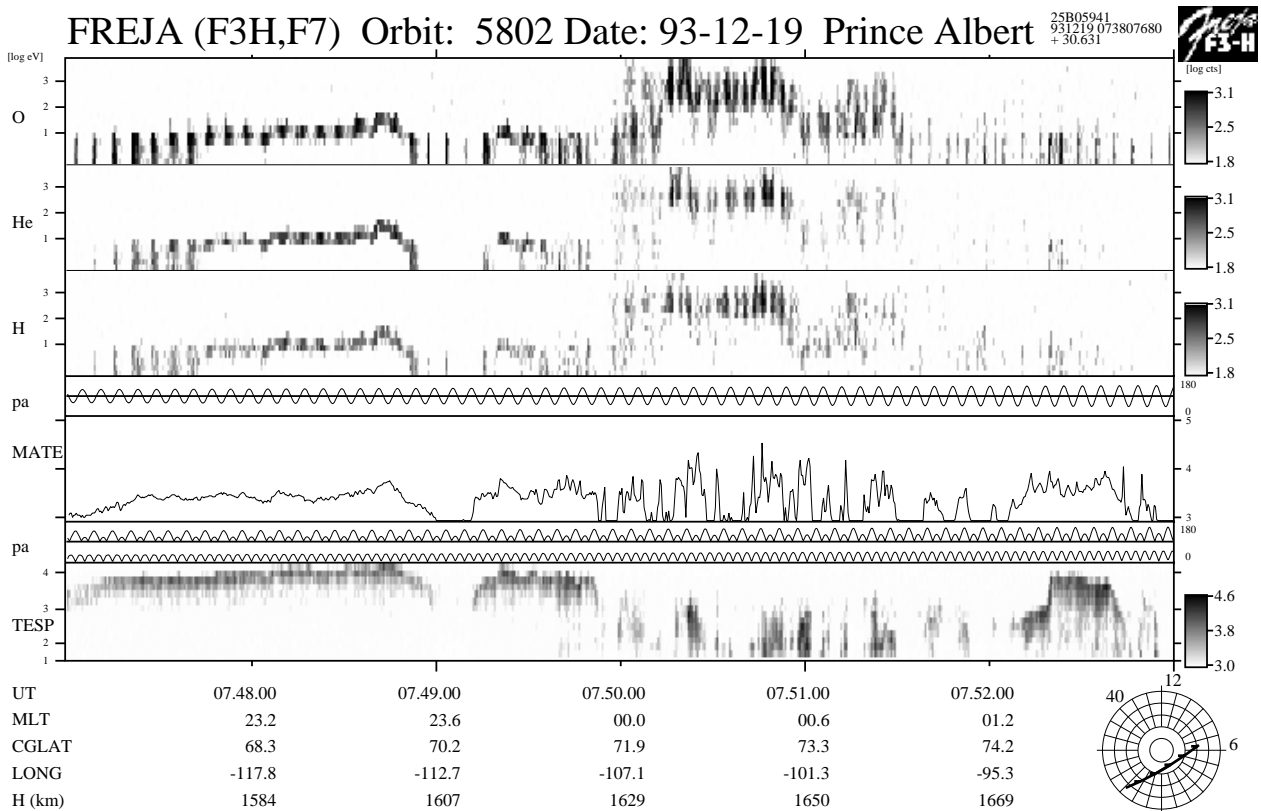


Figure 5.5.2: A blow up of Figure 5.5.1, showing the clear charging event with its associated high energy inverted-V electrons and the transverse ion heating event with its associated suprathermal electron bursts.

Freja F4 Wave Data, Orbit: 5802
Seconds fr. 1993 12 19 074700.000000 UT

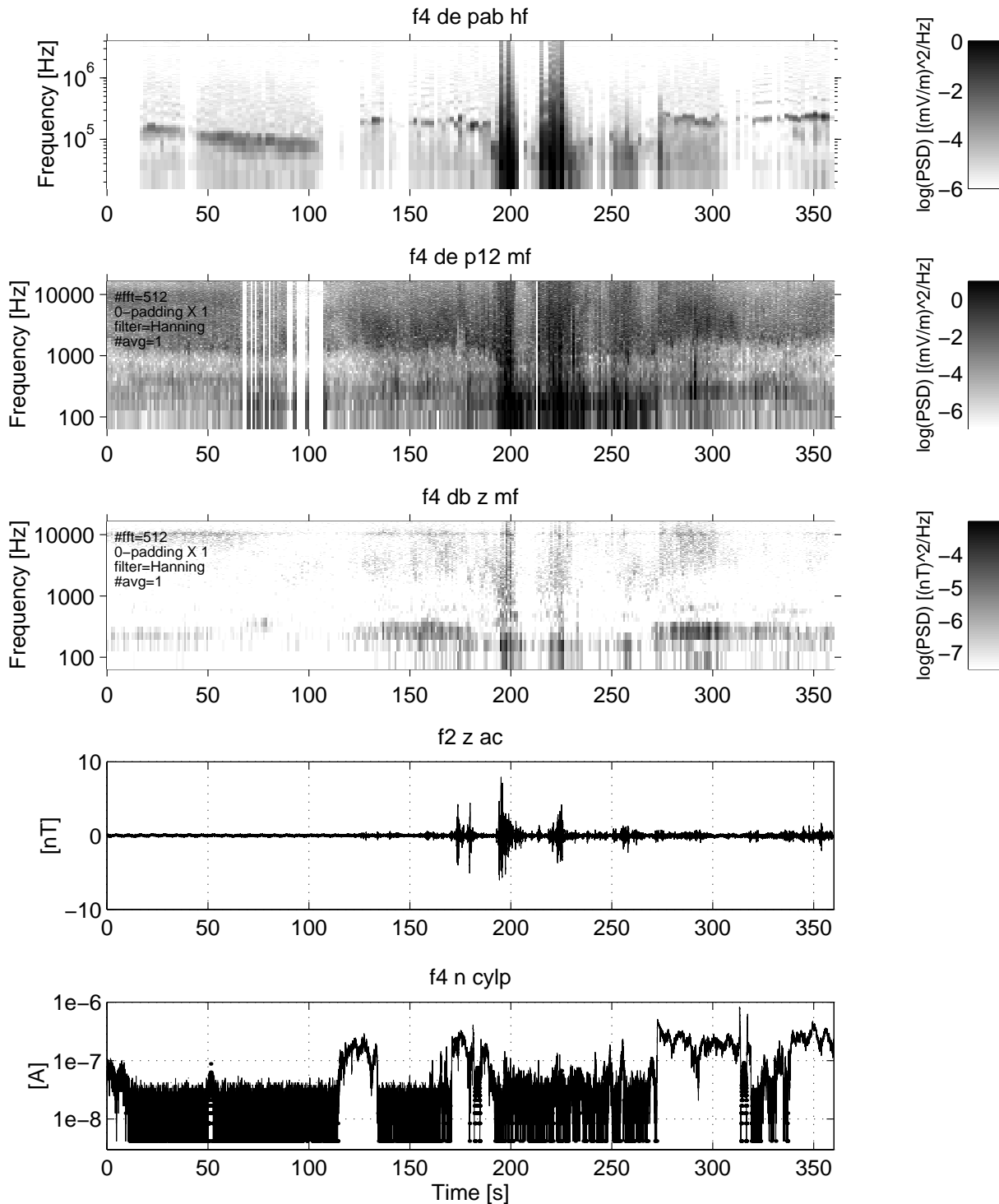


Figure 5.5.3: Plasma wave data corresponding to the particle data in Figure 5.5.2. The density is very low during the transverse ion heating event and the HF emissions correspond well with the low LP currents during that time (+190 s - +270 s). On the other hand, they do not correspond well during the charging events before +170 s.

Detailed Particle Distributions

Figure 5.5.4a and 5.5.5a display the TESP electron spectra and TICS ion distributions for the first charging event near 0748:20 UT. A clear inverted-V electron energy peak near 10 keV can be detected together with uplifted energy distributions of the ions at all pitch-angles. Negative charging levels reaching -12 V are inferred from the ion data.

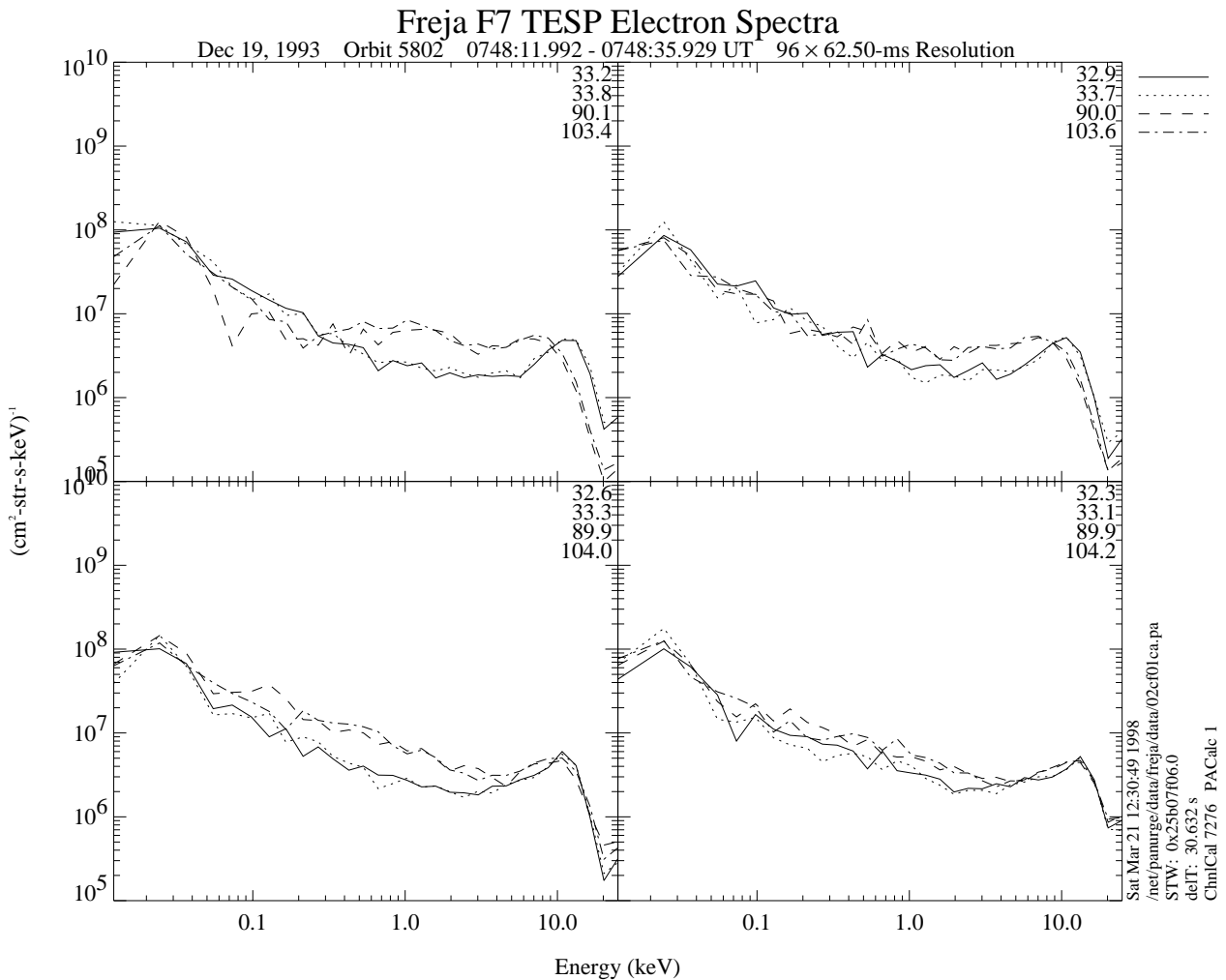


Figure 5.5.4a: TESP electron data from the charging period of this orbit. Auroral inverted-V electron peaks reach 10 keV during charging.

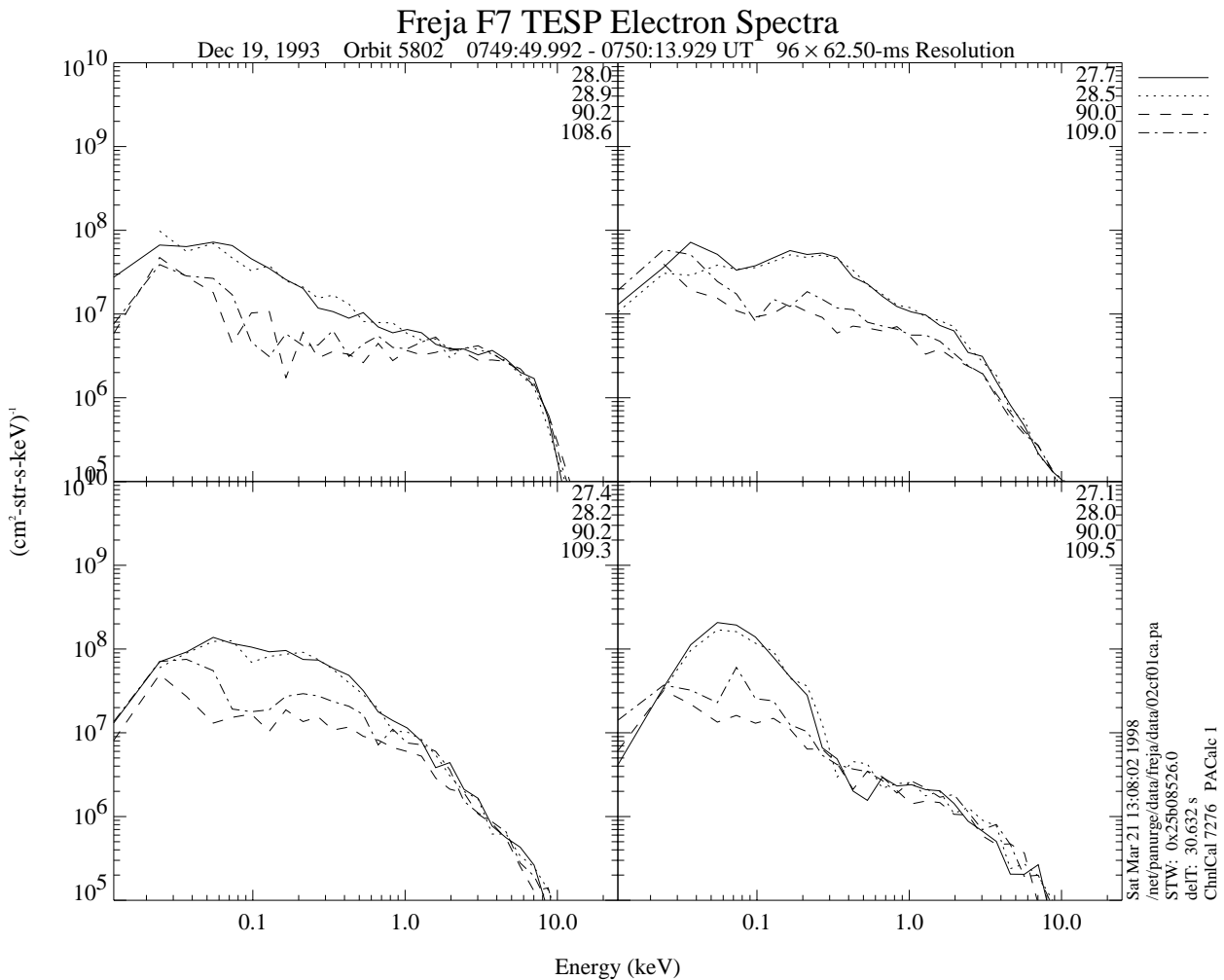


Figure 5.5.4b: TESP electron data from the ion conic period. Intense rather field-aligned low energy (< 1 keV) fluxes are detected.

Detailed TESP electron spectra and TICS ion distributions from the start of the ion conic event are presented in Figures 5.5.4b - 5.5.4c and 5.5.5b respectively. The electron spectra show no trace of high energy inverted-V electrons. Instead rather field-aligned distributed suprathermal electron bursts can be detected at energies below a couple of keV. The corresponding ion distributions evolves from a ram-distribution (panel 1) to an energetic ion conic (panels 2 - 7), which suddenly is lifted to about 250 eV (panels 8 - 9) most probably due to transverse ion heating in connection with the mirror force produced by Earth's diverging magnetic field.

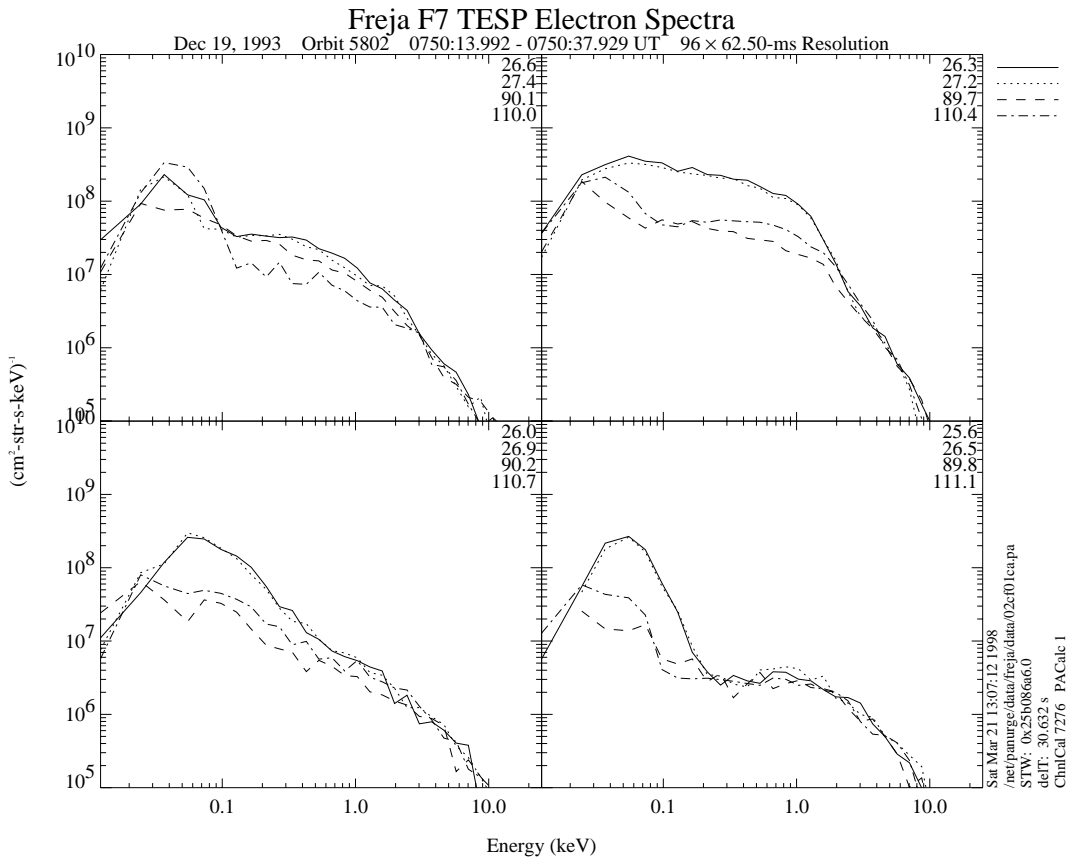


Figure 5.5.4c: TESP electron data. Continuation of Figure 5.5.4b.

FREJA 19 Dec 19930748:13.365 2800-ms Resolution Energy Flu

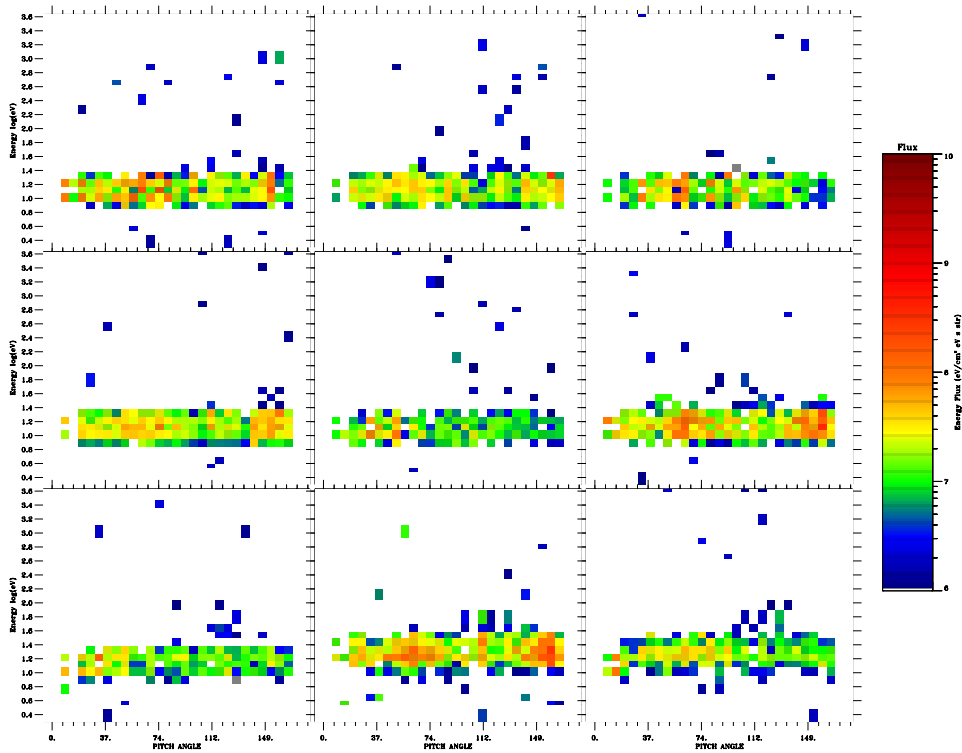


Figure 5.5.5a: The O^+ distribution functions show low level charging of about -12 V.

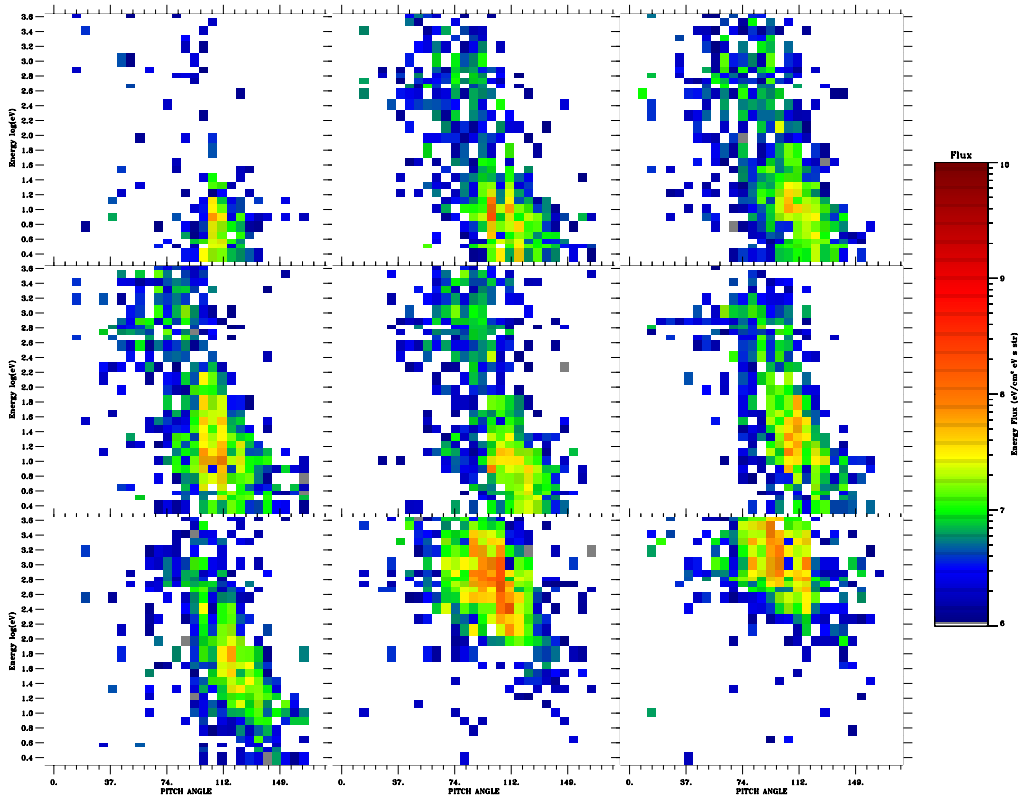


Figure 5.5.5b: These O^+ distribution functions show a nice transition from the spacecraft ram flow signature (panel 1), the transverse energization of the oxygen ions (panels 2 - 6), which in the end of this measurement sequence show the whole ion population accelerated upwards most probably by the action of the magnetic mirror force (panels 7 - 9).

Conclusions from orbit 5802:

- The inverted-V peak energy reached above about 5 keV during the charging events, while no charging was detected when this energy peak fell below 5 keV.
- Transverse ion heating may produce uplifted ion events similar to those during spacecraft charging. However, the detailed ion energy pitch-angle distributions during these two cases are considerably different and can easily be distinguished if accurate analysis is made. Also, transverse ion heating in the Freja data set is most often associated with field-aligned suprathermal electron bursts rather than isotropic inverted-V precipitation.
- There are instrument disturbances due to the charging events in the Langmuir probe, MF and LF electric, and the TICS measurements.

5.6 EVENT 6: ORBIT 1666 (LARGEST CHARGING POTENTIAL)

Overview Data, 93.02.09, Prince Albert

The overview data for the particle measurements from orbit 1666 are presented in Figure 5.6.1. This event represent one of the largest observed charging levels observed in the Freja data set. The ions are lifted in energy between 0916:00 - 0919:00 UT (panels 1-3). The event is associated with enhanced fluxes of high energy electrons which are part of an auroral inverted-V event (panel 7). The whole event occurs during eclipse (panel 4). The MATE measures only the integrated flux during this orbit.

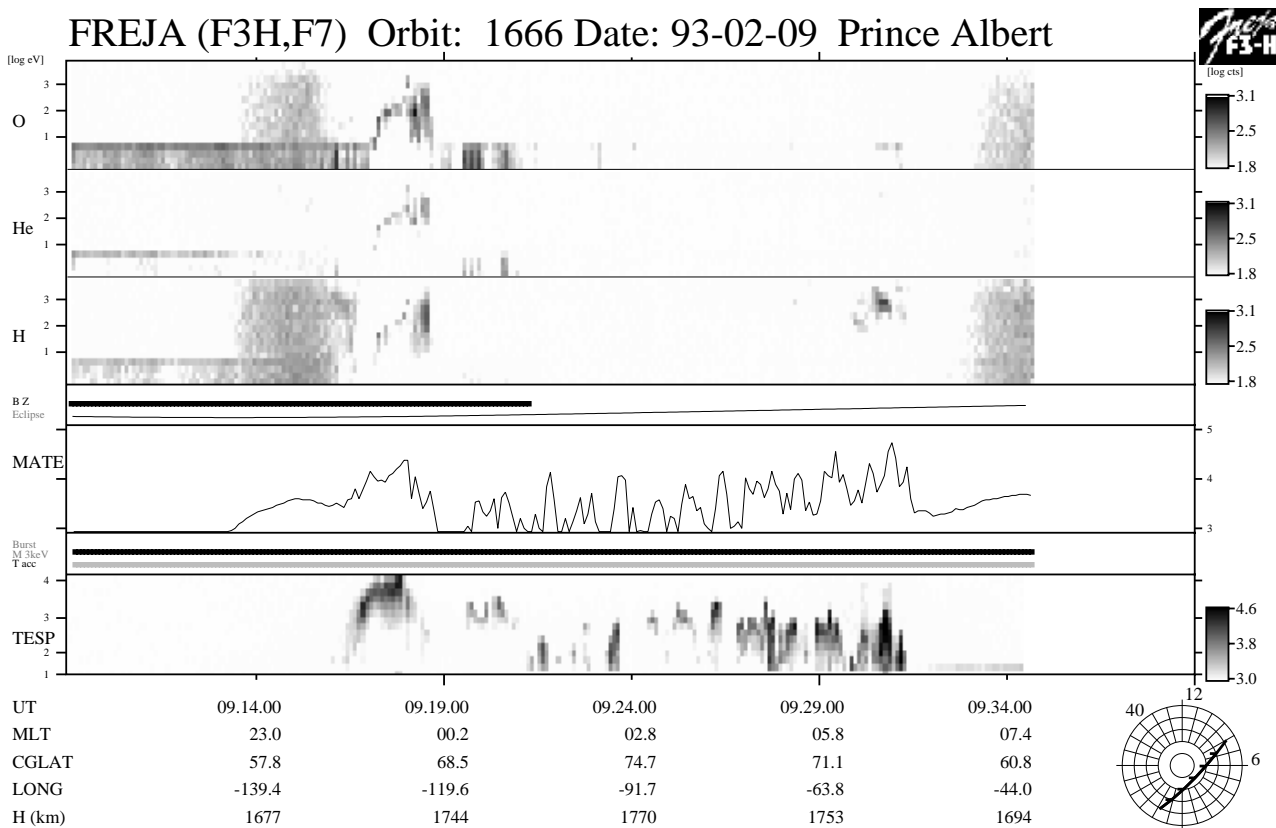


Figure 5.6.1: Overview particle data from the orbit 1666. This orbit reveals one of the highest negative charging levels detected in the Freja data set near 0918:00 UT during eclipse conditions. A clear intense auroral inverted-V event is associated with the charging event.

Figures 5.6.2 and 5.6.3 display the blow up of the particle and plasma wave data around the uplifted ion event. Densities during the charging event vary between $1\text{-}2 \cdot 10^8 \text{ m}^{-3}$ according to the upper cutoff of the HF emissions (panel 1, Figure 5.6.3). In this case the thermal plasma density indeed do decrease when the charging event appears. The ion energy attains values to about -2000 V near 0918:00 UT (panel 1, Figure 5.6.2), a time when the energetic electron fluxes becomes as most intense and the peak energy rise to its largest value (panels 5 and 7, Figure 5.6.2).

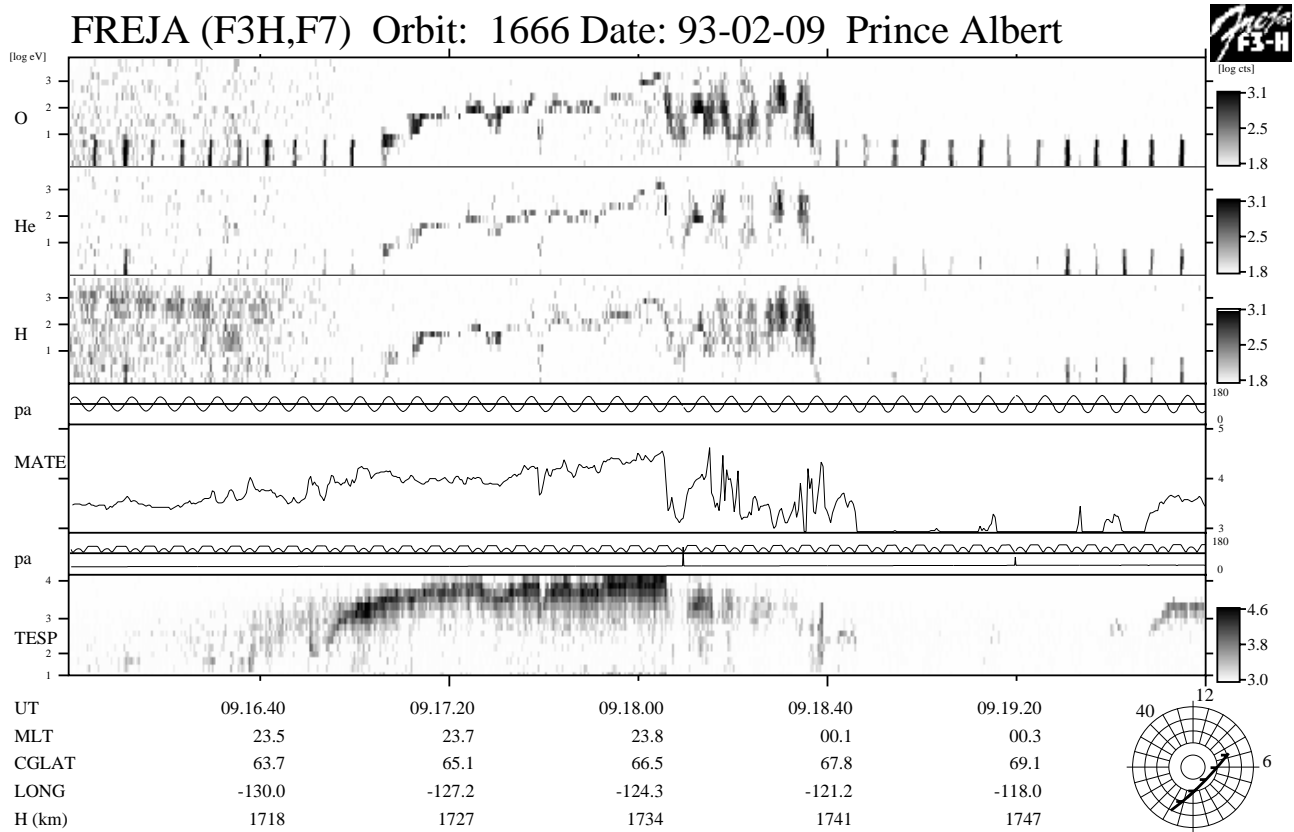


Figure 5.6.2: A blow up of the data around the high level charging event on orbit 1666. The O^+ data (panel 1) show contamination of presumably MeV electrons when maximum charging takes place near 0918:00 UT. Very intense inverted-V electron fluxes (panel 7) matches the time of maximum charging as well.

Freja F4 Wave Data, Orbit: 1666 Seconds fr. 1993 02 09 091600.000000 UT

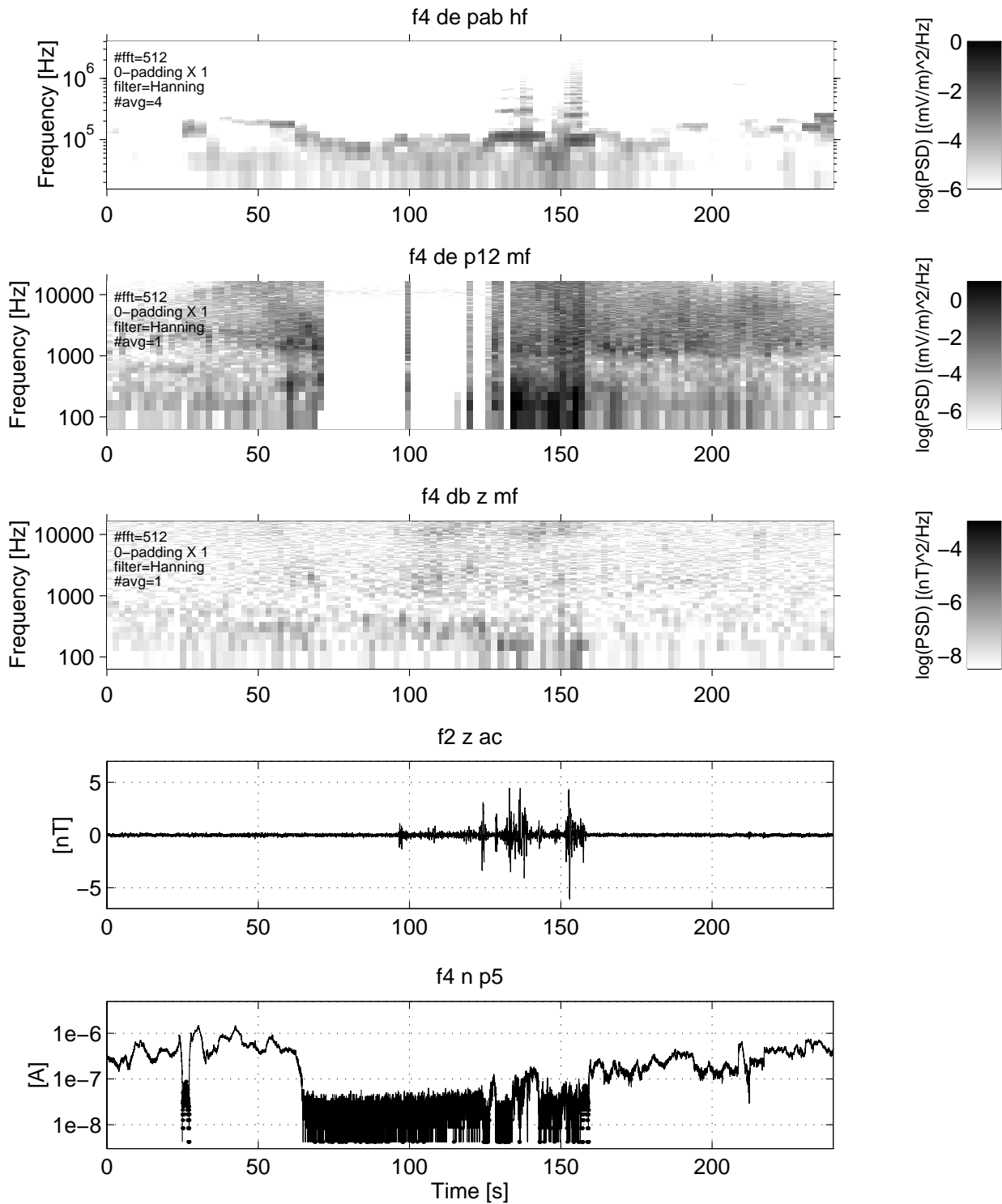


Figure 5.6.3: The plasma density falls to low values during this charging event as indicated by the upper cutoff of the electrostatic whistler type waves around +100 s in panel 1. The MF electric plasma wave data becomes very disturbed during the event, and the Langmuir probe drops due to that no thermal electrons can reach the probe (nor Freja).

Detailed Particle Distributions

Detailed TESP spectra during the event are displayed in Figures 5.6.4a and 5.6.4b. The inverted-V peak becomes displaced upward in energy during maximum charging (panels 3 and 4 in Figure 5.6.4a; panels 1 - 3 in Figure 5.6.4b), and the peak energy is probably even above maximum measured energy (25 keV). The peak flux, on the other hand, stays rather constant during the event. The last panel in Figure 5.6.4b, which is after the time of charging, show evidence of field-aligned suprathermal electron bursts in the energy range 30 - 1000 eV.

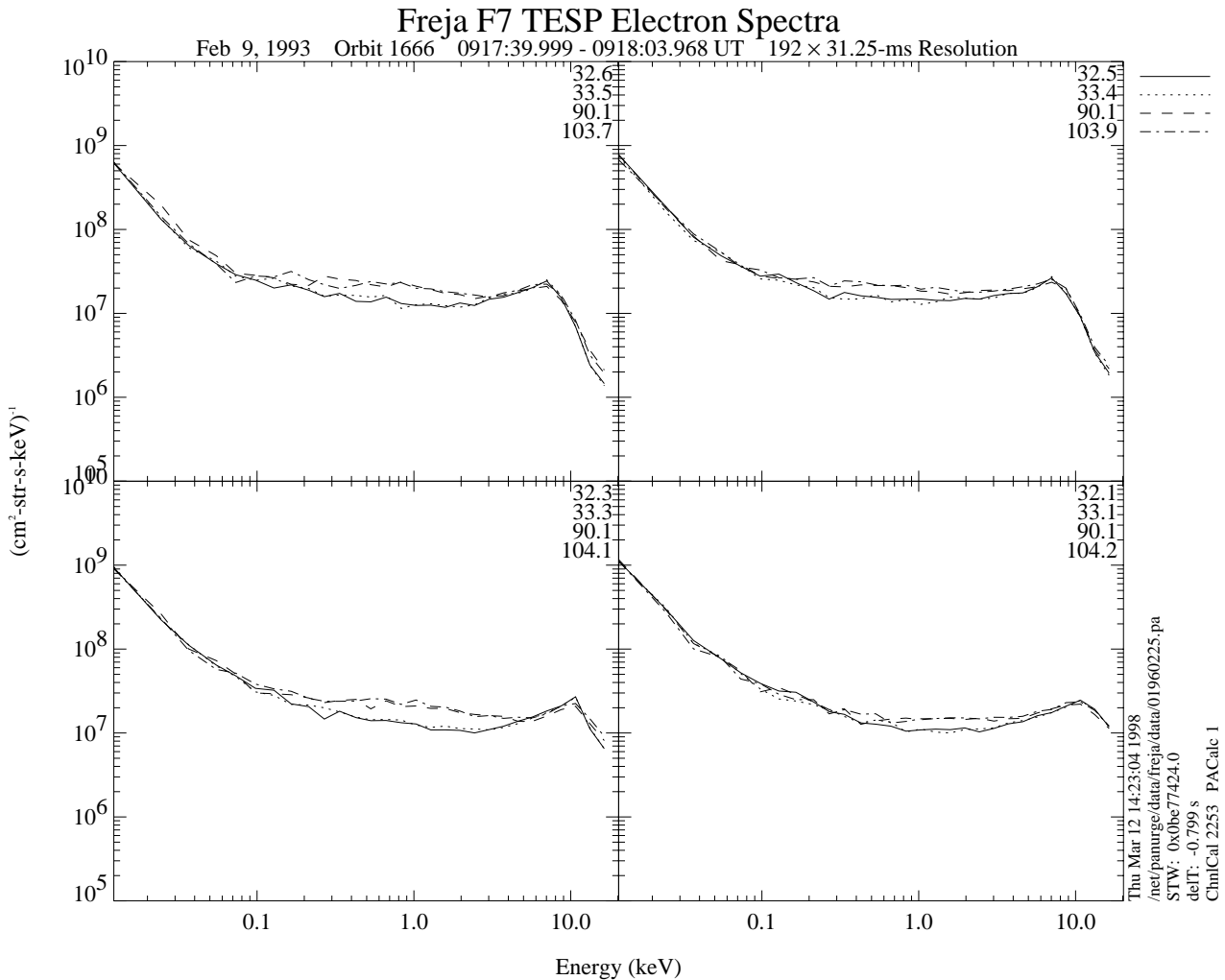


Figure 5.6.4a: TESP electron spectra during the charging event. Maximum charging occurs in panel 3 in the following Figure (Figure 5.6.4b), where the inverted-V peak reaches probably much above maximum measured energy (25 keV).

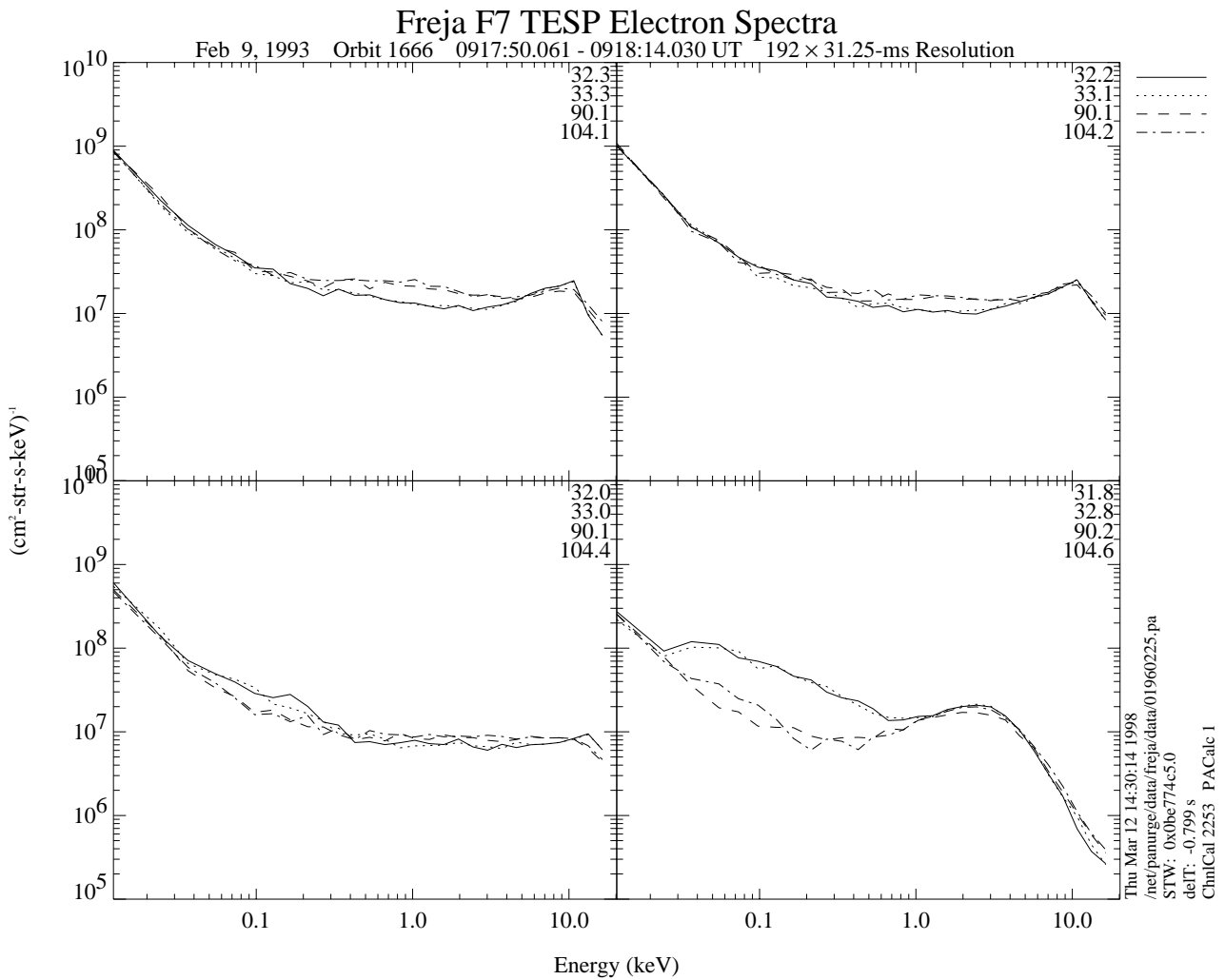


Figure 5.6.4b: See Figure 5.6.4a for text.

The detailed ion distributions around maximum charging are most probably contaminated by large fluxes of high energy electrons in the MeV range. Nevertheless, charging levels up to -1800 V can be inferred from panel 6, where after an ion conic distribution is detected.

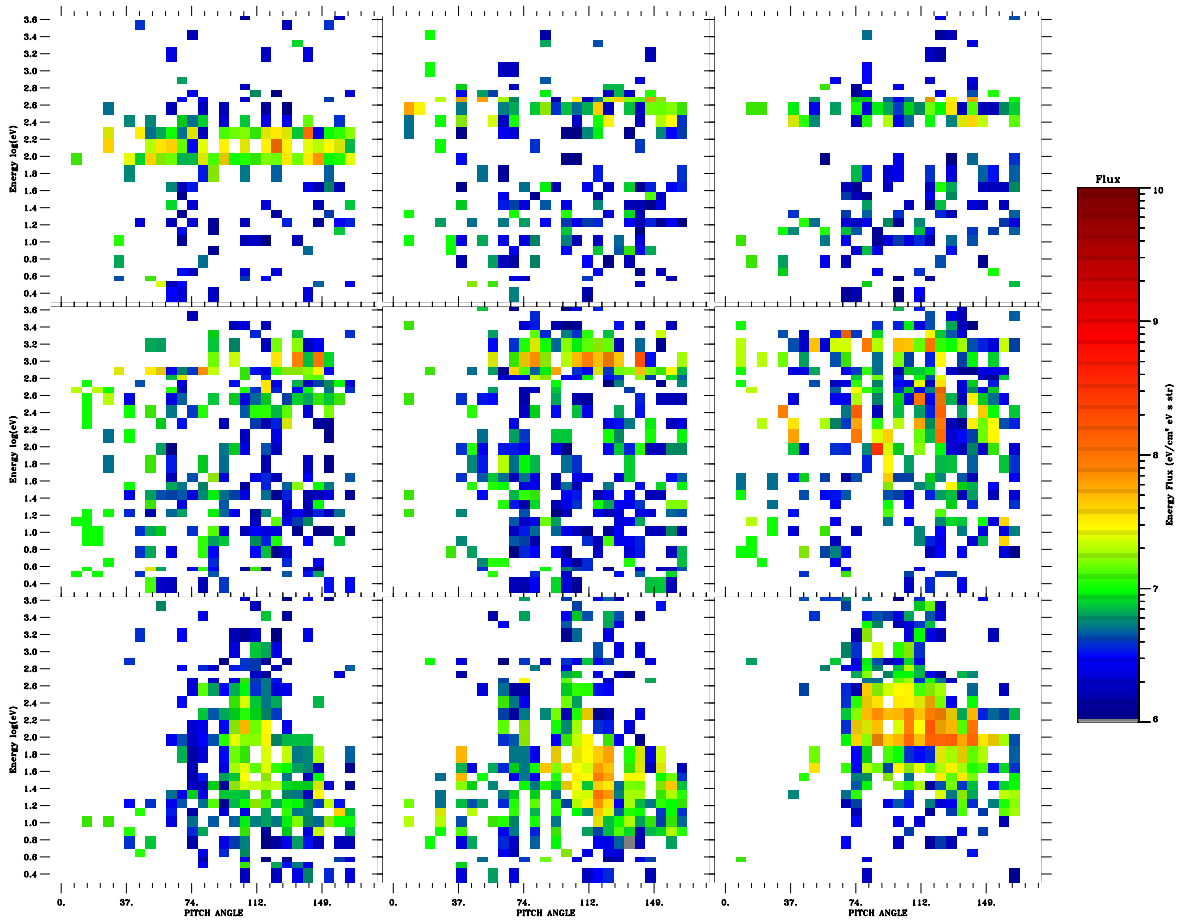


Figure 5.6.5: The O^+ distributions around maximum charging (panel 6). Negative charging levels of -1800 V is inferred.

Conclusions from orbit 1666:

- Freja charging events may reach very large levels despite the efforts of making the Freja spacecraft as electrically clean as possible, in this case near -2000 V.
- The peak energy of the inverted-V event seemed to control the charging level during this event.
- The TICS instrument showed indications of MeV electron fluxes during maximum charging.
- The plasma density decreased to low values during this charging event.
- There are instrument disturbances due to the charging events in the Langmuir probe, MF and LF electric, and the TICS measurements.

5.7 EVENT 7: ORBIT 1785 (CHARGING DURING SUNLIGHT)

Overview Data, 93.02.18, Prince Albert

The overview data for the particle measurements from orbit 1785 are presented in Figure 5.7.1. This charging event is special in that it occurs during sunlight conditions (panel 4, see SPEE-WP130-TN for a detail account on sunlight charging events) around 0932:00 UT. It is clearly associated with high energy (at least up to 25 keV) electrons belonging to an auroral inverted V event (panel 7). Unfortunately no UV photometer data exist for this event, but we are sufficiently confident in the used geometric calculations based on comparisons of such calculations with the photometer data on other orbits.

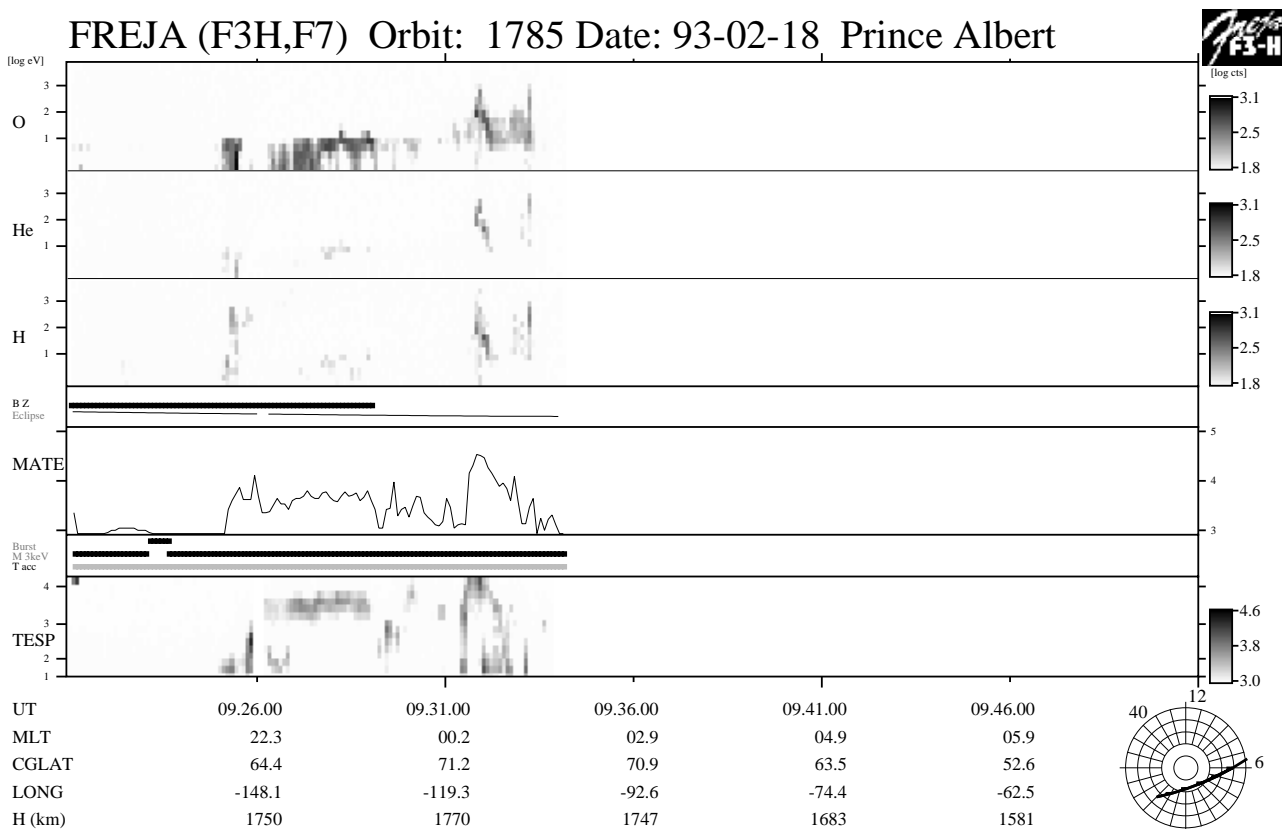


Figure 5.7.1: Overview of the particle data from orbit 1785. A charging event occurs during sunlight conditions around 0932:00 UT, where also a well developed auroral inverted-V structure can be detected (panel 7).

Figures 5.7.2 and 5.7.3 show a blow up of the particle and plasma wave data around the uplifted ion event of interest. The plasma density, as inferred from the HF emissions, stays rather constant during the whole displayed time interval, and estimated densities are nearly constant around $2\text{-}4 \cdot 10^8 \text{ m}^{-3}$. The LP current clearly drops between +43 s to +73 s, while the HF emissions stays constant. Interestingly, a Langmuir sweep exist at the end of the charging event and one may wonder whether the swept potential $\pm 12 \text{ V}$ caused the spacecraft to discharge. However, the LP current drop also corresponds to a drop in energy and flux of the measured high energy inverted V electrons (panel 7,

Figure 5.7.2). The ion data (panels 1-3, Figure 5.7.2) show a lift in energies of up to -500 V. Between 0931:50 - 0931:55 UT it seems extremely high energy electrons hit "through" to the ion detectors, as is otherwise common during ring current passages. Thus, enhanced fluxes of MeV electrons might be associated with the maximum charging part of this charging event. Charging occurs only when the peak energy of the inverted-V electron population reach above about 5 keV, while no detectable charging exists for lower inverted-V peak energies.

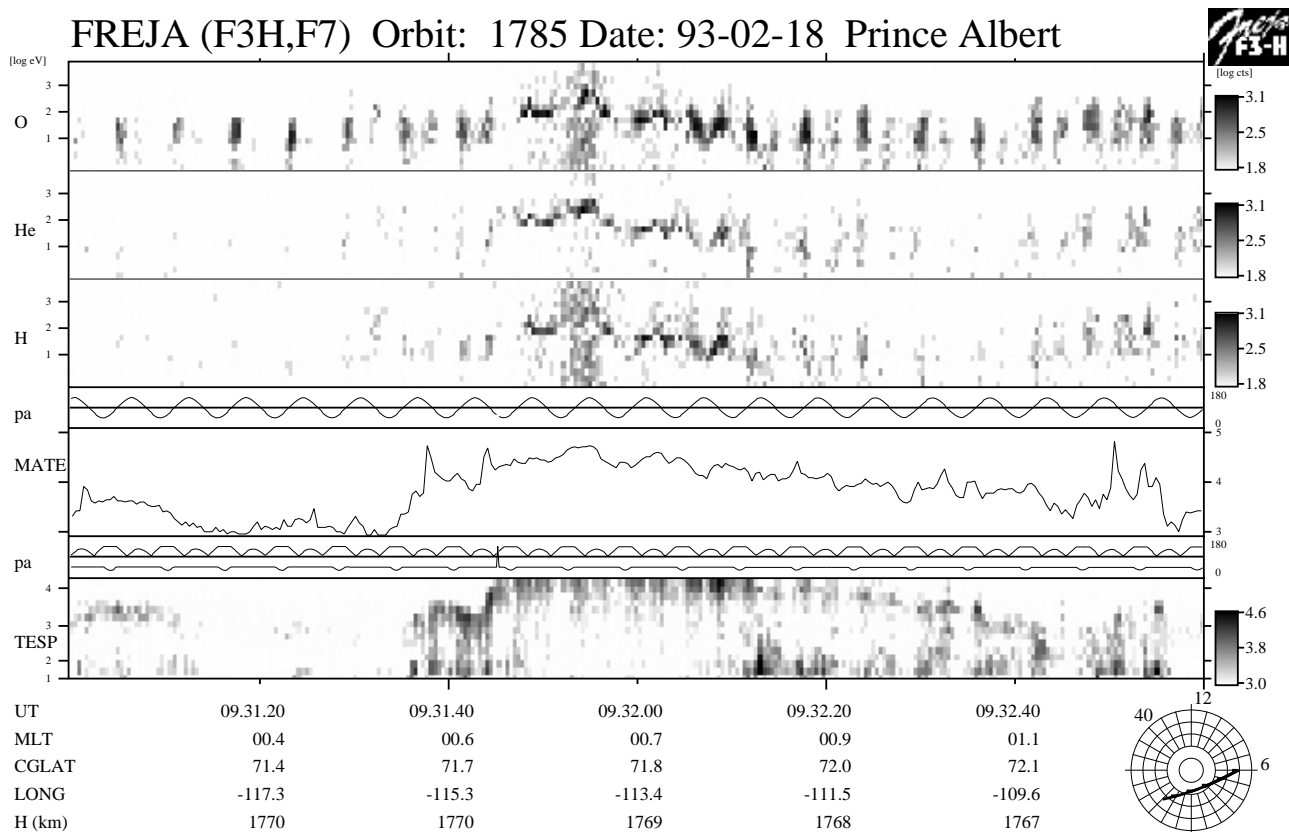


Figure 5.7.2: A blow up of the particle data around the daylight charging event on orbit 1785. It is obvious that the associated auroral inverted-V electron feature (panel 7) reaches at least up to maximum measured energy (25 keV). Contamination most probably from large fluxes of MeV electrons can be detected in all ion channels (panel 1-3).

Freja F4 Wave Data, Orbit: 1785
Seconds fr. 1993 02 18 093100.000000 UT

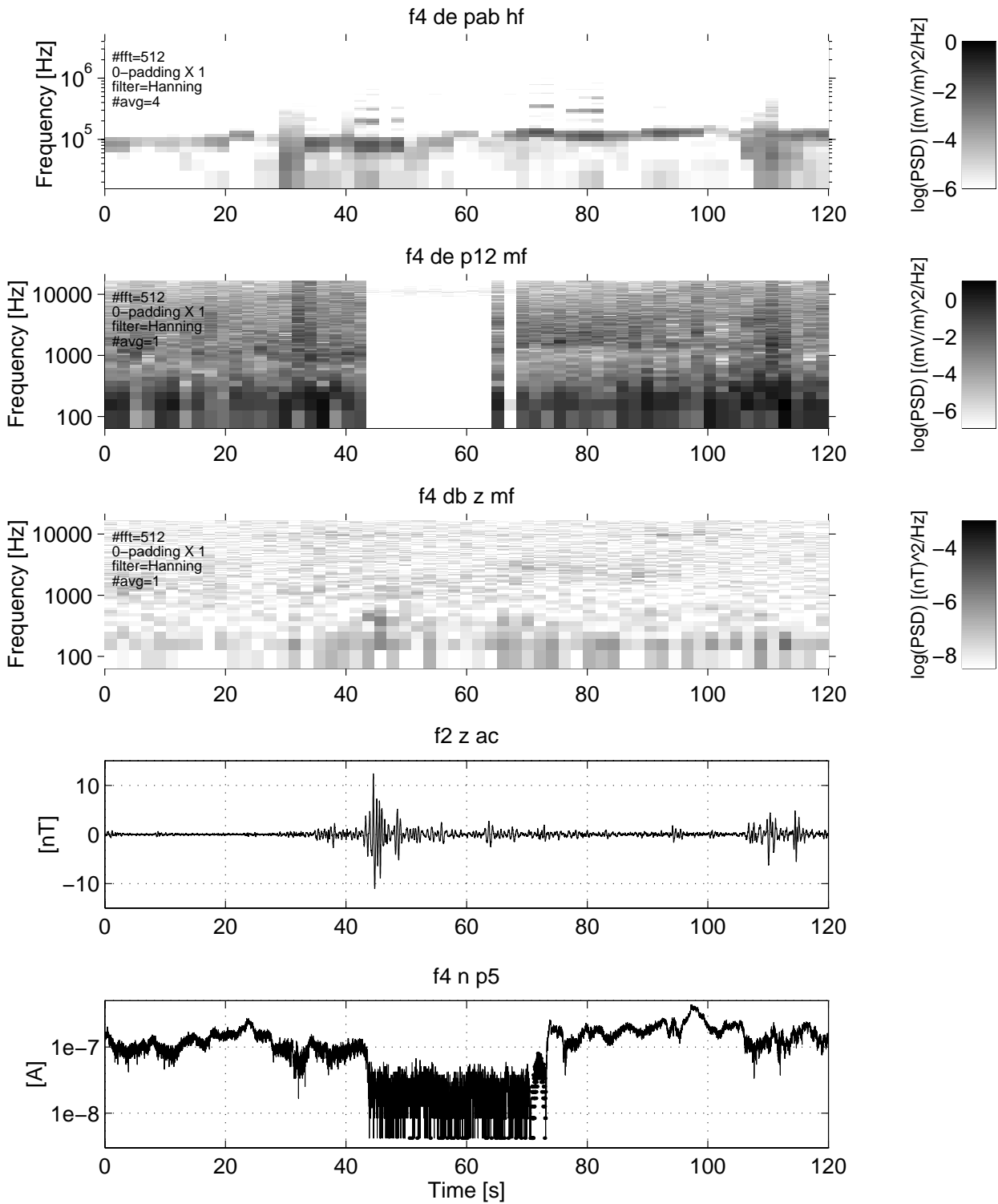


Figure 5.7.3: The cold plasma density is relatively constant during the charging event as inferred from the narrow-band HF Langmuir emissions (panel 1). The charging event is clearly identified by a sharp drop in the Langmuir probe current (panel 5) and disturbances in the MF electric field measurements (panel 2).

Detailed Particle Distributions

Detailed TESP spectra during the charging event are displayed in Figures 5.7.4a and 5.7.4b. Before and after the charging event, field-aligned suprathermal electron beams are detected at energies below 1 keV. These low energy electron beams may inhibit the charging process since maximum yield for secondary electrons occurs around a few hundred eV energy. Unfortunately the inverted-V peak-energy stayed below or around the crossover-yield-threshold energy for Freja charging (few keV) at these occasions, and no final conclusion could be made regarding the inhibiting influence of these low energy electrons. The inverted-V energy peak during the charging event, on the other hand, is probably even above the maximum measured energy of the TESP instrument (25 keV).

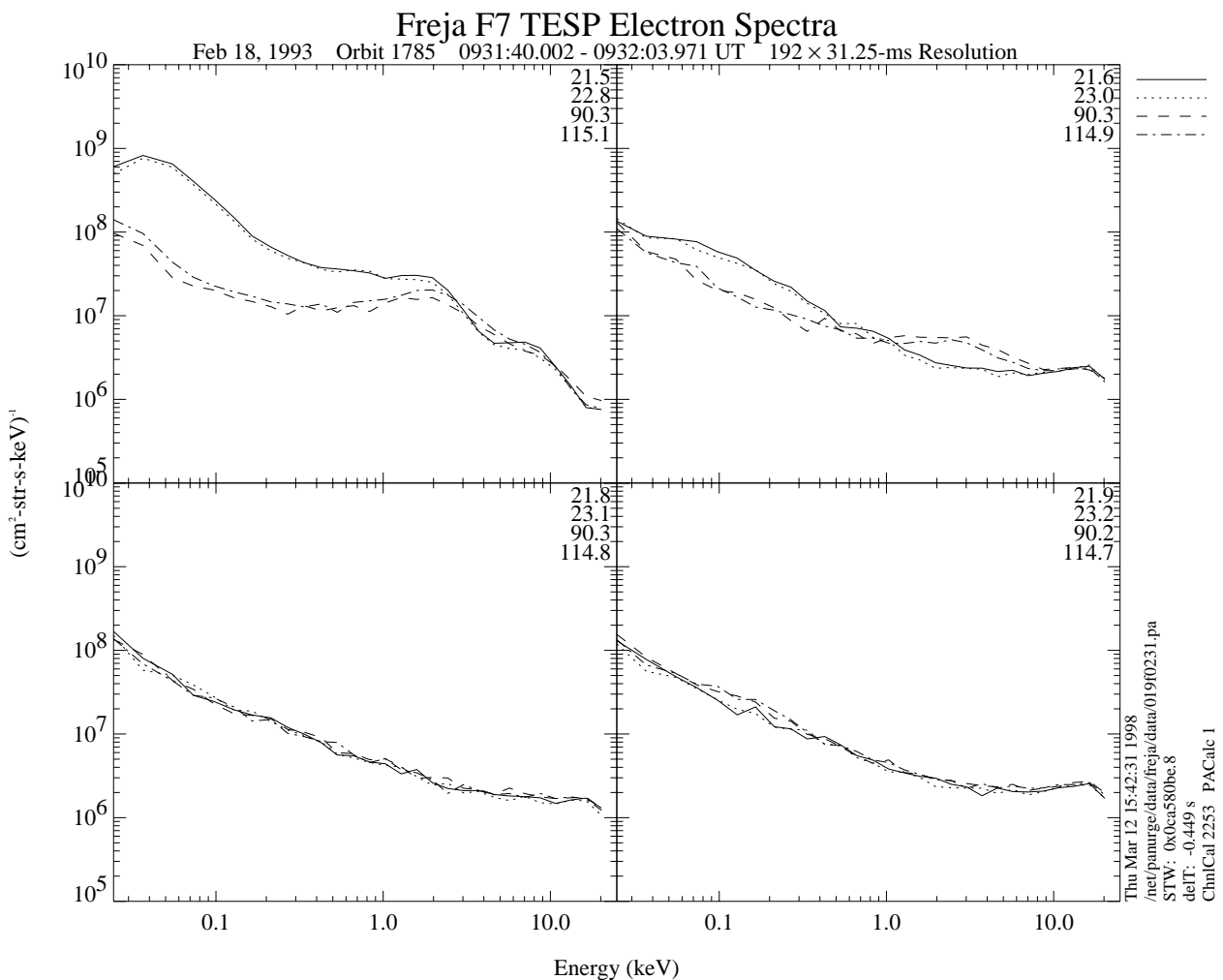


Figure 5.7.4a: TESP electron spectra from the time of the Freja charging event. The inverted-V energy peak reaches up to the maximum measured energy (25 keV) during maximum charging (panel 3).

Detailed ion distributions during the event are shown in Figure 5.7.5a and 5.7.5b. The data is heavily contaminated, most probably by large fluxes of MeV electrons, but charging levels up to -500 V can be inferred.

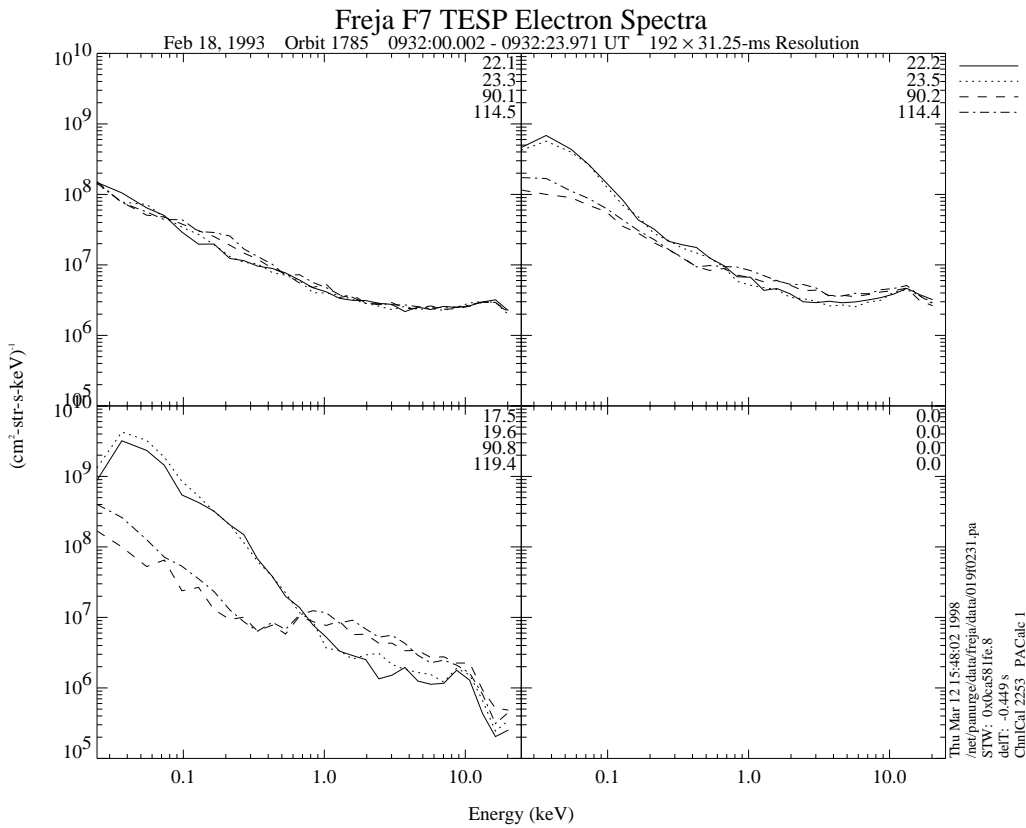


Figure 5.7.4b: TESP electron data. A continuation of Figure 5.7.4a.

FREJA 18 Feb 19930931:33.131 2800-ms Resolution Energy Flu

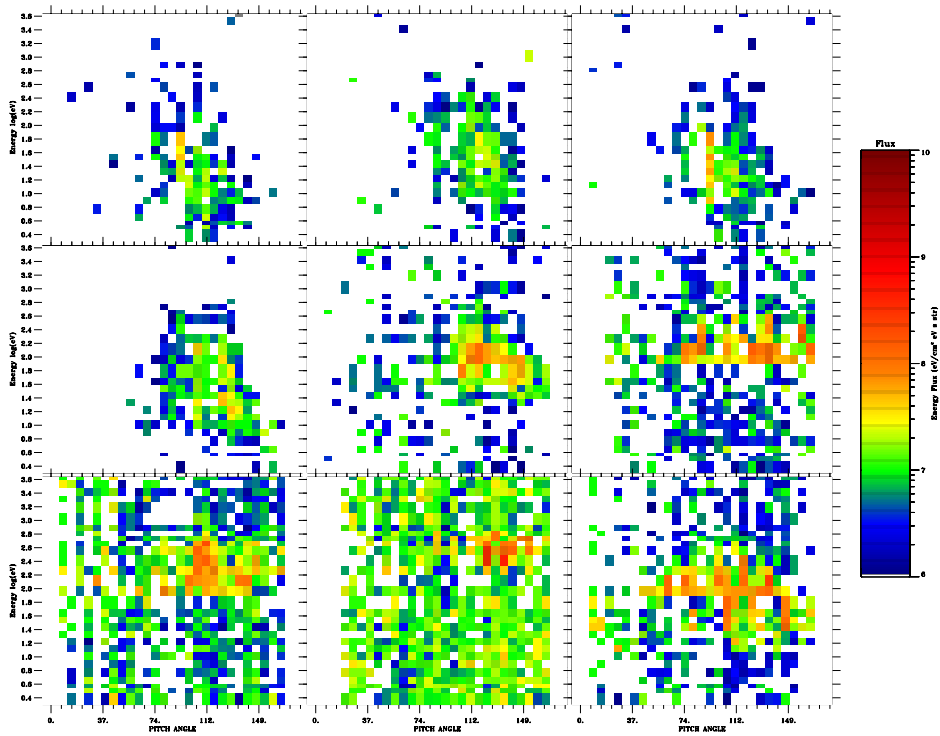


Figure 5.7.5a: Oxygen ion distribution data around maximum charging (panel 8), where negative charging levels of about -500 V can be inferred. The data is heavily contaminated, probably by large fluxes of MeV electrons.

FREJA 18 Feb 19930931:58.333 2800-ms Resolution Energy Flu

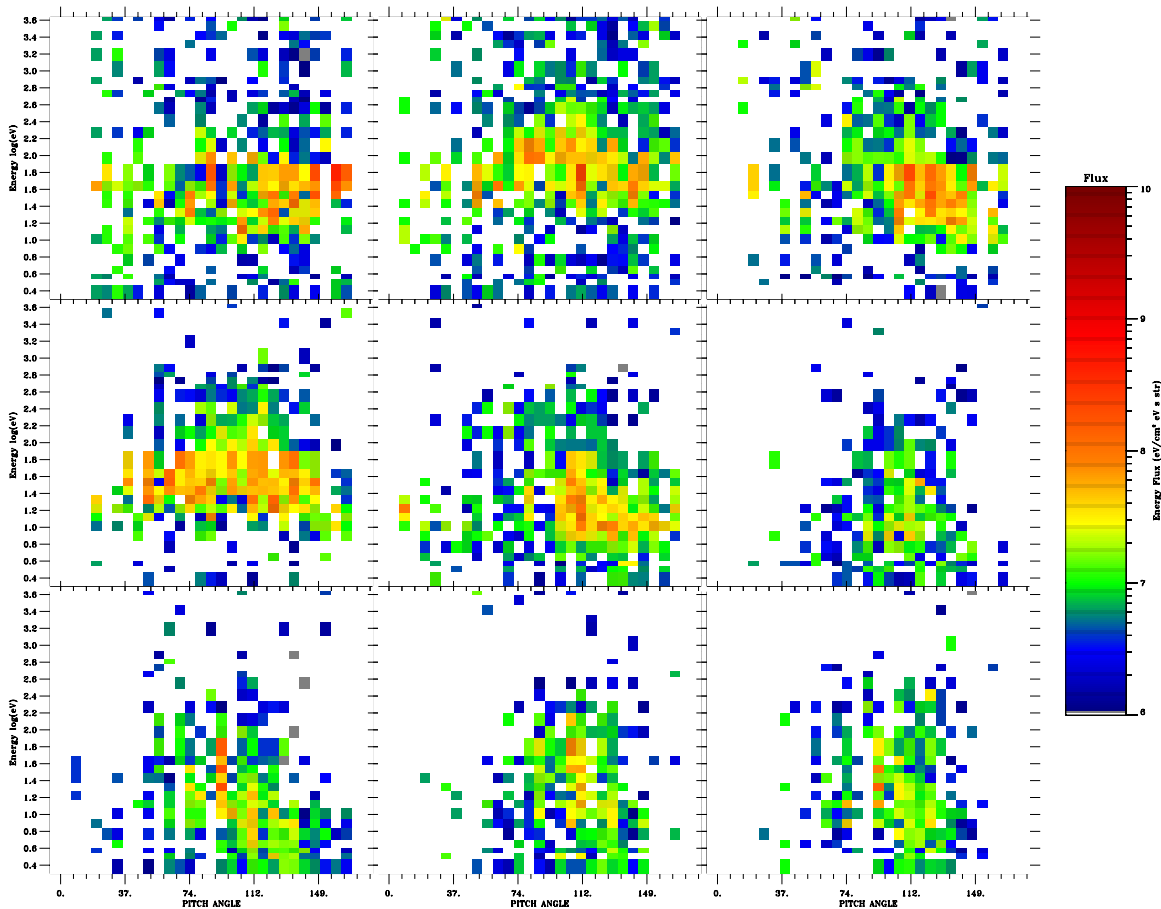


Figure 5.7.5b: Continuation of Figure 5.7.5b.

Conclusions from orbit 1756:

- High level negative charging can occur on Freja when it is situated in sunlight, i.e. despite that large fluxes of photoelectrons are emitted from the spacecraft.
- The inverted-V peak energy is probably above 25 keV and large fluxes of MeV electrons are inferred from the contaminated TICS measurements during maximum charging.
- The plasma density stayed relatively constant during the charging event.
- Charging did not occur if the inverted-V peak energy fell below about a few keV.
- There are instrument disturbances due to the charging events in the Langmuir probe, MF and LF electric, and the TICS measurements.

5.8 EVENT 8: FIVE LOW ALTITUDE SURVEY ORBITS (SUSPECTED CHARGING)

In this section we present the five events of suspected charging of Freja which were found in the low altitude survey orbits (600 - 1000 km). Unfortunately there exist no plasma wave data of reliable quality during these events. These events have been picked out as possible charging events from a database of several hundred low altitude orbits by visual inspection of the survey data. There is no scientific claim made that these low altitude events are real charging events, except for the event on orbit 7945. Neither can we make the claim that charging of Freja is common or not at low altitudes based on this data set. It is merely an indication of that low altitude charging (600 - 1000 km) may indeed have occurred on Freja during auroral conditions. A better study have to wait for the next satellite equipped with suitable instruments, *Astrid 2*, to be launched during December, 1998, into a low altitude polar orbit (about 1000 km).

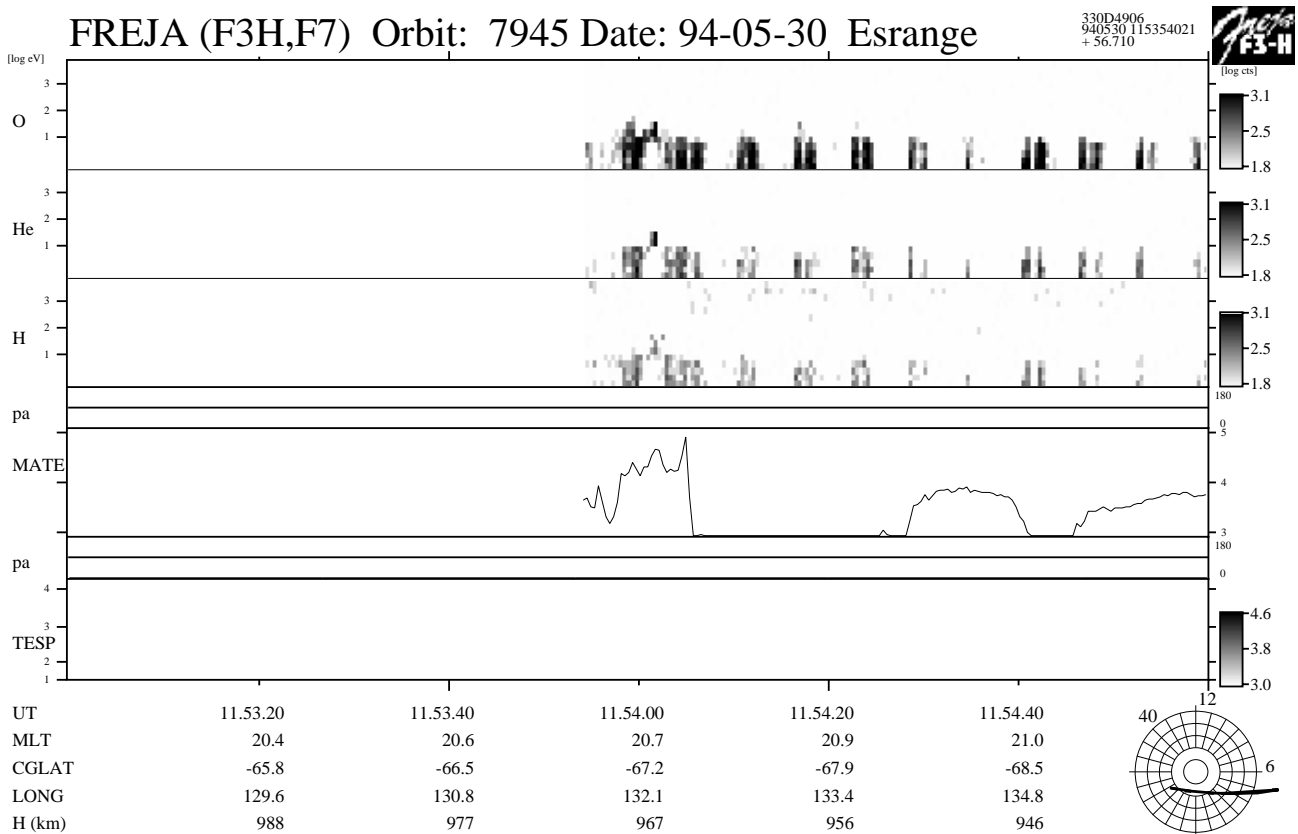


Figure 5.8.1: Orbit 7945. A weak (-10 V) short lived charging event at an altitude of 970 km. The event occurred during eclipse.

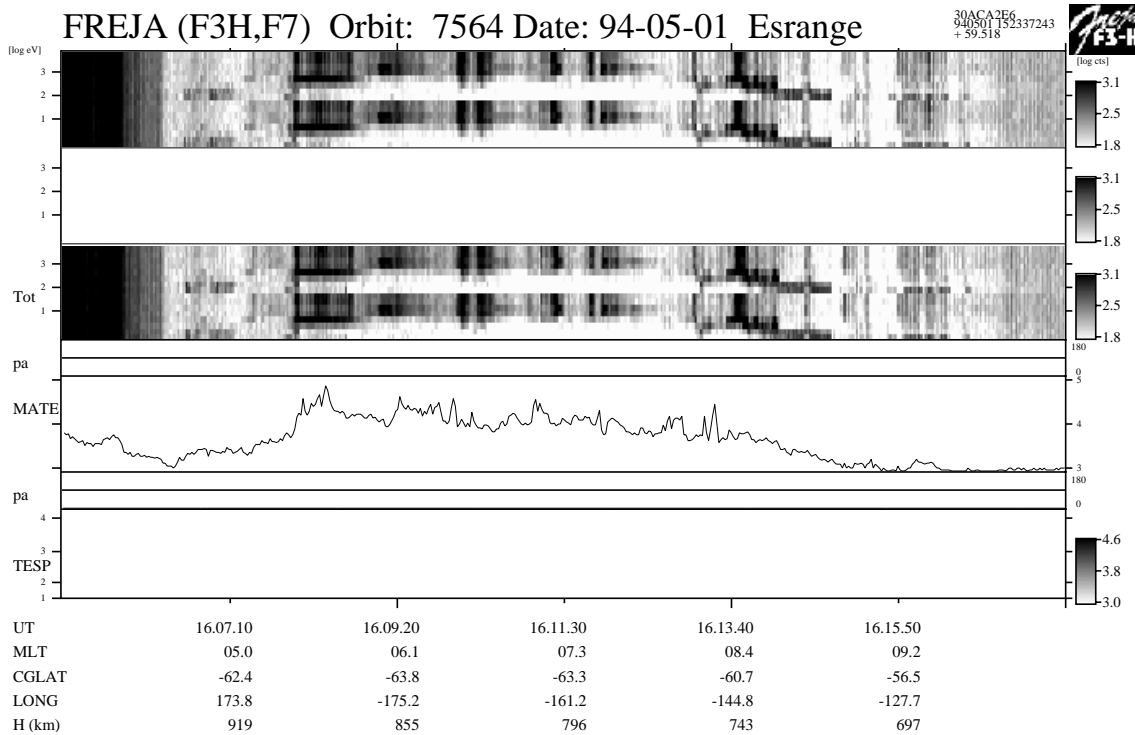


Figure 5.8.2: Orbit 7564. The ion data were unfortunately copied to the high energy part by mistake. The lower portion of the ion data is the correctly measured data, and a possible long duration charging event of about -10 V can be seen. The high energy (MATE) integrated electron flux indicate that high energy electrons could have been present during most of this event. The event occurred mainly in sunlight (from about 1609:00 UT). The altitude varies between 740 km - 900 km.

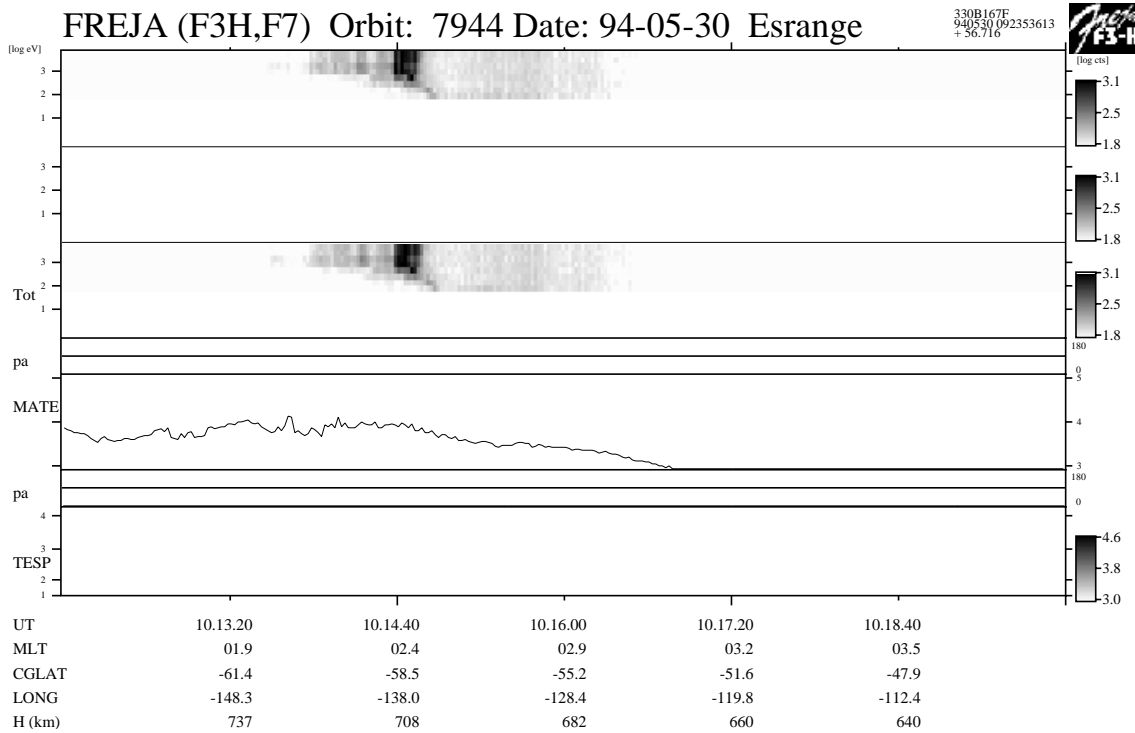


Figure 5.8.3: Orbit 7944. A possible charging event in eclipse near 1014:00 UT (700 km), which is associated with a significant integrated energetic electron flux as measured by the MATE instrument. Charging up to several hundred Volts negative could be inferred if this is a charging event. The event could also be due to ion precipitation.

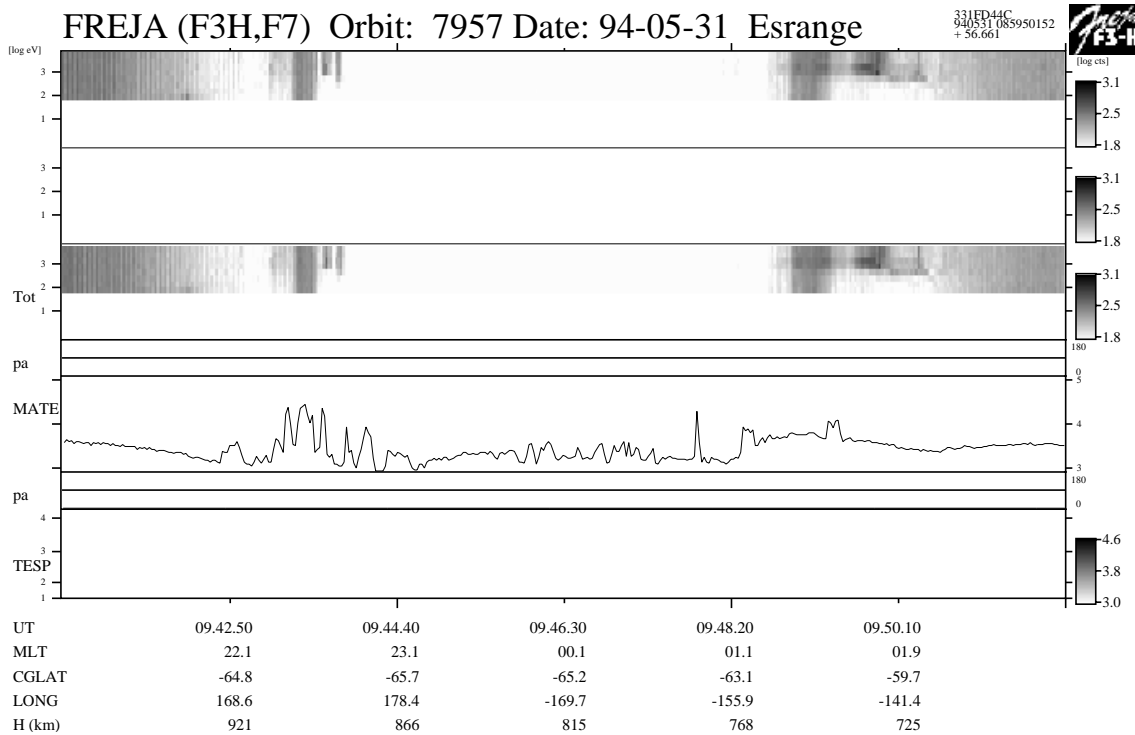


Figure 5.8.4: Orbit 7957. Possible charging event in eclipse near 0943:30 UT and near 0950:00 UT (more probable). Inferred charging levels would in that case be several hundred Volts negative. The first event have an integrated energetic electron flux more characteristic of field-aligned electron bursts (i.e. not charging), while the later event have characteristics of more stable inverted-V type electron precipitation. The events occurred at altitudes around 900 km and 725 km respectively.

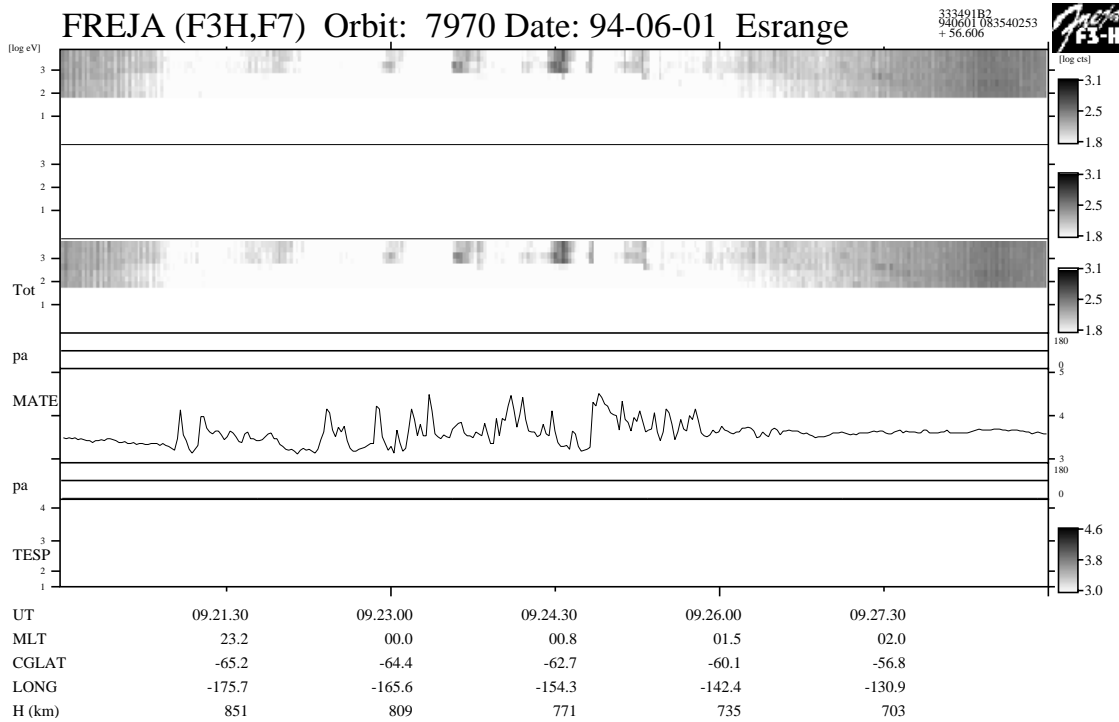


Figure 5.8.5: Orbit 7970. Possible multiple charging events in eclipse of about a few hundred Volts negative. However, the integrated energetic electron flux as measured by the MATE detector (panel 5) show fluctuating characteristics usually more related to low energy field-aligned electron bursts. The altitudes varies between 725 km - 875 km.

5.9 EVENT 9: ORBIT 736 (VARIATION WITH PLASMA DENSITY)

Overview Data, 92.12.01, Esrange

The overview data for the particle measurements from orbit 736 are presented in Figure 5.9.1, and in somewhat more detail in 5.9.2. Three consecutive charging events occur during eclipse in the time period 0034:30 - 0038:00 UT, and all three events are associated with apparently similar energetic electron spectra. Despite this fact, the first charging event near 0035:20 UT reaches a somewhat larger charging level (-50 V) than the two that follows (-5 to -10 V, at 0035:50 UT and 0037:10 UT respectively). The middle event have a somewhat lower electron peak energy, but somewhat larger electron peak flux.

The plasma wave data is presented in Figure 5.9.3. The electron densities during the three events as inferred from the narrow-band HF emissions are $1.0\text{-}1.5\cdot 10^8\text{ m}^{-3}$, $7\text{-}8\cdot 10^8\text{ m}^{-3}$ and $5\cdot 10^8\text{ m}^{-3}$ respectively. Thus, a factor of 5-8 in density increase is associated with a decrease in the charging level by a factor 5-10. Thus, the electron density might determine the charging level to a greater extent during this event.

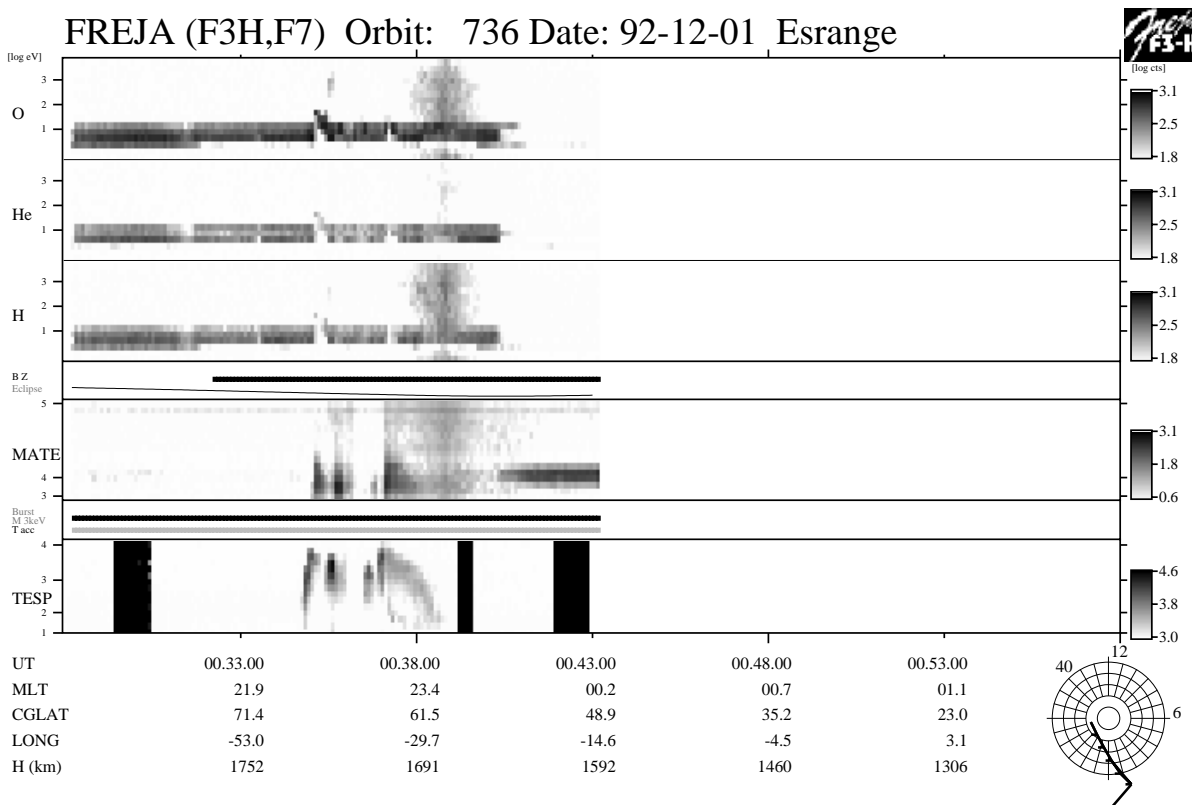


Figure 5.9.1: Overview particle data for orbit 736. Three consecutive relatively low level charging events exist between 0034:00 UT - 0038:00 UT during eclipse conditions. Both MATE (panel 5) and TESP (panel 7) electron data existed during this orbit.

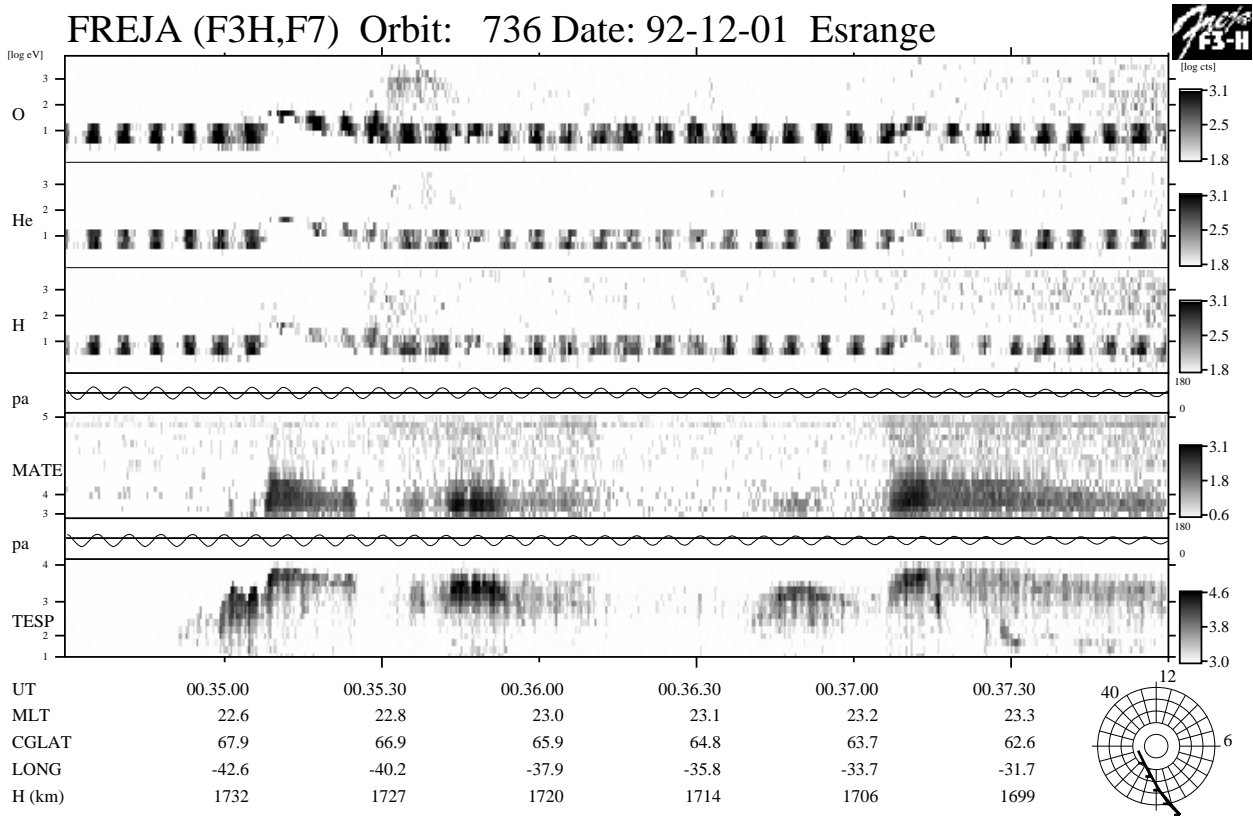
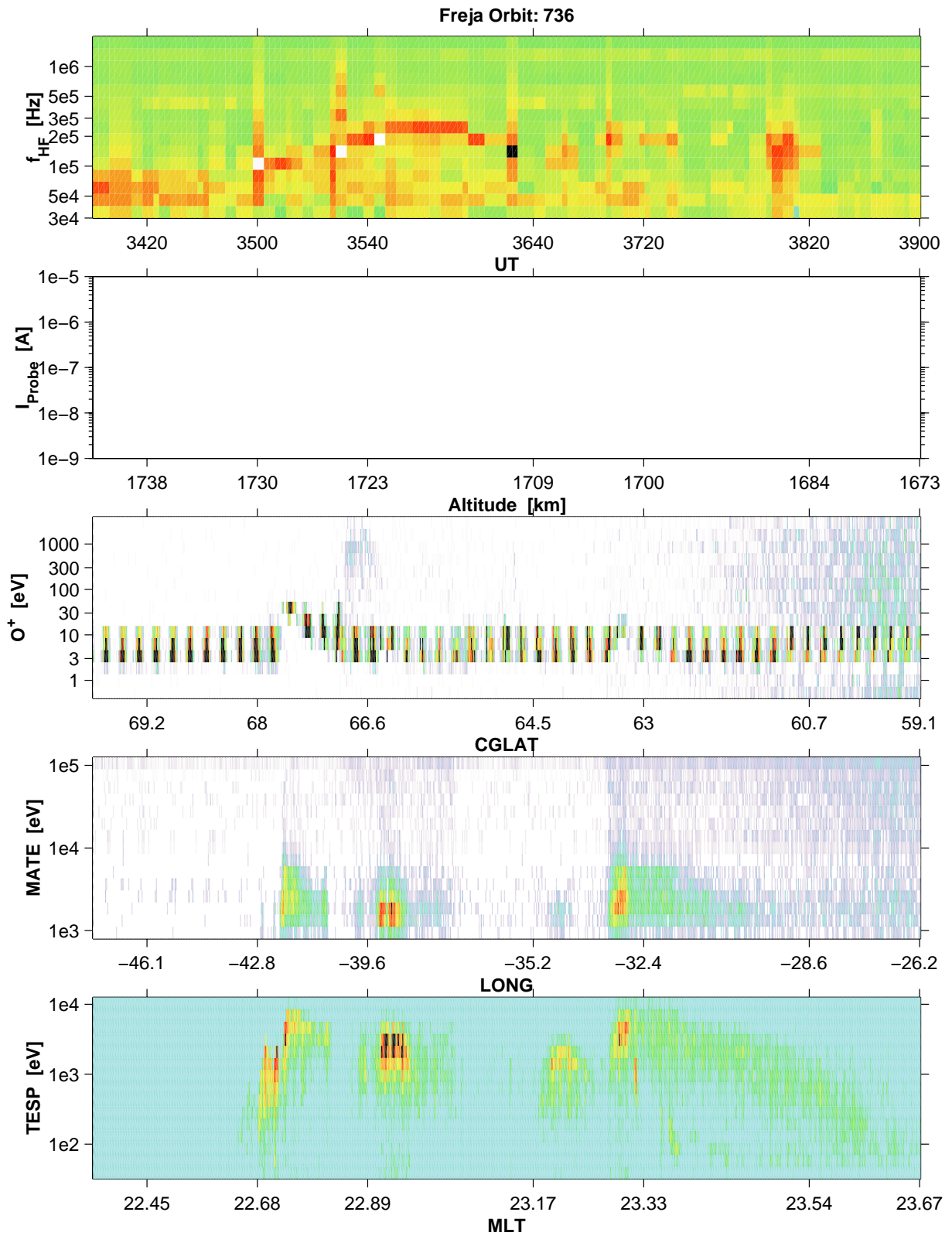


Figure 5.9.2: Three charging events exist around 0035:15 UT, 0035:50 UT, and 0037:15 UT. The electron characteristics appear to be rather similar for these three events (panels 5 and 7).



736

Figure 5.9.3: The electron densities as estimated from the narrow-band HF emissions vary with a factor 5-8, at the same time as the charging level changes by a factor 5-10 (Figure 5.9.2, panels 1-3).

Detailed Particle Distributions

TESP and MATE electron spectra for the charging events are presented in Figures 5.9.4a-d and 5.9.5a-d respectively. Figure 5.9.4a-c shows how the TESP spectra for the first event evolves toward a clear inverted-V type spectra (Figure 5.9.4b, panel 4) with peak energy around 7 - 8 keV for the first event. The electron flux near 1 keV actually decreases at that time. A high energy tail up to about 50 keV is simultaneously developed in the MATE spectra (Figure 5.9.5a, panel 4). The second event (Figure 5.9.4d, panel 2-3) do not reach the same peak energies (more like 3 keV), but has an order of magnitude larger peak flux than the first and the energetic tail is not so developed. It might be so that this larger energetic tail component in the first event is the cause of the charging level difference between the two events. The difference in electron density, i.e. thermal ion return current, might be another reason for the charging level difference. The MATE data from the third event is very similar in its characteristics as the MATE spectra from the first event, and only the difference in plasma density and charging level seems to differ the first and the third events. The TICS data (figure 5.9.1a-c) reveal charging levels of -70 V for the first case and -12 V for the second case.

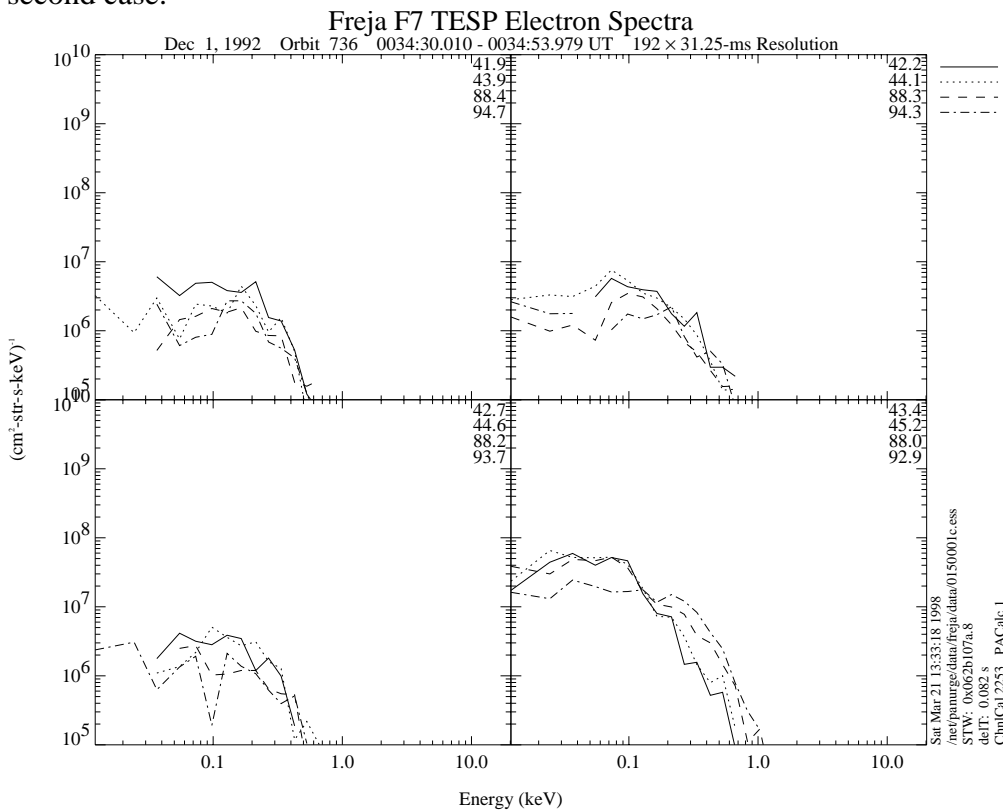


Figure 5.9.4a: TESP and MATE electron spectra for the three charging events are presented in Figures 5.9.4a-d, and Figures 5.9.5a-d. The TESP spectra for the first event evolves toward a clear inverted-V type spectra (panel 4, Figure 5.9.4b) with peak-energy of about 7-8 keV, to be relaxed again in Figure 5.9.4c. The second event is associated with a lower peak energy of about 3-4 keV, but larger flux levels. The MATE spectra of the first event (Figures 5.9.5a-b) show very much the same characteristics as the MATE spectra for the third event (Figures 5.9.5c-d).

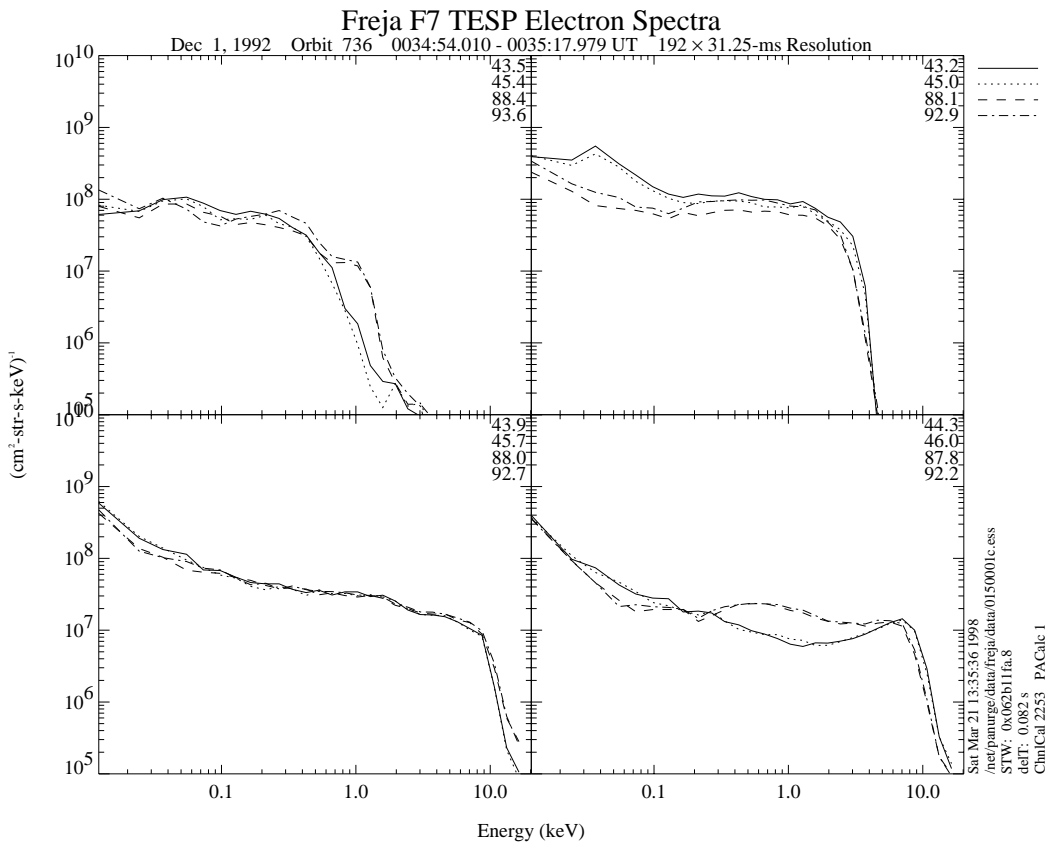


Figure 5.9.4b: TESP spectra from first charging event. See text Figure 5.9.4a.

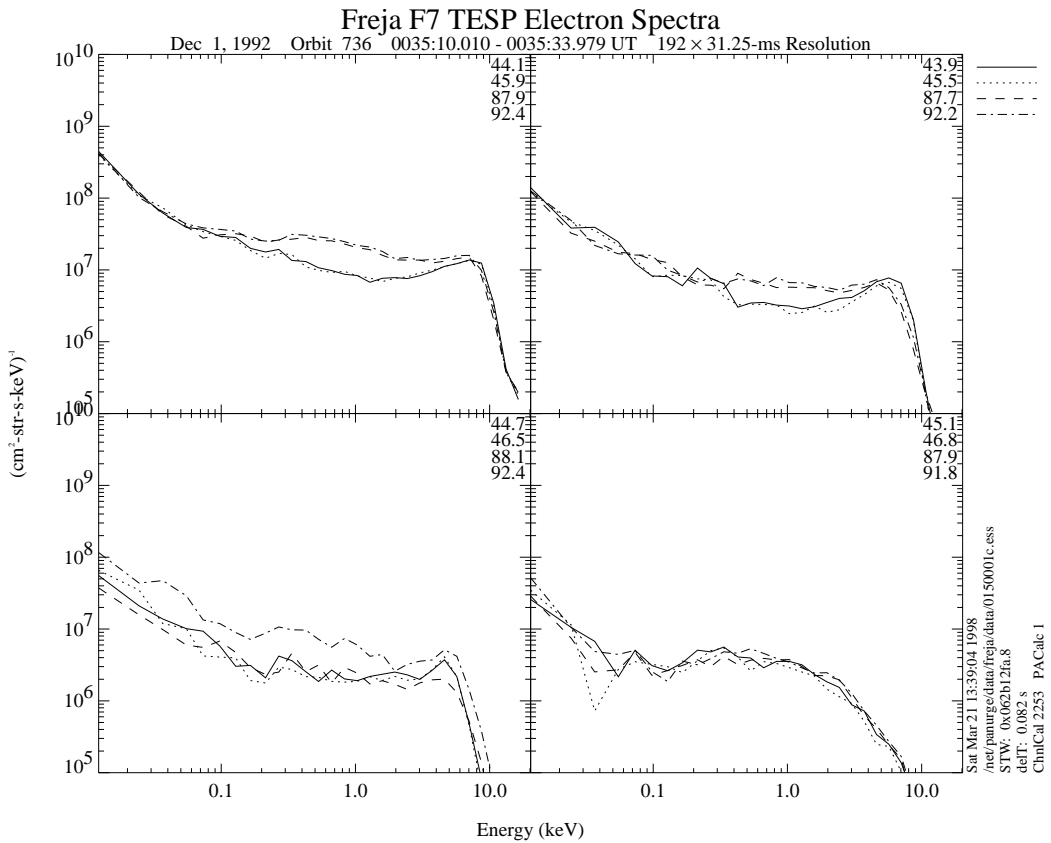


Figure 5.9.4c: TESP spectra from first charging event. See text Figure 5.9.4a.

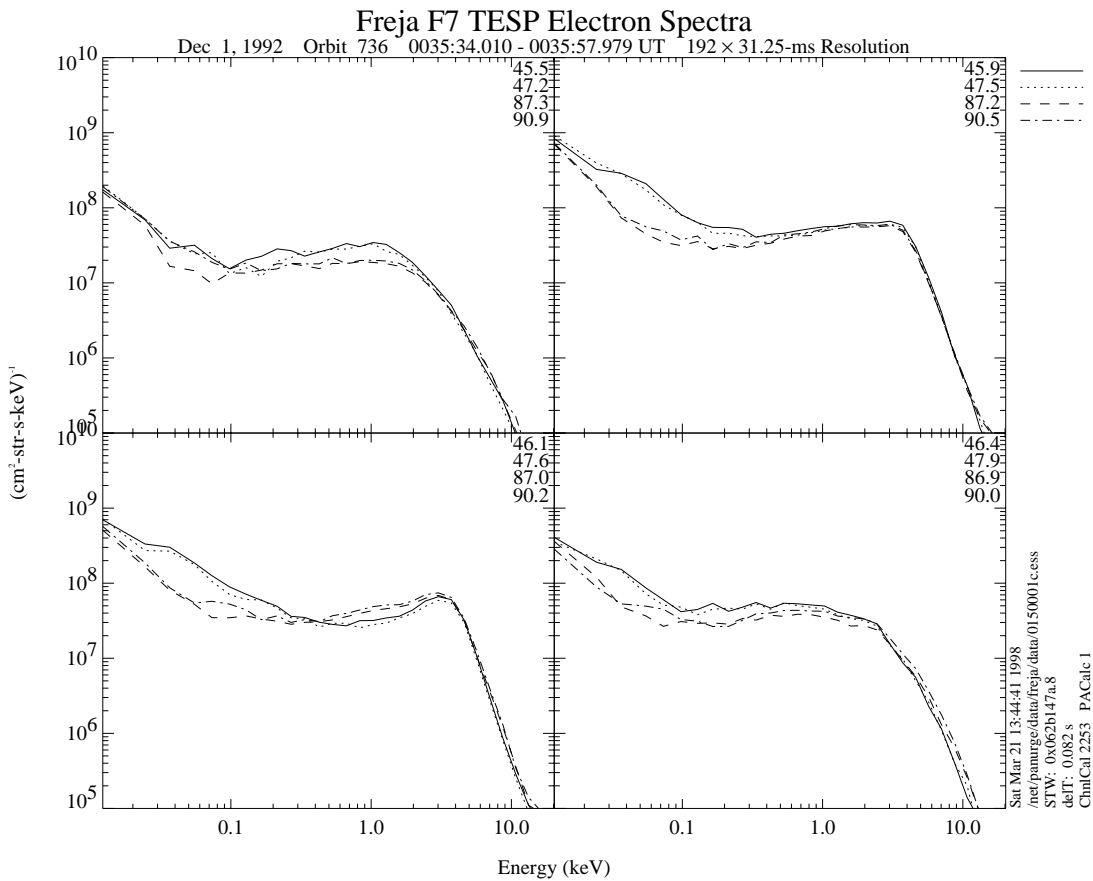


Figure 5.9.4d: TESP spectra from second charging event. See text Figure 5.9.4a.

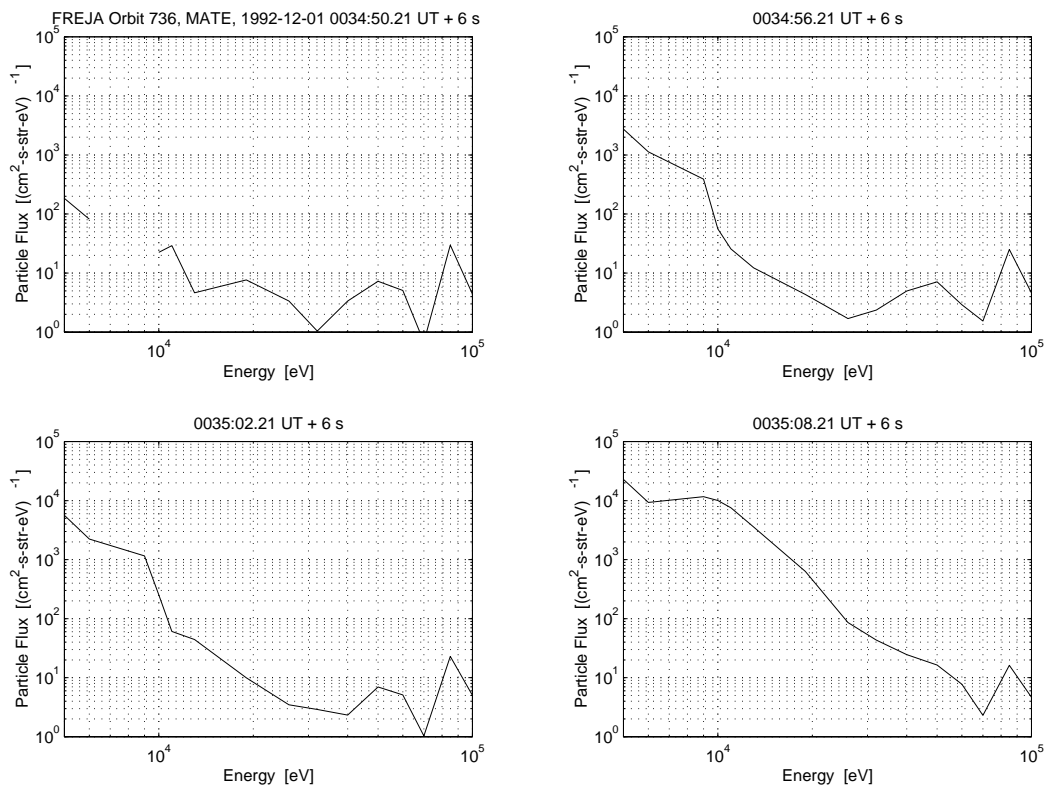


Figure 5.9.5a: MATE spectra from first event. See text Figure 5.9.4a.

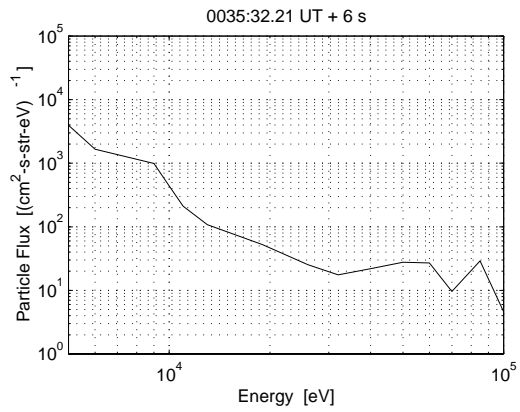
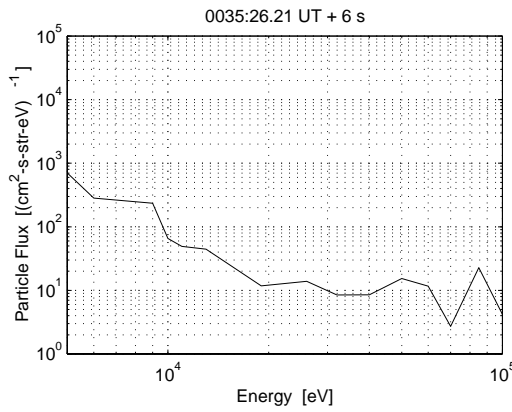
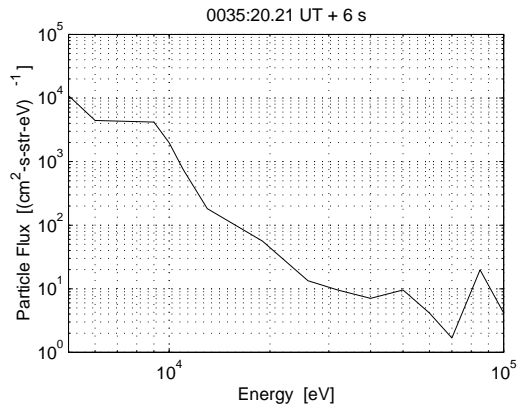
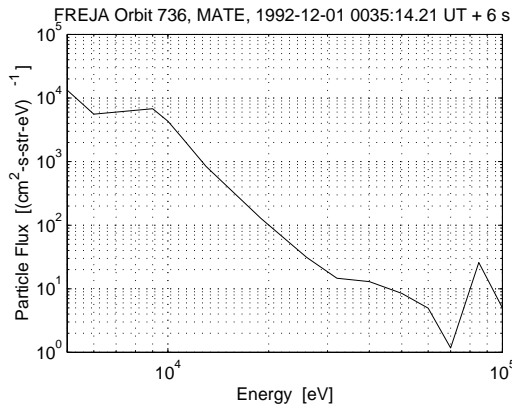


Figure 5.9.5b: MATE spectra from first event. See text Figure 5.9.4a.

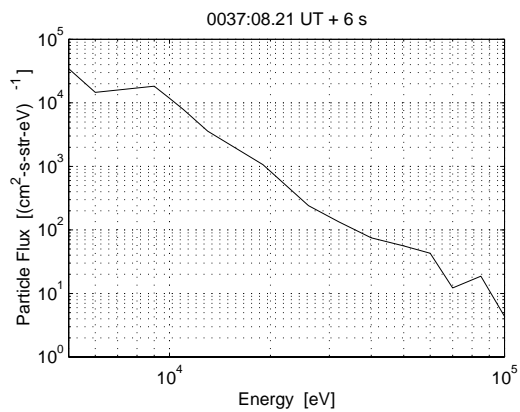
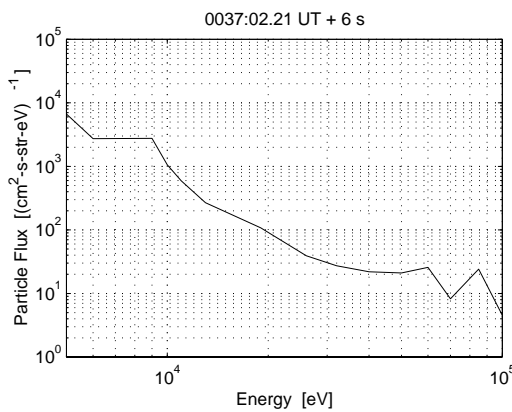
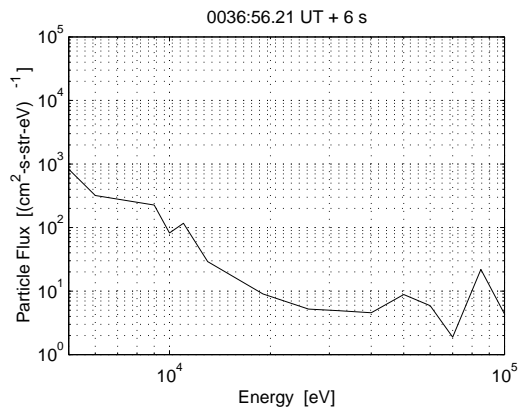
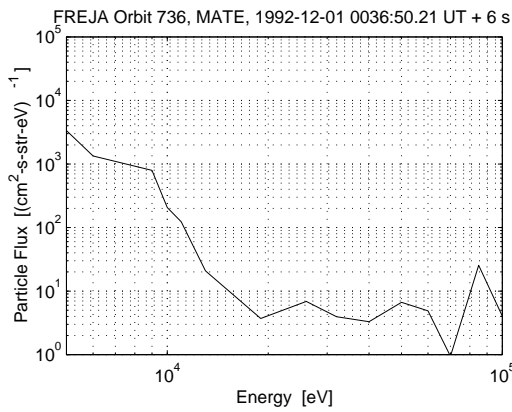


Figure 5.9.5c: MATE spectra from third event. See text Figure 5.9.4a.

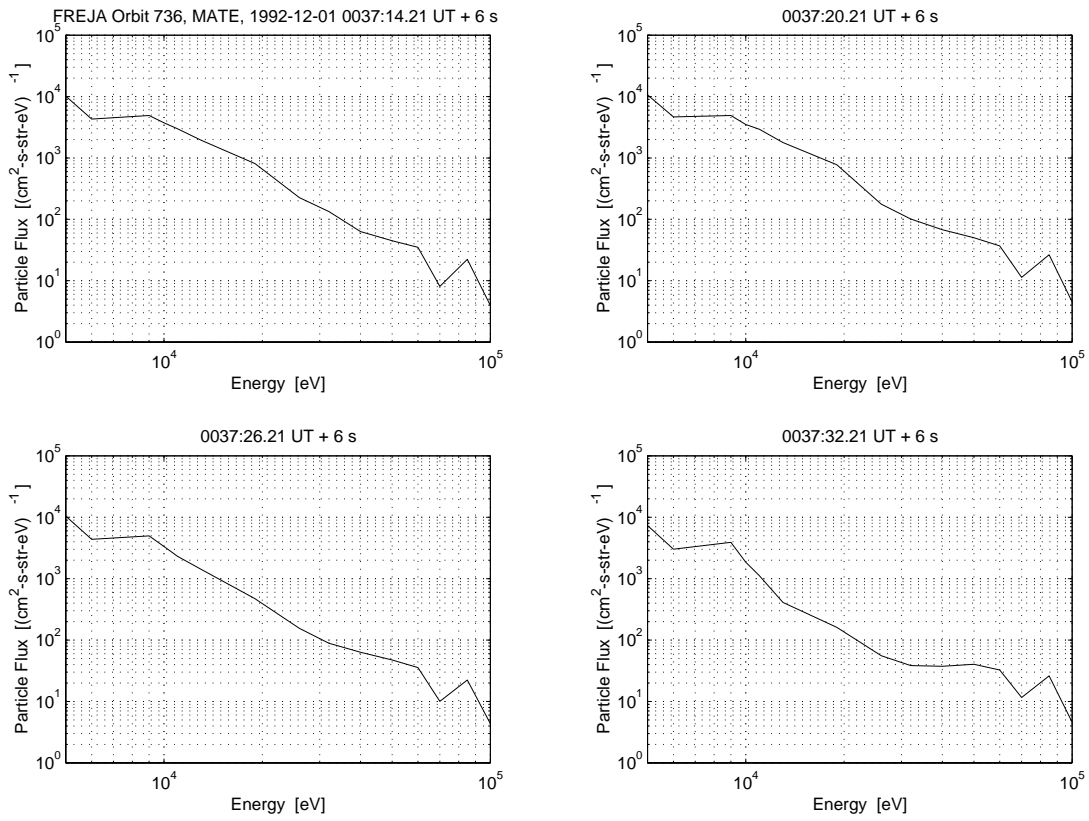


Figure 5.9.5d: MATE spectra from third event. See text Figure 5.9.4a.

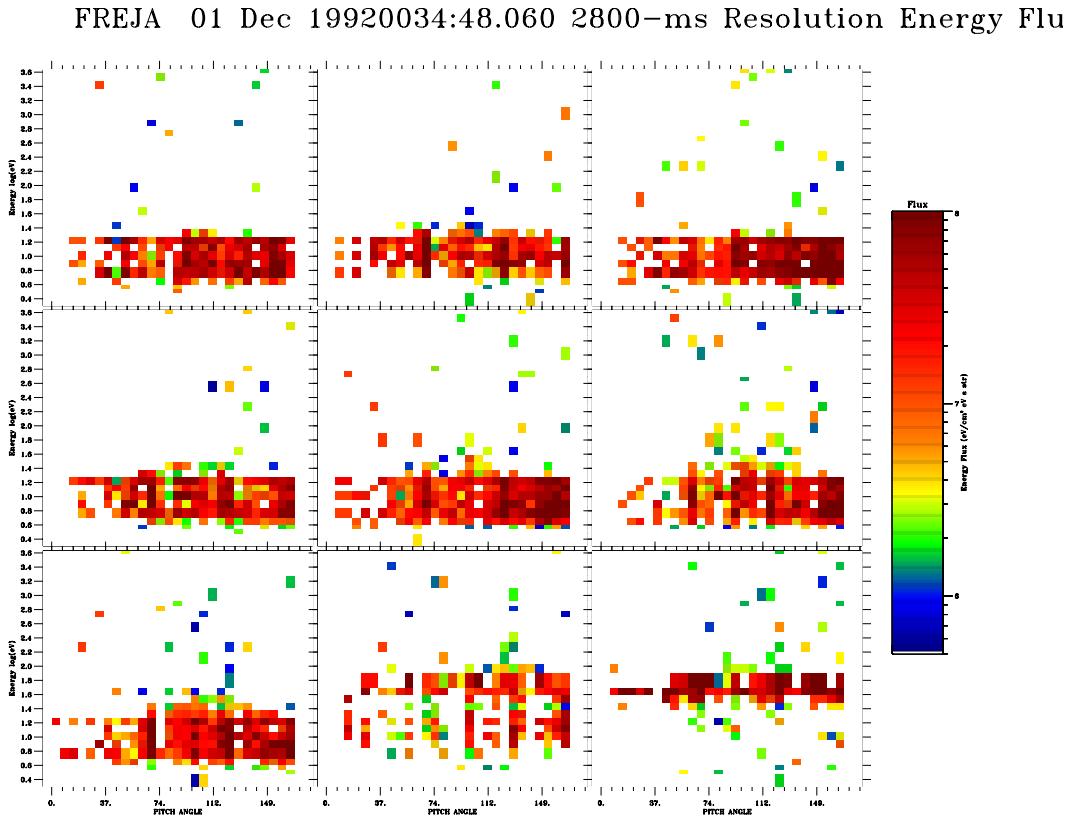


Figure 5.9.6a: Oxygen ion distributions for the first charging event. Negative charging levels of -70 V is inferred.

FREJA 01 Dec 19920035:13.261 2800-ms Resolution Energy Flu

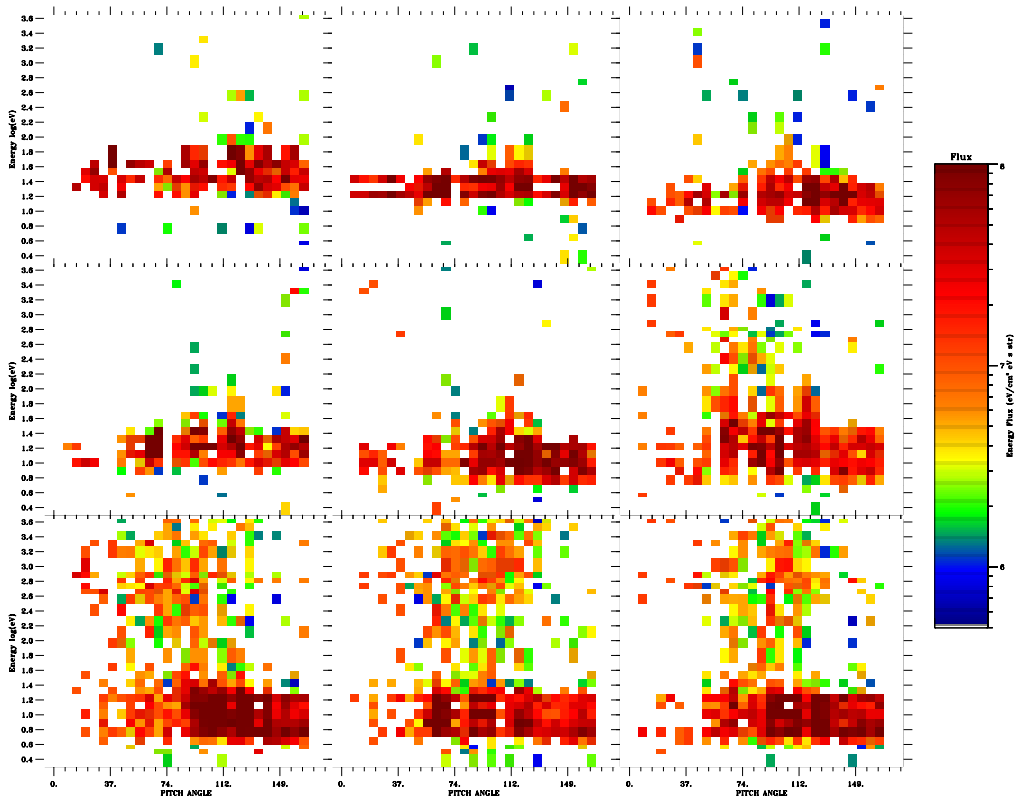


Figure 5.9.6b: Continuation of Figure 5.9.6a.

FREJA 01 Dec 19920035:38.463 2800-ms Resolution Energy Flu

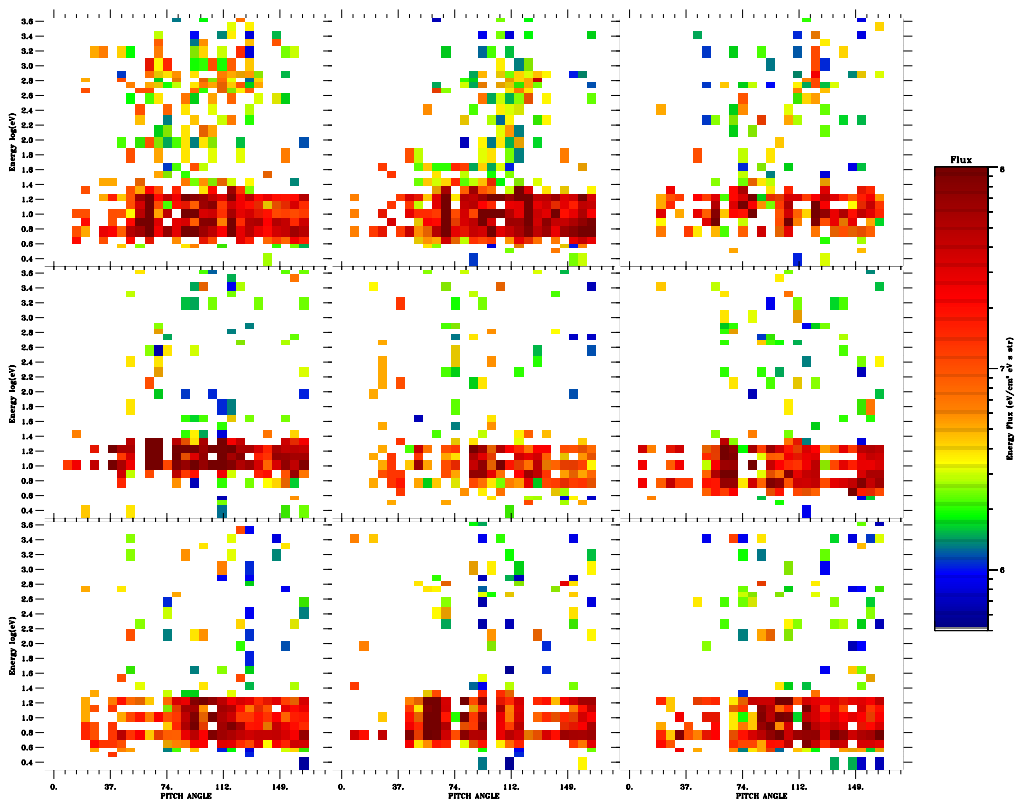


Figure 5.9.6c: Oxygen ion distributions for the second charging event. Negative charging levels of -12 V is inferred.

Conclusions from orbit 736:

- Three cases of Freja charging with rather similar inverted-V electron spectra revealed that the ambient plasma density may affect the charging levels. A change in density by a factor 5-8 seemed to be associated with a change in charging level by a factor 5-10.

5.10 EVENT 10: ORBIT 7279 (LOW ALTITUDE CHARGING)

Overview Data, 94.04.10, Prince Albert

The overview data for the particle measurements from orbit 7279 are presented in Figure 5.10.1, and in somewhat more detail in Figure 5.10.2. The charging event occurs at the rather low altitude of 1395 km during sunlight conditions near 0138:20 UT, which is verified by the UV photometer data (Figure 5.10.3, see also SPEE-WP130-TN). It is the lowest altitude charging event with high resolution Freja data.

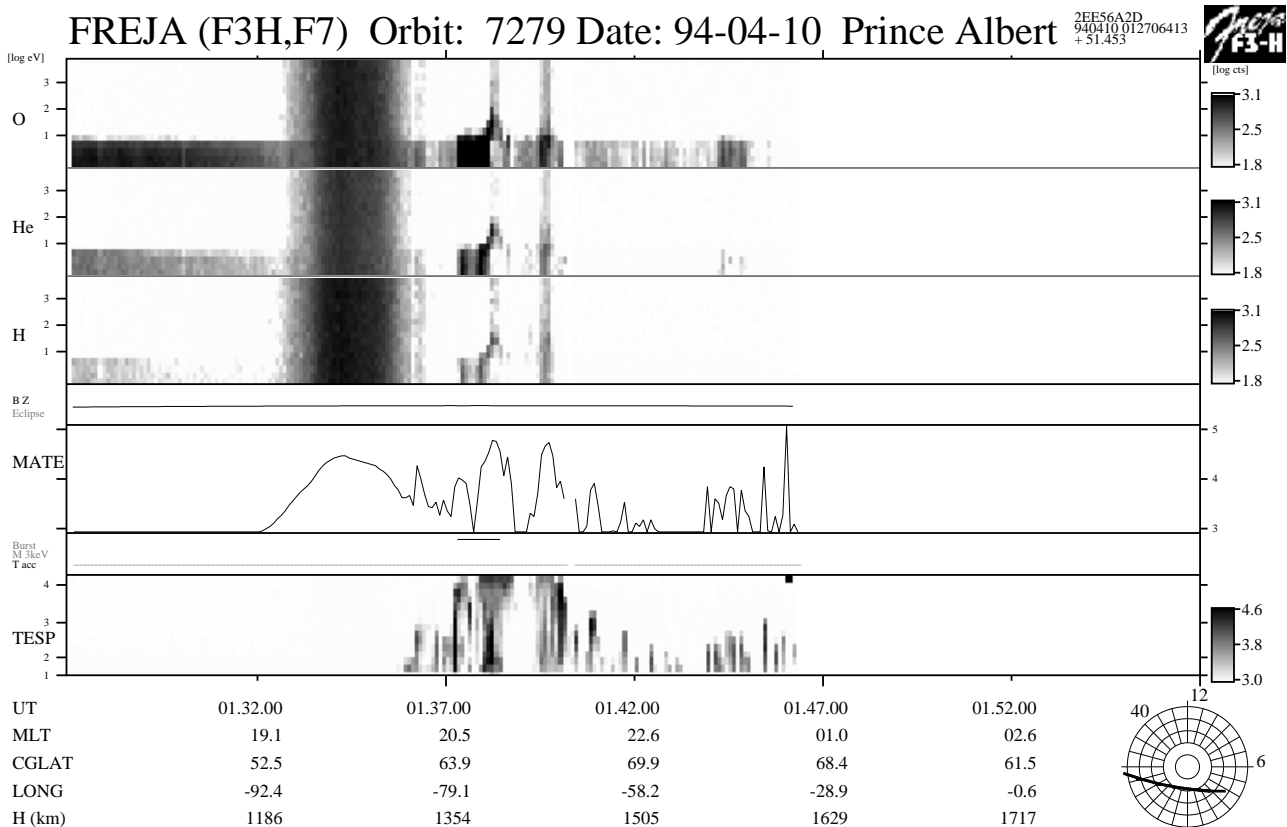


Figure 5.10.1: Overview of the particle data from orbit 7279. The charging event around 0138:20 UT represents the lowest in altitude clearly identified Freja charging event. The event occurs at an altitude of about 1395 km and occurs during sunlight conditions.

The ions (panels 1-3) are lifted to about 20 eV, and a clear inverted-V electron event with superposed low energy suprathermal electron bursts below the inverted-V energies occurs at the same time. The MATE measures only the integrated flux during this orbit. High energy electrons in the MeV range seems to occasionally contaminate the ion data during the charging event. It is interesting to note that the charging increases to its max levels when these supposed MeV electrons exist, while the inverted-V electron spectra just below 25 keV remains constant in its characteristics during the whole charging event. Alternatively, the charging may be inhibited by the lower energy suprathermal electron bursts, by producing secondary electron emission from the Freja surface. The larger charging levels, in fact, occur after these bursts.

An other clear inverted-V event with an even larger peak energy occurs around 0139:40 UT. This later event seems also associated with MeV electrons as indicated from the TICS contamination. Not surprisingly, there is a detectable charging event around this time, even though it is of much lower charging level as compared to the first charging event.

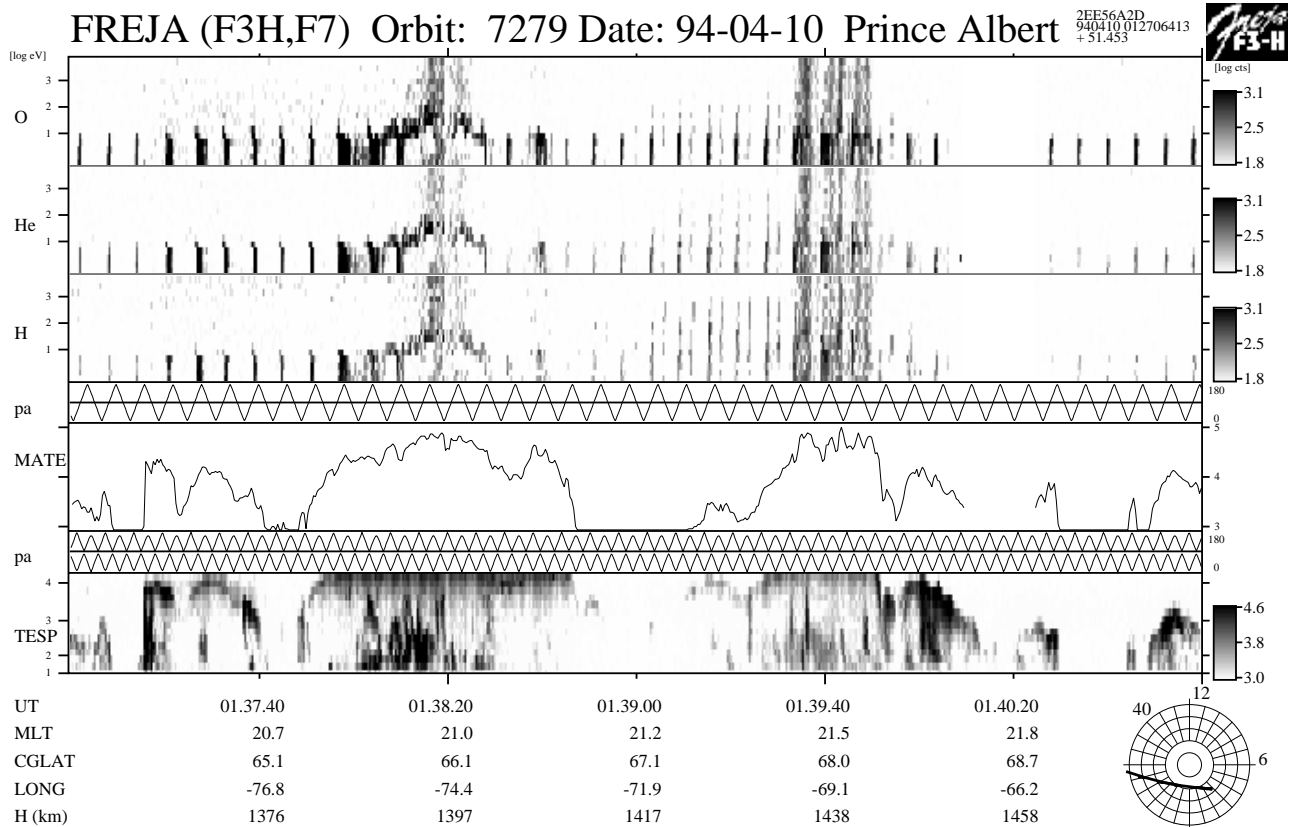


Figure 5.10.2: A blow up of the particle data around the charging event around 0138:20 UT. A clear inverted-V electron event occurs at the same time. The ion channels are contaminated probably by large fluxes of MeV electrons. A similar event which do not seem to be associated with charging occurs around 0139:40 UT.

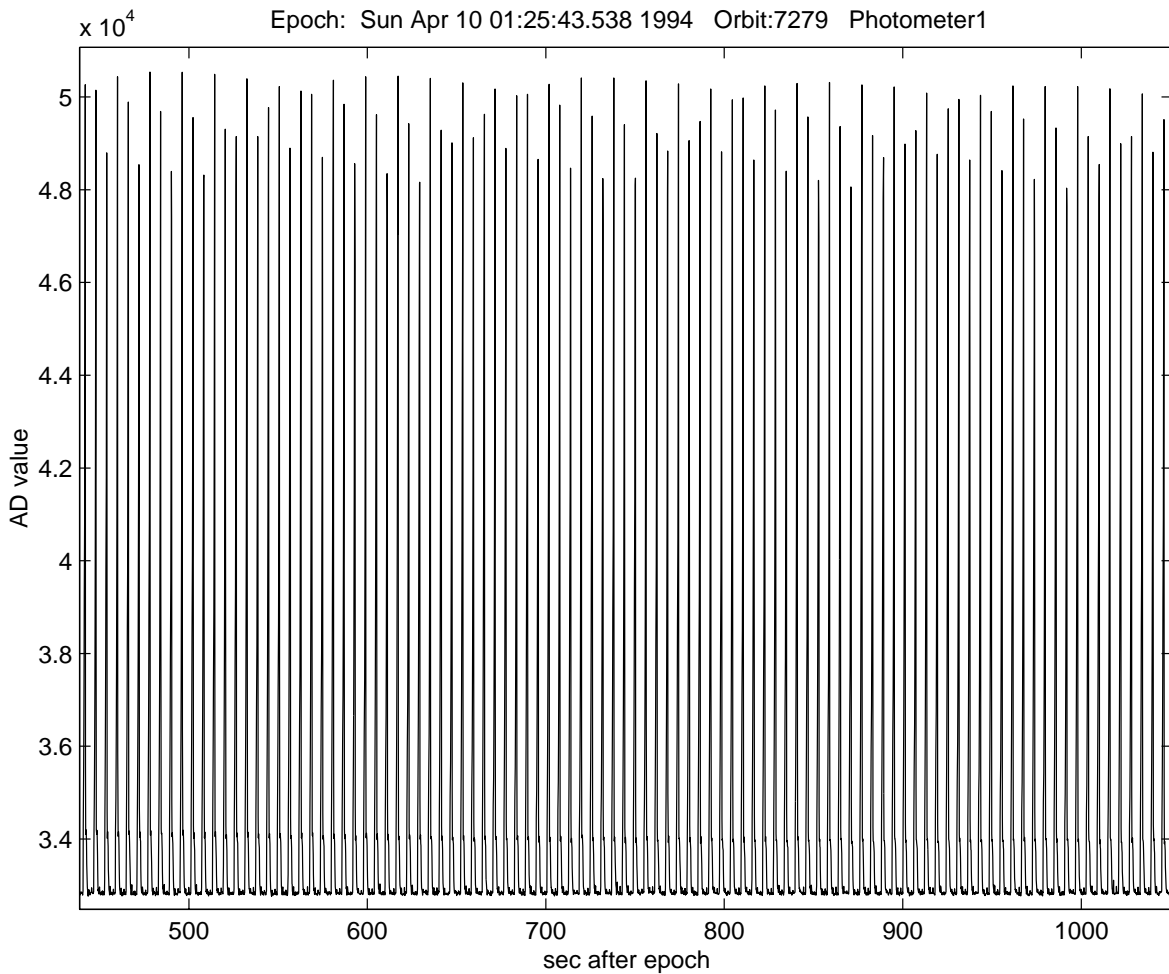
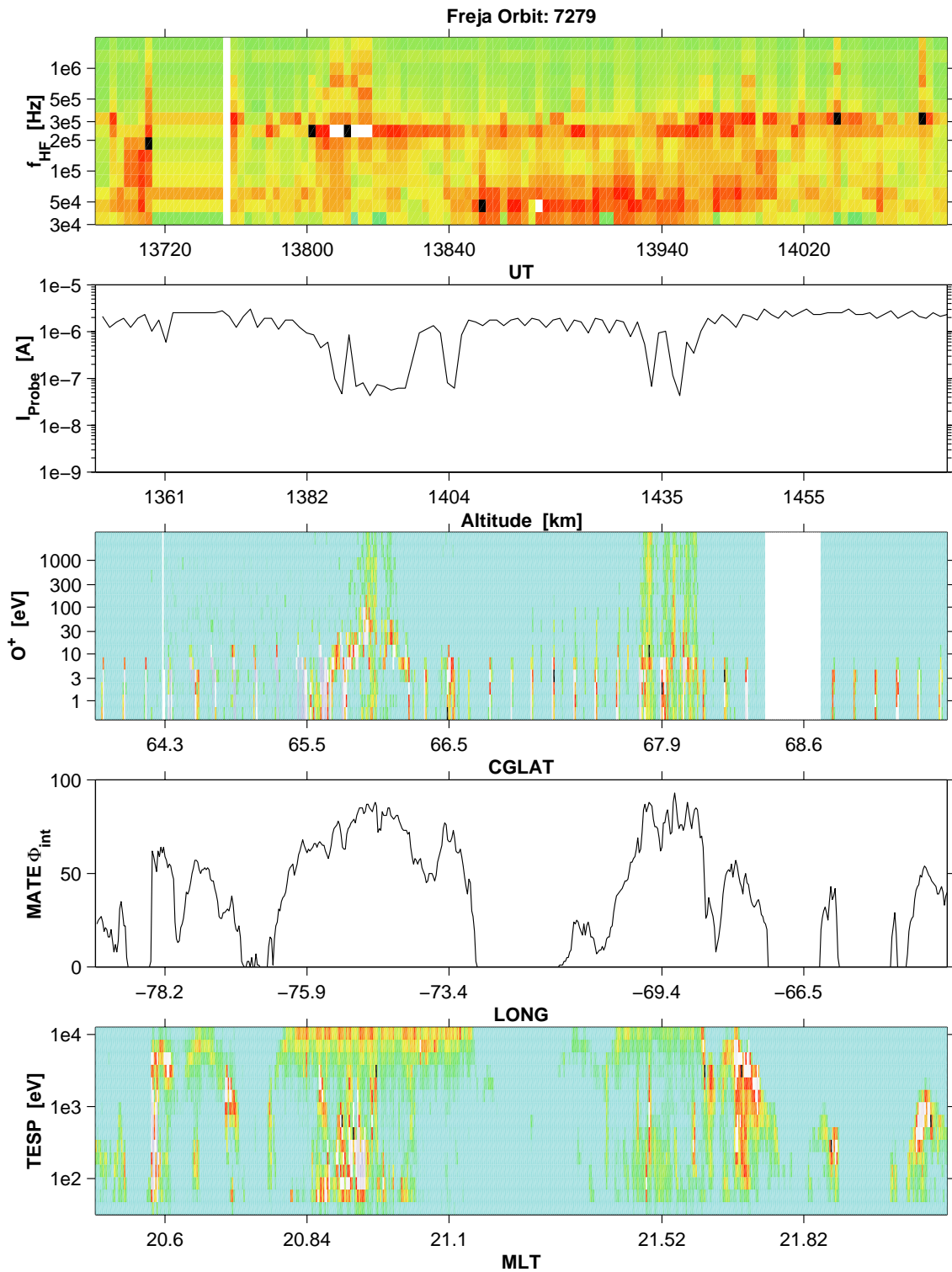


Fig 5.10.3: Photometer data from orbit 7279. Sunlight conditions exist for the whole charging event (750 s to 850 s).

The plasma wave data is displayed in Figure 5.10.4. The inferred density from the narrow-band HF emissions amounts to $7\text{-}8 \cdot 10^8 \text{ m}^{-3}$, which is somewhat lower than the inferred LP density of about $1\text{-}2 \cdot 10^9 \text{ m}^{-3}$ outside the charging events.



7279

Figure 5.10.4: Plasma wave data corresponding to the particle data in Figure 5.10.2. Rather large plasma densities of close to 10^9 m^{-3} are inferred from the HF narrow-band Langmuir emissions and Langmuir probe current just outside the charging event. Such plasma densities are unusual during charging events, even though densities generally encountered by Freja are a few times this value.

Detailed Particle Distributions

The detailed TESP electron spectra for the time period 0137:48 - 0138:36 UT is displayed in Figures 5.10.4a and 5.10.4b. Unusually many field-aligned suprathermal electron bursts exist below a few keV during this event. Such electron bursts are not common during charging events and are probably unrelated to them since such electrons presumably would rather inhibit the charging process than enhancing it. The inverted-V energy peak is located close to or above the maximum possible measured energy (25 keV). One of the displayed TESP sectors (near 168° pitch-angle) is within the atmospheric loss cone, and therefore shows much lower flux levels above 2 - 3 keV energy.

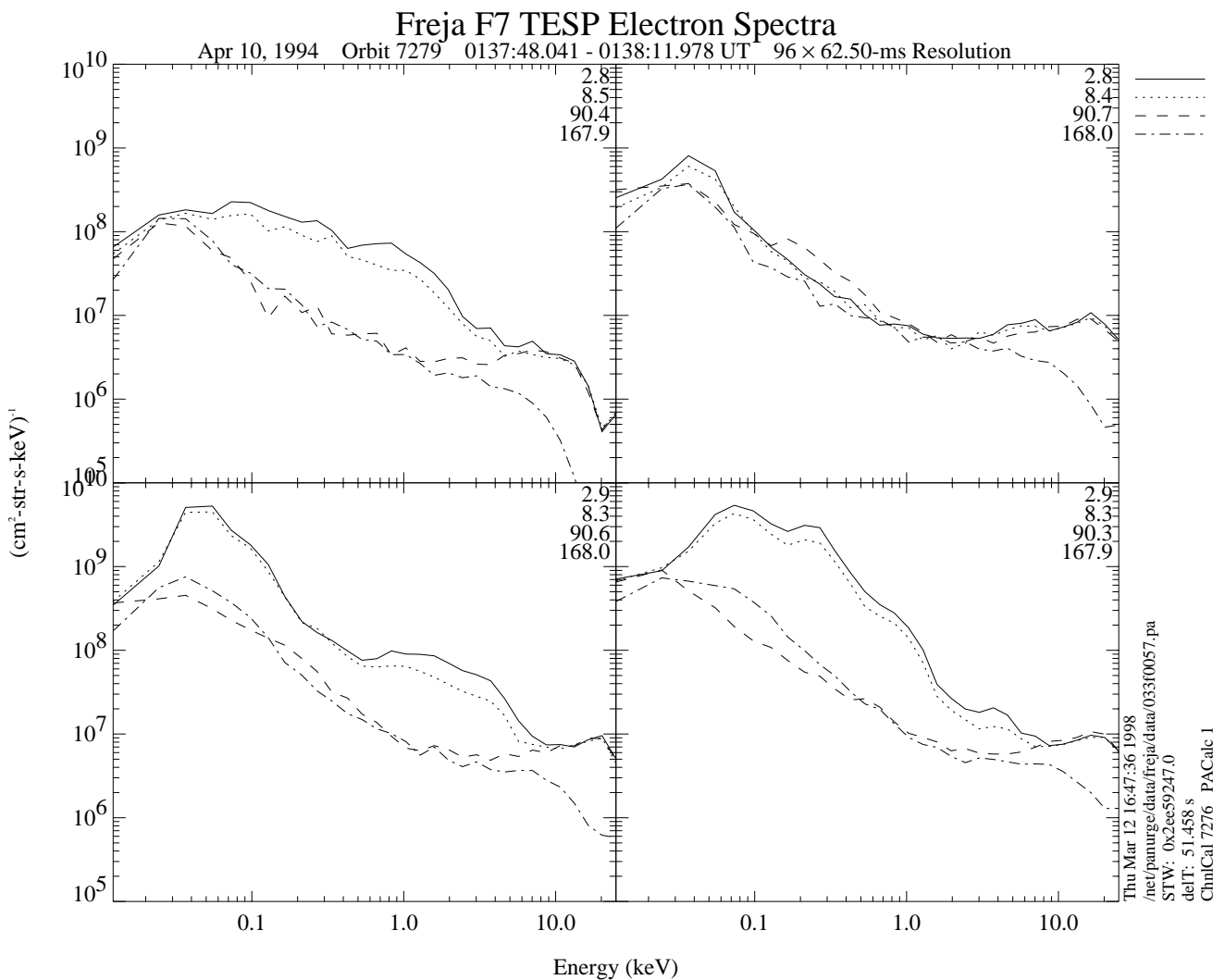


Figure 5.10.4a: TESP electron data from the charging event. Unusually much low energy field-aligned electron bursts appeared during this event. The inverted-V energy peak is close to or possibly above maximum measured energy (25 keV, panels 3-4, this Figure; all panels in next Figure). The 168° channel is measuring within the atmospheric loss cone.

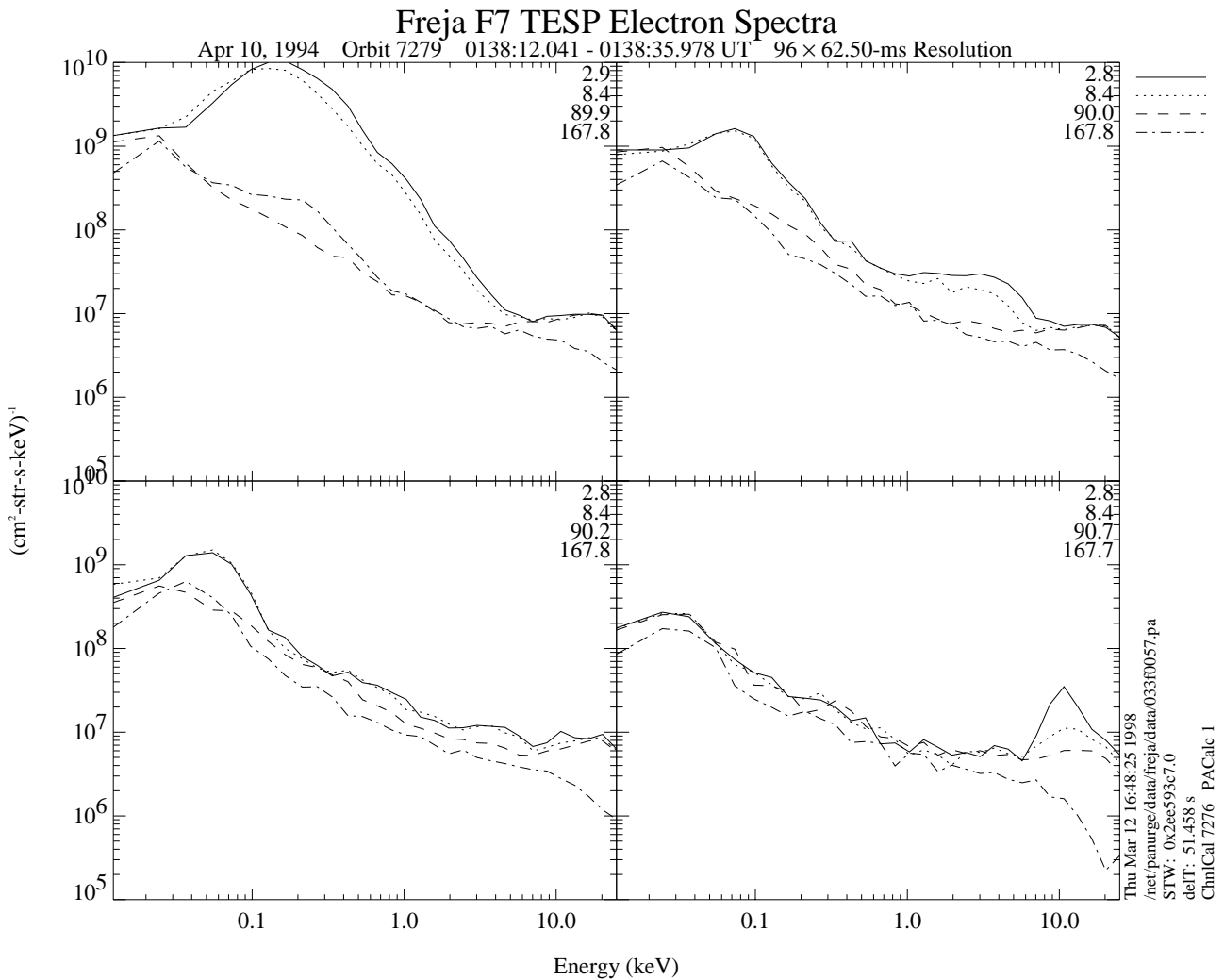


Figure 5.10.4b: See text of previous Figure.

Conclusions from orbit 7279:

- This charging event occurred during sunlight conditions at a low altitude (i.e. somewhat larger magnetic field strength and smaller electron gyro-radii). The gyroradius of emitted photoelectrons (expected to have energies of a few eV) will be 0.1-0.3 m, which is smaller than the size of Freja (about 1.5 m radius). These electrons are therefore expected to return to the spacecraft to a large degree unless large negative potentials accelerate them away from the spacecraft.
- The high energy electron tail seems to enhance the charging levels.
- The influence of low energy suprathermal electron bursts on charging level is not obvious in the data.

6. DISCUSSION OF THE EVENTS

6.1 IDENTIFIED FREJA CHARGING EVENT TYPES

By far the most common type of charging detected on the Freja satellite occurs during high-latitude auroral inverted-V events when extreme fluxes of high energy (5-80 keV or more) electrons hits the spacecraft. Usually the cold ambient plasma density is rather low ($<2 \cdot 10^9 \text{ m}^{-3}$) during these events, and a majority of these events occurred during eclipse. Two other types of charging have been found, but these were associated with very low level charging ($< -10 \text{ V}$). One of these just reflects the spacecraft ground potential change when it moves from sunlight to eclipse. An example of such a change in satellite ground potential is shown in Figure 6.1.1 (orbit 709). Almost every sunset/sunrise case have similar charging characteristics; a few Volts negative on the eclipse side and no detectable charging during sunlight conditions. *No charging events of this type has been included in the statistical study [see SPEE-WP130-TN].*

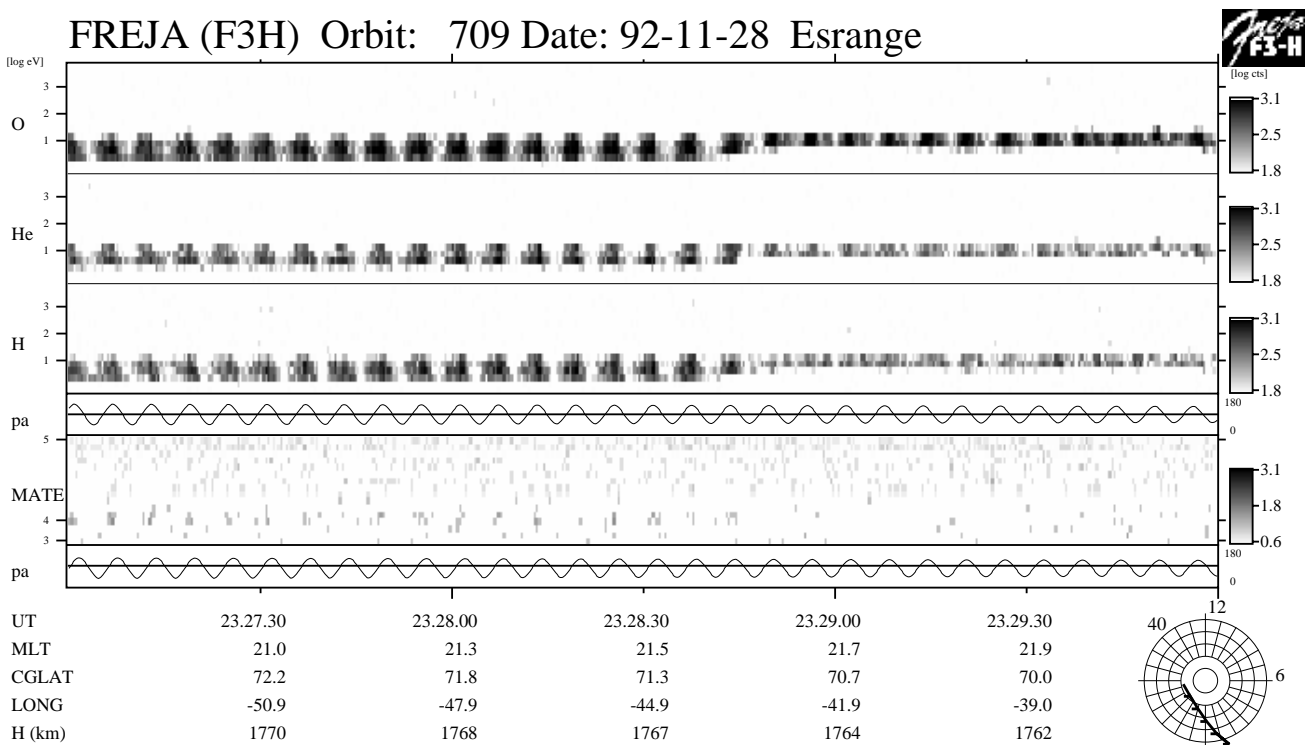


Figure 6.1.1: Overview of the particle data from orbit 709. This event illustrates the normal charging behaviour which occur during every transition from sunlight to eclipse (or vice verse) conditions. A small negative charging of a few Volts appears during eclipse.

The three types of charging detected onboard Freja can therefore be summarised as follows:

- High level charging to about -2000 V associated with energetic electrons in connection with auroral high-latitude inverted-V precipitation events. These can be of two types
 - Eclipse events (most common)
 - Sunlight events (rare, but may still reach high charging levels)
- Low level charging to -10 V due to that the Freja spacecraft enters eclipse conditions during otherwise calm plasma conditions. The photoelectron emission current from the spacecraft disappears when Freja traverses into the darkness, which shift the normal spacecraft potential somewhat to the negative.
- Low level charging to -15 V most probably due to changes in the thermal electron plasma (e.g. electron temperature increase to 2-3 eV perhaps due to heated thermal electrons produced from various plasma instability processes near auroral arcs). There exist unfortunately no data to support this hypothesis for the charging mechanism of these events, and further speculation is therefore meanings-less.

In the continuation all conclusions stated will refer to the first type of auroral (inverted-V) type charging.

6.2 ARCING ?

A majority (if not all) high level charging events detected by the Freja instruments are closely correlated with an increase in the inverted-V peak energy as well as the simultaneous increase in electron flux. This usually occurs over a time span of a few seconds and is therefore not related to sudden discharges (or arcing) in the vicinity of Freja. The charging state of the Freja satellite can therefore be said to have occurred during close to current balance equilibrium conditions, and “violent” discharges have therefore not been confirmed to occur on Freja. This study cannot tell much about so called micro-discharges (micro-arcing) possibly occurring on Freja, because the time resolutions of the Freja detectors are at best 32 ms (TESP), 0.4 s (MATE) and 0.2 s (TICS) respectively.

6.3 COMPARISONS WITH OTHER SPACECRAFT RESULTS

In Chapter 2 the various results from earlier spacecraft studies were addressed, and here we compare them with the results from this study. The Freja satellite was designed to be highly conductive and as electromagnetically clean as possible, and therefore should be better prepared for charging effects compared to the DMSP satellites. The DMSP results suggest that a somewhat lower threshold energy for charging existed and that high level charging could occur at densities an order of magnitude higher than for Freja. Also, the POLAR code simulation results presented in SPEE-WP120-TN indicate that DMSP should be charged to much higher values given the same environment. Yet, the Freja spacecraft achieved somewhat larger max charging levels and did indeed charge during sunlight conditions, which the DMSP satellites never did [Gussenhoven, private communication, *Gussenhoven et al.*, 1985]. It should be noted, though, that the Freja mission occurred close to solar minimum, which have been proven to be the most prone period with

regard to charging [*Frooninckx and Sojka, 1992*]. One DMSP result that could not be confirmed by the Freja data was the thermal plasma decrease coincident with most charging events measured by DMSP [e.g. *Yeh and Gussenhoven, 1987*]. We suspect that the plasma density measurements onboard DMSP were jeopardised by the charging events themselves and produced this artefact.

The gyroradius at Freja/DMSP altitudes for around 2 eV secondary electrons are 0.1 - 0.4 m, which is still a significant fraction of the size of Freja. Even so, only a fraction of these electrons will return to Freja through gyromotion, depending on orientation with respect to the Earth's magnetic field direction [*Laframboise, 1988*]. For a larger spacecraft a larger fraction of these secondaries will return to the spacecraft surface, and a larger spacecraft will therefore likely gain somewhat higher charging levels. The same argument is true with regard to sunlight conditions, when large amounts of photoelectrons are emitted from the surface. A smaller spacecraft will not see the photoelectrons return as easily as a larger spacecraft, and the larger spacecraft is therefore more easily charged.

7. CONCLUSIONS FROM THE CHARGING EVENTS CASE STUDY

In this report a detailed description of plasma measurements performed during several Freja electrostatic charging events was given. From this survey, the following observational conclusions can be made:

- All detected charging events were related to the presence of auroral inverted-V energetic electrons, at least down to time scales of the order of 1 second.
- Charging levels up to -2000 kV have been observed in eclipse although the main coating material, Indium Tin Oxide (ITO), is known to have high secondary electron emission properties.
- There exists a clear proportionality between charging level and the rise of the energetic electron peak energy (and the electron flux is most often enhanced an order of magnitude at the peak energy). The highest level charging events have the highest energy peaks and fluxes.
- A high energy tail up to at least 80 keV is observed during the charging events. In some cases large fluxes of MeV electrons occur simultaneously as inferred from the contamination of the ion detector measurements. Such MeV electrons only appears during the most extreme charging events and most probably is the extension of the enhanced high energy tail. MeV electrons could penetrate the upper surface layers and possibly cause internal charging.
- A threshold energy for the inverted-V peak of about 5 keV is inferred, where no charging developed below this value. Even the low level charging events of just a few volts negative were associated with energetic electrons above this threshold.
- Most charging events occurred during eclipse, but a few existed during sunlight conditions. The peak energy threshold were larger ($> 10\text{-}15$ keV) during sunlight conditions.
- Only weak indications exist that low energy suprathermal electron bursts below 1 keV inhibited charging on Freja.
- The thermal plasma density did not usually change significantly when Freja encountered a charging event as compared to the surrounding densities. Also, only weak indications (from orbit 736) exist that the thermal plasma density affected the charging levels significantly.
- The thermal plasma density was rather low ($< 10^9$ m⁻³) during charging events.
- Several of the plasma instruments showed serious operation disturbances during charging events (above a few tens of volts negative). The Langmuir probe currents dropped to almost zero current due to the fact that few thermal electrons reached the probes. The same effect made the LF and MF plasma wave measurements impossible, and the TICS instrument showed almost ring distributed ions due to the fact that the ions were accelerated toward the spacecraft.
- Transverse ion heating show similar characteristics in the ion spectrometer data (TICS) as those during a charging event. Only careful analysis or the trained eye can easily

differ between the two interpretations.

- No arcing or EMC problems have been identified during the charging events presumably because most of the spacecraft surface was very conductive.

Because Freja was a spacecraft devoted to the scientific investigation of auroral processes, including the measurement of charged particles at low energy, the designers had made special care to provide conductive surfaces of high secondary electron emission material, mainly Indium Tin Oxide (ITO). It has been shown that the charging levels of several thousand volts negative observed occasionally during auroral active conditions may have affected the quality of the data especially for the low energy plasma and the electric field measurements. However, no charging induced problems have been observed on Freja presumably thanks to the careful design regarding conductivity and grounding of the surfaces. However, it should be emphasized that an ordinary spacecraft without strong requirements regarding surface material properties (conductivity, secondary electron emission, ...) could have suffered from electrical problems (e.g. arcing) but also an enhanced erosion rate of the surface due to sputtering by the accelerated O^+ ions encountered at low altitude (= 4000 km).

For a high latitude orbiting spacecraft highly conductive surface materials are needed to avoid differential charging and risk of arcing during auroral arcs crossings. To avoid absolute high level charging, surfaces with high secondary electron emission properties are required. The use of ITOC (conductive Indium Tin Oxide Coating) wherever it is possible on the surface appears to be a good regarding electrostatic discharge problems. However, it does not prevent for occasional high level charging. This is because ITOC has a cross over energy of about 2.5 - 3 keV, above which the secondary yield falls below unity, whereas the spectral characteristics of a typical auroral inverted-V events are associated with insignificant low-energy fluxes (< 1 keV) and large fluxes of high energy electrons. These electron events are therefore especially prone to produce high charging levels on *any spacecraft* where the secondary yield crossover-energy for the surface material is a few keV. Search for more appropriate coating materials is a possible line of investigation to mitigate charging. An alternative solution could be provided by active charge control systems, like plasma contactors that are expelling a cold rather dense plasma around the spacecraft. However, such techniques may induce contamination problems and are not recommended onboard spacecrafts used for science.

8. REFERENCES

- Anderson, P. C., and H. C. Koons, Spacecraft charging anomaly on a low-altitude satellite in an aurora, *J. Spacecraft and Rockets*, vol. 33, no. 5, 1996.
- André, M., et al., Ion energization mechanisms at 1700 km in the auroral region, *J. Geophys. Res.*, vol. 103, no A3, pp 4199, 1998.
- Carlson, M., The Langmuir probes on Freja, IRF Uppsala internal report, 1994.
- Carruth, M. R., and M. E. Brady, Measurement of the charge-exchange plasma flow from an ion thruster, *J. Spacecraft Rockets*, 18(5), 457-461, 1981.
- DeForest, S. E., Spacecraft charging at synchronous orbit, *J. Geophys. Res.*, 77, 651, 1972.
- Dettleff, G., Plume flow and impingement in space technology, *Prog. Aerospace Sci.*, 77, 3587-3611, 1991.
- Eviatar, A., and J. D. Richardson, Corotation of the kronian magnetosphere, *J. Geophys. Res.*, vol. 91, no A3, pp 3299, 1986.
- Frooninckx, T. B., and J. J. Sojka, Solar cycle dependence of spacecraft charging in low earth orbit, *J. Geophys. Res.*, vol. 97, no. A3, pp 2985, 1992.
- Garrett, H. B., The charging of spacecraft surfaces, *Rev. Geophys. Space Phys.*, vol. 19, no. 4, pp 577, 1981.
- Garrett, H. B., and C. P. Pine, Eds., *Space systems and their interactions with earth's space environment*, vol. 71, Progress in Astronautics and Aeronautics Series, American Institute of Aeronautics and Astronautics, New York, 1980.
- Gussenhoven, M. S., D. A. Hardy, F. Rich, and W. J. Burke, and H.-C. Yeh, High-level spacecraft charging in the low-altitude polar auroral environment, *J. Geophys. Res.* vol. 90, no. A11, pp 11009, 1985.
- Gussenhoven, M. S., and E. G. Mullen, Geosynchronous environment for severe spacecraft charging, *J. Spacecraft Rockets*, 20, 26, 1983.
- Hall, W. N., P. Leung, I. Katz, G. A. Jongeward, J. R. Lilley, Jr., J. E. Nanevicz, J. S. Tayler, and N. J. Stevens, Polar-auroral charging of the space shuttle and EVA astronaut, in *The aerospace environment at high altitudes and its implications for spacecraft charging and communications*, AGARD-CP-406. p. 34-1, North Atlantic Treaty Organization, France, 1987.

Hastings, D. E., A review of plasma interactions with spacecraft in low Earth orbit, *J. Geophys. Res.*, vol. 100, no. A8, pp 14457, 1995.

Hastings, D., and H. Garret, Eds., *Spacecraft environment interactions*, Cambridge University Press, Atmospheric and Space Science Series, 1996.

Katz, I., M. Mandell, G. Jongeward, and M. S. Gussenhoven, The importance of accurate secondary electron yields in modelling spacecraft charging, *J. Geophys. Res.*, vol. 91, no A12, pp 13739, 1986.

Katz, I., and D. E. Parks, Space shuttle orbiter charging, *J. Spacecraft Rockets*, 20, 22, 1983.

Koons, H. C., and D. J. Gorney, Relationship between electrostatic discharges on spacecraft P78-2 and the electron environment, *J. Spacecraft*, vol. 28, no. 6, 1991.

Laframboise, J. G., Calculation of escape currents of electrons emitted from negatively charged spacecraft surfaces in a magnetic field, *J. Geophys. Res.*, vol. 93, no. A3, pp 1933, 1988.

Lazarus, A. J., R. L. McNutt, and Jr., Low-energy plasma ion observations in Saturn's Magnetosphere, *J. Geophys. Res.*, vol. 88, no A11, pp 8831, 1983.

Leach, R. D., and M. B. Alexander, Failures and anomalies attributed to spacecraft charging, NASA Reference Publication 1375, 1995.

Lundin, R., G. Haerendel, and S. Grahn, .Eds., *The Freja mission*, Space Science Reviews, vol. 70, Nos. 3-4, 1994.

Mullen, E. G., M. S. Gussenhoven, D. A. Hardy, T. A. Aggson, B. G. Ledley, and E. Whipple, SCATHA survey of high-level spacecraft charging in sunlight, *J. Geophys. Res.*, vol. 91, no. A2, pp 1474, 1986.

Newell, P. T., Review of critical ionization velocity effect in space, *Rev. Geophys. Res.*, 23, 93-104, 1985.

Olsen, R. C., A threshold effect for spacecraft charging, *J. Geophys. Res.*, vol. 88, no. A1, pp 493, 1983.

Rosen, A., *Spacecraft charging by magnetospheric plasmas*, American Institute of Aeronautics and Astronautics, Washington DC, 1976.

Shaw, R. R., J. E. Nanevicz, and R. C. Adamo, Observations of electrical discharges caused by differential satellite charging, in *Spacecraft Charging by Magnetospheric Plasmas*, Prog. Astronaut. Aeronaut., ed. A. Rosen, AIAA Press, New York, 47, 61-76, 1976.

Sittler, E. C., Jr., K. W. Ogilvie, and J. D. Scudder, Survey of low-energy plasma electrons in Saturn's magnetosphere: Voyager 1 and 2, *J. Geophys. Res.*, vol. 88, no A11, pp 8847, 1983.

Stevens, N. J., and M. R. Jones, Comparison of auroral charging predictions to DMSP data, AIAA 95-0370, 33rd Aerospace Sciences Meeting and Exhibit, January 9-12, 1995.

Wahlund, J-E., et al., Broadband ELF plasma emission during auroral energization 1. Slow ion acoustic waves, *J. Geophys. Res.*, vol. 103, A3, pp 4343, 1998.

Yeh, H.-C., and M. S. Gussenhoven, The statistical electron environment for defence meteorological satellite program eclipse charging, *J. Geophys. Res.*, vol. 92, no. A7, pp 7705, 1987.